Department of Physics and Astronomy

Ruprecht-Karls-University of Heidelberg

Master thesis in Physics

submitted by

Moritz Hornung

born in Heidenheim an der Brenz

2023

Memory Effects and Aging – Ergodicity Breaking Behaviour in Isolated Quantum Systems

This Master thesis has been carried out by Moritz Hornung

at the

Physikalisches Institut Heidelberg

under the supervision of

Prof. Dr. Matthias Weidemüller

Memory Effects and Aging –
Ergodicity Breaking Behaviour in Isolated Quantum Systems:

Spin glass models have established themselves as a paradigm for the investigation of complex systems. Since their discovery in the early 1960s, they were extensively studied and played a key role for important breakthroughs in statistical physics. With the rise of modern quantum simulation, new platforms opens up for the study of these systems that provide unprecedented access and control over the spins. This possibility to study spin glasses in a truly isolated setting might help to address open questions regarding the ground state of the glassy phase. Furthermore, it could stimulate the development of new theoretical methods to describe the wealth of phenomena displayed by a spin glass. In the course of this thesis, we investigate the behaviour of an isolated Heisenberg XY model on a Rydberg quantum simulator for a possible glass transition. To this end, we introduce a new state preparation that is utilized to probe the system for memory effects over a large range of internal energies. Finally, we are going to discuss first measurements of a key signature of the ergodicity breaking phase that is known as aging effect.

Memory-Effekte und Aging –
Nichtergodisches Verhalten in Isolierten Quanten Systemen:

Spin-Glas-Modelle haben sich als Einstieg in das Forschungsgebiet komplexer Systeme etabliert. Seit ihrer Entdeckung Anfang der 1960er Jahre wurden sie ausgiebig erforscht und hatten eine Schlüsselrolle bei wichtigen Durchbrüchen der statistischen Physik inne. Durch moderne Quantensimulatoren eröffnen sich nun neue Möglichkeiten für ihre Erforschung in Experimenten die beispiellosen Zugang zu den Spins bieten. Die dadurch gegebene Möglichkeit Spin-Gläser in einer isolierten Umgebung zu untersuchen könnte dazu beitragen offene Fragen hinsichtlich deren Grundzustand zu klären. Darüber hinaus könnte es die Entwicklung neuer theoretischer Methoden anregen, um die Vielzahl von Phänomenen zu beschreiben, die an einem Spin-Glas beobachtet werden. Diese Arbeit untersucht das Verhalten eines isolierten Heisenberg-XY-Modells auf einem Rydberg-Quantensimulator hinsichtlich eines möglichen Glasübergangs. Zu diesem Zweck führen wir eine neue Zustandsvorbereitung ein, die genutzt wird, um das System auf Memory-Effekte zu untersuchen. Abschließend werden wir erste Messungen eines Aging-Effekts diskutieren, einer klaren Signatur der nicht-ergodischen Phase.

Contents

1 Introduction

In our daily lives, we are constantly surrounded by an intricate interplay of an unimaginable number of microscopic particles. When looking at these particles at a specific snapshot in time, often times their microscopic orientation appears to be totally random, yet the emergent macroscopic behaviour is stable to the point that we do not even think of it as special. What is more, the amount of different large-scale behaviour that might originate is astonishing – a mere glance outside the window already reveals more distinct features than we can even begin to fathom.

Be it in physical, biological or even social problems, the field of complex systems science [1] addresses the study of how such collective behavior emerges from the interactions among individual components within a system. While it may initially appear counterintuitive to investigate systems comprised of vastly different constituents within a unified framework, a simple example gives reason to this approach. For instance, various gases exhibit similar macroscopic behaviors despite their dissimilar constituents. Conversely, a block of ice displays completely different behavior from liquid water, even though they are composed of identical particles.

The relevance of studying complex systems has recently been highlighted with the awardment of one half of the 2021 Nobel Prize in physics for the ”discovery of the interplay of disorder and fluctuations in physical systems from atomic to planetary scales”. The prize was granted in half to Giorgio Parisi for his development of the replica symmetry breaking method [2], a highly sophisticated application of statistical physics to disordered systems. While it nowadays finds wide application across a variety of complex problems such as protein folding [3], neural networks [4] and numerical optimization problems [5], it was initially developed in the context of spin glass theory.

Conventional spin glasses form a branch of condensed matter physics that deals with the study of disordered magnetic materials. Originally discovered in metallic alloys of non-magnetic metals doped with a small fraction of magnetic atoms, they nowadays serve as a paradigm for the study of disordered systems in general. Being characterized by randomly interacting spins, spin glasses exhibit a rugged free energy landscape with numerous local minima separated by both energy and entropy barriers, a feature that results in a plethora of metastable states. The variety of different phenomena [6] arising from this property is astounding and despite substantial progress over the last decades, theoretical models are as of now still not fully compatible with experimental data [7].

In this context, the modern concept of quantum simulation [8–10] could potentially help with addressing the unanswered questions by providing an additional platform to study such systems. Quantum simulation offers the potential to isolate and precisely manipulate spin systems [11, 12], providing access on the individual spin level. Through the use of precisely tuned experiments, it might be possible to obtain deeper insights into the true nature of the ground state, the growth of correlation lengths at the glass transition or the study of fluctuation-dissipation relations in the aging regime, which could also serve to advance the broader understanding of disordered systems in general.

Within this thesis, we strive to answer the question of whether phenomena resembling a spin glass phase can be found in a system of isolated spin interacting via dipole-dipole interactions. To this end, we want to make use of the Rydberg quantum simulation platform that has been developed in our group over the last years and uses thousands of interacting Rydberg atoms in a disordered cloud that are mapped onto a spin system. The viability of Rydberg atoms as a means for quantum simulation has already been ascertained in the past [11, 13, 14] and we have found interesting behaviour in our system such as sub-exponential relaxation [15] and ergodicity breaking on experimental timescales [16] that point towards the occurrence of a spin glass phase in the system.

We aim to extend these findings and accumulate further evidence for a possible existence of the spin glass phase in our system. To this end, we introduce a new state-preparation protocol using an external field ramp that allows to initialize states at different internal energies. By means of numerical simulation of this procedure for small system sizes, we obtain a first intuition of the phenomena we would expect at larger scales which include memory effects depending on the history of the system. We also use the high controllability provided by numerical simulations to discuss the influence of the disorder strength on the behaviour of the system. Finally, we discuss new experimental measurements that show for the first time a response to an external field after the magnetization has decayed to zero. We observe a key signature of the glass phase that is known as aging effect [17], a distinct feature where the spin glass superficially looks to be in thermal equilibrium but at the same time there are still ongoing internal dynamics that manifest in the shape of the response function when probed with an external field.

2 Ergodicity in Isolated Quantum Systems and its Breakdown

Since its foundation, during the 18^{th} and 19^{th} century, thermodynamics has been hugely successful at describing the physics of many-body systems. The key to this success lies in the abandonment of a microscopic description and the sole focus on macroscopic energy conservation and the conversion between different forms of energy.

While the fact that such an abstraction is possible is on its own quite astounding, it is classically well understood how it can come to pass. Indeed, the statistical mechanics interpretation allows for the derivation of thermodynamic principles based on the single assumption of equal probabilities for microstates in thermal equilibrium.

At the heart of this interpretation lies the ergodic hypothesis, which implies that the system, if left alone for long times, will explore the whole phase space equally. In figure 2.1 this concept is visualized. For integrable systems, due to the existence of an extensive number of conserved quantities, the trajectory is periodic and the system stays non-ergodic at all times. On the other hand, dynamics of generic many-body systems usually lead to chaotic phase space trajectories and thus an ergodic behaviour of the system. In this case, all available states are weighted equally in time, justifying the postulation of equal probabilities.

Difficulties arise when trying to unify these concepts with quantum mechanical time evolution of isolated systems. Due to the linearity of the Schrödinger equation, the classical notion of chaos does not apply to a quantum system and the state retains information about the initial conditions at all times. So how is it possible that in spite of this apparent violation of the one fundamental concept underlying all of statistical mechanics, its

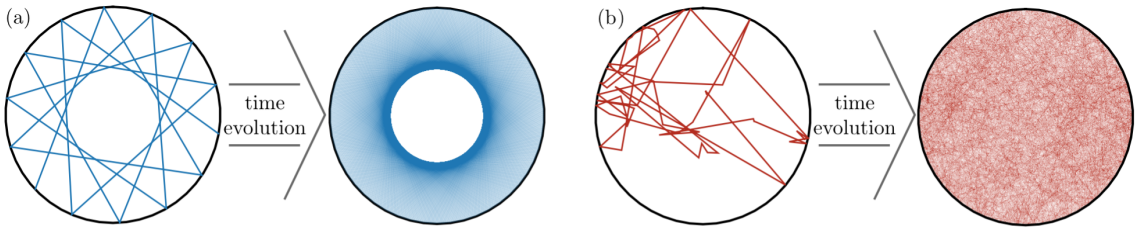

Figure 2.1: Demonstration of the concept of ergodicity. (a) For integrable systems, phase space trajectories tend to be periodic which prevents a full exploration. (b) For a classical many-body system, the phase space trajectories become chaotic. Eventually, the whole of it will be traversed. Figure taken from [18]

predictions still retain credibility for a vast range of quantum mechanical systems?
Within this introductory chapter, we are going to address the questions of how ergodicity and the process of thermalization can be interpreted in the context of an isolated quantum system. We are then going to give a short recap on how thermal concepts can be used for the descriptions of magnetic systems, assuming that they are ergodic. Magnetic systems are of special interest for the question of quantum thermalization, due to the ease of theoretical modeling [19] and direct experimental access in modern quantum simulators [11]. This combination allows for the study of fundamental questions in a truly isolated setting. Finally, we are going to discuss the special case of a spin glass as an example of a magnetic system where ergodicity is broken.

2.1 Quantum Thermalization

Although there is extensive experimental evidence supporting the relevance of statistical physics principles for non-integrable quantum systems, the emergence of equilibrium statistical physics from the unitary evolution governed by the Schrödinger equation remains poorly understood. In view of recent findings of ergodicity breaking such as quantum many-body scars [20, 21] and many-body localization [22–24], the questions of why and especially under which conditions statistical methods are applicable are currently a subject of intense debate.
As early as 1929, von Neumann [25] started this discussion with the proof of the quantum ergodic theorem, providing a first interpretation of how isolated dynamics can agree with microcanonical ensemble predictions. The constraints he imposed on the system for his proof are however quite strict and nowadays thermalization is expected to occur for a much broader class of systems.
An extension of his work over many decades has lead to the postulation of the Eigenstate Thermalization Hypothesis (ETH), a term first coined by Srednicki [26]. It explains thermalization from a microscopic perspective based on the properties of individual eigenstates of a many-body system. While the basic statements of the ETH are going to be laid out below, a more complete introduction to the topic can be found in the review of Deutsch [27].

2.1.1 Thermal Equilibrium in Isolated Systems

Before talking about the mechanisms underlying the process of thermalization, we first have to establish what we mean by this expression in the context of an isolated quantum system.
Assuming a generic, time-independent hamiltonian $\hat{H}$ with eigenvectors $|\alpha\rangle$ and eigenvalues E_α, as a direct consequence of the Schrödinger equation the time development for an arbitrary initial state $|\psi_0\rangle$ with population coefficients $c_\alpha = \langle\alpha|\psi_0\rangle$ is given by

$$|\psi(t)\rangle = \sum_\alpha c_\alpha e^{-iE_\alpha t}|\alpha\rangle. \tag{1}$$

Accordingly, the time dependent expectation value of any observable $\hat{A}$ can be expressed in terms of the matrix elements $A_{\alpha\beta} \equiv \langle\alpha|\hat{A}|\beta\rangle$ via

$$\langle\hat{A}\rangle(t) \equiv \langle\psi(t)|\hat{A}|\psi(t)\rangle = \sum_\alpha |c_\alpha|^2 A_{\alpha\alpha} + \sum_{\alpha,\beta\neq\alpha} c_\alpha^* c_\beta e^{i(E_\alpha - E_\beta)t} A_{\alpha\beta}. \tag{2}$$

Following the approach taken by D'Alessio et al. [28], we now define thermalization via late time expectation values of observables

$$\langle\langle\hat{A}\rangle\rangle_t \equiv \lim_{t_0\to\infty} \frac{1}{t_0}\int_0^{t_0} dt\langle\hat{A}\rangle(t). \tag{3}$$

Thus, when saying that a system thermalizes, we imply the following two conditions to be valid:

(i) The system develops in such a way that expectation values of observables relax to an equilibrium value and temporal fluctuations of this value are small at most later times.

(ii) The equilibrium value agrees with the predictions based on the microcanonical density operator $\hat{\rho}_{\mathrm{mc}}$ of the system

$$\langle\hat{A}\rangle \stackrel{!}{=} \mathrm{Tr}(\hat{\rho}_{\mathrm{mc}}\hat{A}), \qquad \hat{\rho}_{\mathrm{mc}} = \frac{1}{\mathcal{N}} \sum_{\substack{\alpha,\\ |E_\alpha - E| < \frac{\Delta E}{2}}} |\alpha\rangle\langle\alpha|. \tag{4}$$

The first statement ensures that the long-time average (3) gives an accurate prediction of the equilibrium value at almost all times. While an expansion of this statement to all

Figure 2.2: The process of thermalization in an isolated quantum system. The expectation values of individual spins relax towards their equilibrium values. Figure taken from [18].

times is impossible due to the existence of quantum revivals in any isolated system, the difference is irrelevant for most practical purposes.

The second statement guarantees ergodicity of the system, meaning that the temporal average can be substituted by a configurational average over the accessible state space.

We note that by this definition, ergodicity is no longer tied to the classical notion of the system slowly exploring all of its available configurations, which leads to an apparent contradiction. For isolated dynamics, all population coefficients are constants of motion and it follows that the system is stationary with respect to the phase space formed by the underlying eigenstates. The classical picture of ergodicity is clearly not fulfilled, which poses the question of why we should be able to replace a temporal average with a configurational one in the first place. There seems to be no physical reasoning for such an exchange to have any meaning.

A second prime example of why it is difficult to reconcile statistical mechanics and quantum mechanics becomes apparent when considering the evolution of a state that is initially pure in the quantum mechanical sense. Quantum mechanics tells us that this will stay a pure state at all times, whereas statistical mechanics tells us that after a relaxation time, the system can be described via a mixed density matrix where all coherences can be neglected. In physical terms, this conflict can be interpreted as the loss of information about the initial state in a statistical description compared to retaining said information in the quantum mechanical picture.

We are going to explicitly address these issues in the next section and want to conclude here with a common interpretation for how thermalization occurs in an isolated system. We start by subdividing the total system into a smaller, local system and the comparable

much larger rest. Within this setting, the large system can then act as a bath on the smaller one. Hence, local expectation values of individual spins that are obtained by tracing out the rest of the system can relax to their thermodynamic equilibrium values described by a mixed density matrix, a process illustrated in figure 2.2.

2.1.2 The Diagonal Ensemble

Although the previously highlighted interpretation of thermalization prints an intuitive picture of how it can come to pass locally, it still does not change the fact that the total system remains pure at all times. This imposes the question of why it would naturally develop towards an equilibrium value in the first place, especially since we know for a fact that at a quantum revival, the initial state will be recovered.
To tackle this problem, we first want to take a small step backwards from a thermal ensemble and introduce another equilibrium ensemble that is applicable under very general conditions. Assuming that there are no degeneracies in the system, we now have a closer look at equation (3) and evaluate the late-time average by plugging in the explicit formula for the expectation values (2). Using that the terms in the second sum average out, the expression simplifies and we are left with an equation containing only the diagonal terms

$$\langle\langle \hat{A} \rangle\rangle_t \equiv \lim_{t_0 \to \infty} \frac{1}{t_0} \int_0^{t_0} dt \langle \hat{A} \rangle(t) = \sum_\alpha |c_\alpha|^2 A_{\alpha\alpha} \equiv \mathrm{Tr}(\hat{\rho}_\mathrm{d} \hat{A}). \tag{5}$$

In the last step, we introduced the diagonal ensemble density matrix

$$\hat{\rho}_\mathrm{d} \equiv \sum_\alpha |c_\alpha|^2 |\alpha\rangle\langle\alpha|, \tag{6}$$

a rigorous prove of the equality to the temporal average can be found in Reimann [29].
Based solely on quantum mechanical dephasing of the coherences, this result discloses very interesting properties of a generic quantum system. Taking a look at the definition of the diagonal ensemble (6), it is plain that the equilibrium expectation value of an observable is fully determined by the occupation probabilities of the initial state and the the matrix elements with respect to the energy eigenstates. Since both of these quantities are stationary, this means that all information about the late-time steady state is already encoded in the initial state of the system.
Additionaly, the diagonal ensemble also restores meaning to the notion of ergodicity. In an isolated system, the off-diagonal terms of the pure density matrix will vanish under a

long time average. This implies that the system can effectively be described by a mixed density matrix, even though it might not necessarily be a thermal one.
Predicting the long time average of a generic system [30], the diagonal ensemble is a very useful tool for the study of many-body systems. There is however a large disadvantage it has compared to a thermal ensemble. Since it requires knowledge of all eigenstates and their corresponding occupation numbers, it does not reduce the complexity of the description as it is the case for thermal ensembles. The complexity of calculating the diagonal ensemble essentially corresponds to what is needed for numerically simulating the exact dynamics and is therefore exponentially hard in the number of particles involved. It is thus still a question of considerable interest under which conditions predictions obtained from a thermal ensemble converge to the exact predictions from the diagonal ensemble.

2.1.3 Eigenstate Thermalization Hypothesis (ETH)

In view of the equilibrium state predicted by the diagonal ensemble, the question of thermalization narrows down to the question under which conditions a thermal ensembles approximates the results from the diagonal ensemble. Hence, for an isolated quantum system to thermalize, we need the equality

$$\mathrm{Tr}(\hat{\rho}_{\mathrm{d}}\hat{A}) = \sum_{\alpha} |c_\alpha|^2 A_{\alpha\alpha} \stackrel{!}{=} \frac{1}{\mathcal{N}} \sum_{\substack{\alpha, \\ |E_\alpha - E| < \frac{\Delta E}{2}}} A_{\alpha\alpha} = \mathrm{Tr}(\hat{\rho}_{\mathrm{mc}}\hat{A}) \tag{7}$$

to hold. This is where the eigenstate thermalization hypothesis (ETH) comes in to play. Stating that the matrix elements are a smooth function of the average energy $A_{\alpha\alpha} = A(E)$, it allows to prove equation (7) in a very general setting. If the state is localized in the energy spectrum, meaning that in the limit of large system size the energy fluctuations in the diagonal ensemble

$$\sigma_{\mathrm{E}} \equiv \sqrt{\langle\psi_0|\hat{H}^2|\psi_0\rangle - \langle\psi_0|\hat{H}|\psi_0\rangle^2} \tag{8}$$

are subextensive, the equality holds up to second order in σ_{E}. This can be verified through a direct calculation:

$$\begin{aligned}\mathrm{Tr}(\hat{\rho}_{\mathrm{d}}\hat{A}) &= \sum_{\alpha} |c_\alpha|^2 A_{\alpha\alpha} \\ &\approx A(E)\sum_{\alpha}|c_\alpha|^2 = A(E) = A(E)\frac{1}{\mathcal{N}} \sum_{\substack{\alpha, \\ |E_\alpha - E| < \frac{\Delta E}{2}}} 1 \\ &\approx \frac{1}{\mathcal{N}} \sum_{\substack{\alpha, \\ |E_\alpha - E| < \frac{\Delta E}{2}}} A_{\alpha\alpha} = \mathrm{Tr}(\hat{\rho}_{\mathrm{mc}}\hat{A}). \end{aligned} \tag{9}$$

A more concise treatment of the ETH statement and when these equalities are fulfilled can be found in the review of Mori et al. [31]. Central to this approximation lies the fact that all eigenstates within a narrow window of the average energy yield the same expectation values. This leads to the conclusion that every eigenstate is, by itself, thermal and the complex out of equilibrium dynamics that can be observed are seen because of phase coherence that is retained as a consequence of the preparation of the initial state.

As of now, for most systems there is no real microscopic theory that would explain why the ETH is fulfilled. Connections can be made to random matrix theory [28, 32], in the framework of which some rigorous statements can be proven, but definite criteria for the validity have not been found as of know. Accordingly, the ETH does not really offer a priori predictive power, since it is not clear whether it will be fulfilled in a system or not. We first need to investigate the nature of the eigenstates to extract information on the system based on ETH.

Moreover, ETH as it was discussed here does not provide any information about the timescale at which equilibration occurs. While there are some approaches to extend ETH to a statement about the off-diagonal matrix elements [32], we are not going to further elaborate on this topic for this work.

Nevertheless, using exact diagonalization, ETH has been found to apply to a vast range of systems [33–37] and once ETH has been verified, it provides a nice explanation for how thermalization occurs under unitary dynamics.

Summing up this discussion about quantum thermalization, considerable insights have been gained on how equilibration arises from unitary quantum mechanics over the past decades. Three properties are needed for a generic system to thermalize. First, the system relaxes towards an equilibrium value determined by the diagonal ensemble. Second, the

initial state of the system is concentrated in energy according to equation (8). While this condition might seem rather specific, it has been shown that it is generically fulfilled in the scenario of a quantum quench, where the system is initially in an eigenstate and then brought out of equilibrium through a sudden change of the Hamiltonian [38]. Third, the ETH has to be fulfilled, which concludes this set of three conditions that is sufficient for any system to be assumed thermalizing.

2.2 Methodology for Ergodic Systems

After having established the framework of thermalization in the context of isolated quantum systems, we now want to look at the benefits this provides when trying to predict the behaviour thereof. For thermal systems, we can use the well established tools from statistical mechanics and thermodynamic to describe the relevant physical processes. Since thermodynamics does not take into account microscopic details of the system it deals with, this enables accurate predictions for a vast range of microscopically different systems.
Throughout this section, we are going to outline the most important techniques when dealing with ergodic systems. We are going to focus on how to apply these to magnetic models, since this is seldomly done in an explicit way within the textbooks when introducing thermodynamics. Due to lazy notation in many books, there even is some confusion in literature about identifying the correct thermodynamic potentials from statistical ensembles [39]. This confusion arises from the wrong identification of quantum mechanical energy encorporating the interaction with the external field as inner energy of the system, a point that will be clarified in the subsequent introduction. In the end, we are going to elaborate on the notion of self-averaging in large systems and the important role this plays when dealing with disordered systems.

2.2.1 Macroscopic Thermodynamics of Magnetic Systems

For any macroscopic system with fixed particle number, the first law of thermodynamics tells us that a change of the internal energy is always a consequence of either heat transport or generalized work performed by the system. Mathematically speaking, the variation of the inner energy is given as

$$dU = TdS - \delta W, \tag{10}$$

where TdS represents heat transfer and δW a generalized work. We adapt the convention that positive work implies that the system performs work whereas negative work is done

to the system.
In the case of a system formed by magnetic dipoles, the work done by an external magnetic field B to produce a variation of the magnetization is given through

$$\delta W = -BdM, \tag{11}$$

the alignment with an external field thus corresponds to negative work and increases the energy of the system. Initially, this statement might seem a little counterintuitive, since we know that an alignment reduces the energy between the field and the dipoles. The crucial observation to clarify this conundrum is that this interaction energy is not part of the system of dipoles. When it is minimized through the build-up of magnetization, as a consequence of energy conservation, there has to be some excess energy. With nowhere else to go, this excess energy is absorbed by the system and thereby increases its inner energy.
It is important to note, that contrary to the notation of most textbooks on electrodynamics, in the above formulas, B indicates the external magnetic H-field which does not include the magnetization of the system. The reason for this deviation from conventional nomenclature is the introduction of the magnetic enthalpy below, which unfortunately is also labeled with H in most textbooks on statistical physics.
Combining equations (10) and (11) yields the following fundamental equation for the internal energy of a magnetic system

$$dU(S, M) = TdS + BdM, \tag{12}$$

where the natural variables are entropy S and magnetization M. The equations of state for the system follow in the usual way by evaluating the partial derivatives

$$T = \left(\frac{\partial U}{\partial S}\right)_M, \qquad B = \left(\frac{\partial U}{\partial M}\right)_S. \tag{13}$$

Once again, we stress that the energy that is stored in the interaction between the dipoles and the external field is not part of the inner energy $U(S, M)$ of the system as defined above. This is an easy to make mistake when coming from the perspective of quantum mechanics, where usually interactions and external field are combined into a single Hamiltonian, which is then used to derive thermodynamic potentials according to statistical mechanics.

As addressed by Castellano [39], the thermodynamic potential obtained when considering a composite system of both dipoles and external field is in fact the magnetic enthalpy $H(S, B)$ and not the inner energy. They are of course related via the Legendre transformation

$$H(S, B) = U - BM, \tag{14}$$

which immediately makes it clear that now the interaction energy is considered part of the system. Consequently, the total differential is

$$dH(S, B) = TdS - MdB \tag{15}$$

and we find for the arising equations of state

$$T = \left(\frac{\partial H}{\partial S}\right)_B, \qquad M = -\left(\frac{\partial H}{\partial B}\right)_S. \tag{16}$$

As it turns out, it is more useful to interpret the fundamental equation (15) in a slightly different way. Since entropy is a lot harder to control than the energy of the system, we derive a thermodynamic potential from the entropy

$$dS(H, B) = \frac{dH}{T} + M\frac{dB}{T}, \tag{17}$$

where now we interpret Entropy as a function of magnetic enthalpy and external field. Evaluating the partial derivatives shows that

$$\frac{1}{T} = \left(\frac{\partial S}{\partial H}\right)_B, \qquad M = T\left(\frac{\partial S}{\partial B}\right)_H. \tag{18}$$

Thus, knowing entropy as a function of magnetic enthalpy and external field fully determines the system.

There is one last quantity that is going to be very important throughout this thesis and can be readily computed by means of a second derivative upon knowledge of the thermodynamic potentials stated above. The magnetic susceptibility is defined as

$$\chi_{\mathrm{mag}} \equiv \frac{\partial M}{\partial B} = -\frac{\partial^2 H}{\partial B^2} = T\frac{\partial^2 S}{\partial B^2}, \tag{19}$$

the equalities being a direct consequence of equations (16) and (18).

An important result that cannot be obtained from a macroscopic thermodynamic description relates this response function to thermal fluctuations in equilibrium

$$\chi_{\mathrm{mag}} = \langle M^2 \rangle - \langle M \rangle^2. \tag{20}$$

This statement, which holds for small external field strengths, will not be derived here since one needs the microscopical framework of the canonical ensemble to do so. It is however a very important and somewhat surprising result, as it allows to calculate out of equilibrium behaviour of the system based on equilibrium properties.
For the sake of completeness, we also mention the Helmholtz and Gibbs free energy, that are obtained by applying the Legendre transformation $X - TS$, where X stands for the inner energy or magnetic enthalpy respectively. While both free energies are very important for the study of open quantum systems, where Temperature is easy to control, they have less relevance for isolated systems that feature a fixed energy.
To conclude this short introduction to thermodynamic potentials, we elaborate on why they are important and on how to use them. For each thermodynamic potential, the phase space is spanned by the two natural variables. All other macroscopic quantities defining the system then follow from the equations of state. Hence, knowledge of the thermodynamic potential over the phase space of the natural variables fully determines the possible states of the system.
So far, this does not give us any information about the nature of the thermal state of the system. To predict the steady state, we need an additional postulate which is the second law of thermodynamics and tells us that the system will evolve towards the state with highest entropy while at the same time respecting external constraints. These constraints comprise for example conserved quantities such as the total energy under unitary evolution in an isolated quantum system or a constant magnetic field that is fixed from the outside.

2.2.2 Microscopic Statistical Interpretation and Paramagnetism

Having laid out the macroscopic theory, we now want to demonstrate how we can use a microscopic statistical mechanics point of view to calculate the corresponding thermodynamic potentials. This will also bring back the connection to quantum mechanics, since we need detailed knowledge about the possible states that the system can adopt. We do so using the example of paramagnetism, which is a common feature displayed by many

magnetic materials, above a critical energy density.

By definition, a paramagnet is a system of non-interacting dipoles. Working in units where $\hbar = k_\mathrm{b} = 1$ and restricting ourselves to a quantum mechanical spin half system with external field applied in x-direction $B = (b, 0, 0)^T$, the corresponding Hamiltonian reads

$$\hat{H}_\mathrm{para} = -b \sum_{\mathrm{i}=1}^{N} \hat{\sigma}_\mathrm{x}^{(\mathrm{i})}, \tag{21}$$

where σ_x denotes the Pauli-x matrix, the index i labels the spins and the magnetic moment is assumed to be $\mu = 1$. The stationary (eigen-) states are simply the product states in x-basis of the form $|\psi\rangle = |{\rightarrow}{\rightarrow}\cdots{\rightarrow}\rangle$, which we can use to derive the thermodynamic properties in the framework of the microcanonical ensemble.

For a given state, energy[1] $\epsilon = E/N$ and Magnetization $m = M/N$ per unit spin are uniquely determined from the number of spins aligned $N_\uparrow$ and antialigned $N_\downarrow$ with the external field according to

$$m = \frac{N_\uparrow - N_\downarrow}{2N}, \qquad \epsilon = -bm. \tag{22}$$

The number of possible configurations $\Omega(N, \epsilon)$ for a specific ϵ is determined by the possible ways of distributing $N_\uparrow$ among N spins and therefore equals the binomial coefficient

$$\Omega(N, \epsilon) = \binom{N}{N_\uparrow(\epsilon)} = \frac{N!}{N_\uparrow(\epsilon)! N_\downarrow!}. \tag{23}$$

Finally, we can use the definition of the Boltzmann entropy in the microcanonical ensemble and find

$$\begin{aligned} S(N, \epsilon) &\equiv \ln \Omega(N, \epsilon) = \ln N! - \ln N_\uparrow! - \ln N_\downarrow! \\ &\approx N \ln N - N - N_\uparrow \ln N_\uparrow + N_\uparrow - N_\downarrow \ln N_\downarrow + N_\downarrow \\ &= N \ln N - N_\uparrow \ln N_\uparrow - (N - N_\uparrow) \ln(N - N_\uparrow) \\ &= -N \left[\left(\frac{1}{2} - \frac{\epsilon}{b} \right) \ln \left(\frac{1}{2} - \frac{\epsilon}{b} \right) + \left(\frac{1}{2} + \frac{\epsilon}{b} \right) \ln \left(\frac{1}{2} + \frac{\epsilon}{b} \right) \right], \end{aligned} \tag{24}$$

where we used the Stirling approximation for large N.

[1] Note that here we adopt the quantum mechanical approach and simply call the quantity determined by the Hamiltonian the energy of the system. However, from a thermodynamical point of view, we are dealing with the magnetic enthalpy

This result is visualised in figure 2.3, where entropy and magnetization are plotted as a function of energy and we reinsert the magnetic moment for dimensional reasons.
The first thing to notice is that, as laid out above, by including the mutual interaction between field and dipoles in the Hamiltonian, from a thermodynamical point of view, we obtain the entropy as a function of magnetic enthalpy and not inner energy when doing the microcanonical computations. Second, up to an arbitrary additive constant, enthalpy in this system is bounded from below and above. The minimum is reached when all spins are aligned with the external field and there is no configuration that further reduces enthalpy. In the same way, maximum enthalpy is obtained when all spins are antialigned with the field. The boundaries are readily computed from equation (22) to be $\epsilon_{\pm} = \pm b/2$.
Within the allowed enthalpy window, entropy increases monotonously throughout negative enthalpies, has a maximum at zero and then decreases towards positive enthalpy values. Once again we can make two interesting observations.
First, there is a regime where the derivative with respect to the energy is negative which implies the existence of negative temperatures. Second, entropy is maximized at zero energy, which seems to imply a demagnetized equilibrium state independent of the external field strength if we consider the second law of thermodynamics.
This apparent contradiction can be resolved by taking a more careful look at how to apply the second law to specific scenarios. As stated in the previous section, it tells us that the system will evolve in the available phase space such that entropy is maximized. We also know from the previous section that phase space is spanned by H and B, while T and M are derived quantities. Now, since the isolated system conserves enthalpy and the magnetic field is determined from the exterior, the constraints on the system are so strong

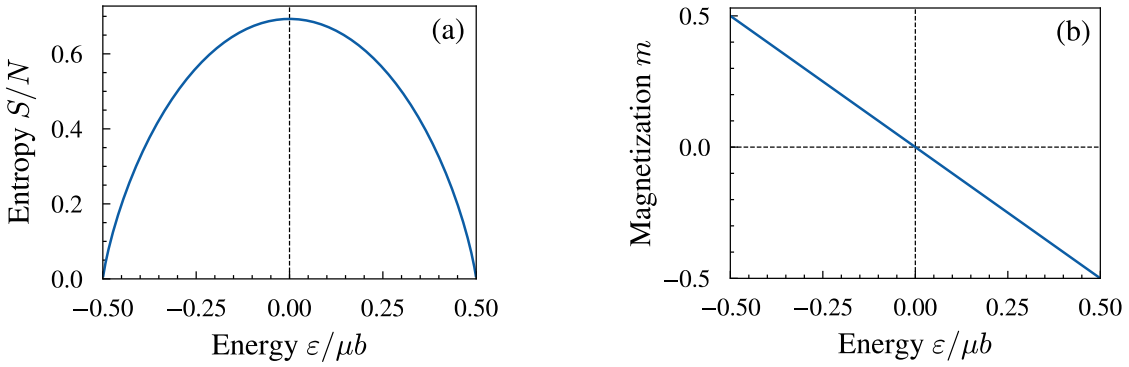

Figure 2.3: (a) Entropy of a paramagnet as function of energy density. We find a single maximum at zero for a paramagnet. (b) The magnetization is a linear function of energy.

that there is only a single allowed point in the phase space that simultaneously satisfies both the enthalpy and magnetic field constraints. Hence there is no allowed configuration that increases entropy, which is thus maximized in accordance with the second law at non-zero magnetization.

While paramagnetism is a very instructive model to study and is even able to describe materials with very weak interactions over a large range of temperatures or energy densities, the model breaks down in most known materials as soon as interactions become relevant. To circumvent this, one can expand the model by including a mean field interaction. With this ansatz, which is known as Weiss molecular field theory, it is possible to significantly improve the predictions using a self consistent approach to the magnetization and even gain estimates for critical temperatures for a phase transition as is present in for example a ferromagnetic Ising model. The main idea behind this approach is to substitute interaction terms in the Hamiltonian with the mean value for a given spin configuration and then solve self-consistently, a very instructive explanation can be found in the lecture notes of Likharev [40]. Since this procedure depends very much on the actual model, we will come back to this topic when analysing the specific model realized in the Rydberg experiment of our group.

2.2.3 Self-averaging in disordered systems

To finish the discussion about thermodynamics of magnetic systems, we want to take a look at an important property of disordered systems, known as self averaging. When dealing with a disordered system, in principle one would have to average over all possible disorder realizations when expressing thermal expectation values. Such an average is called disorder average and defined as

$$\overline{\langle A \rangle} = \frac{1}{\mathcal{N}} \int_\lambda p(\lambda) \langle A \rangle_\lambda = \frac{1}{N} \sum_\lambda p_\lambda \langle A \rangle_\lambda, \tag{25}$$

where the overbar $\overline{\cdots}$ denotes the disorder average and $\langle \cdots \rangle_\lambda$ the thermal expectation value for configuration λ that is realised with probability p_λ.

In most use cases, the number of possible disorder realizations increases dramatically with the number of particles, and while it might be possible to calculate the disorder average in specific cases, it is nigh on impossible to experimentally access all configurations in an experiment. Nonetheless, we can often use measurements from a single, large sample to make statements about not just this specific but any realization with a similar distribution.

Essentially, we are able to determine the full disorder average for many systems from just a single realization. This is due to the phenomenon of self averaging, which implies that as the sample gets larger, global quantities depend less and less on the individual configuration.
Mathematically this is expressed by the relative variance with respect to the disorder average going to zero in the limit of large N

$$\lim_{N\to\infty} \frac{\overline{\langle A\rangle^2} - \overline{\langle A\rangle}^2}{\overline{\langle A\rangle}^2} = 0. \tag{26}$$

For extensive thermodynamic quantities such as entropy or free energy in a system with weak interactions, self-averaging is usually given, which can be shown by subdividing the system and using the central limit theorem [41]. This statement is very important, both from an experimental and numerical point of view, as it allows for a determination of the quantities from only a small subspace of the possible configurations of quenched disorder.
An important class of operators where self-averaging fails is for local operators. Quantities such as individual correlations between two spins or local magnetization values still fluctuate very much from realization to realization, even in the thermodynamic limit. For such quantities, a disorder average as defined above is essentially meaningless, as it does not allow any predictions for a specific realization.

2.3 Spin Glass Phenomenology

Eigenstate thermalization as it has been discussed so far holds for a variety of different systems. Combined with the universality of thermodynamics and the computational power of statistical mechanics, this allows for powerful predictions in a large number of physical settings.
There are however exceptions, where thermal predictions are known to fail. The most notable case being within integrable systems, where due to an extensive number of conserved quantities, the proper equilibrium state is not determined by a thermal ensemble and has to be determined according to a generalized Gibbs ensemble instead [42]. The breakdown of thermalization in this case is quite well understood and an immediate consequence of integrability.
A case that is as of now less well understood is when the defiance of thermalization occurs in a system that is non-integrable, a scenario occurring for example in many-body

localized systems and spin glasses. While the former defy thermalization due to a lack of transport in the system [22], ergodicity breakdown in the latter is a result of astronomically long relaxation times [7].
Throughout this thesis, we want to investigate the possibility of such an ergodicity breaking spin glass phase in our system. Therefore, we will present a short introduction to this kind of system and highlight its main experimental signatures and important theoretic questions in the following.

2.3.1 Introducing the Spin Glass Model

Originally found in non-magnetic metals that have been doped to a small percentage with magnetic atoms, spin glasses have been extensively studied for many decades and over the course of this time, many empirical and theoretical results have been accumulated [43].
A spin glass is characterized by a temporal freezing out of the spins below a critical temperature. The spins in this frozen state of matter feature long correlation times, while no long-range magnetic ordering can be found and the total magnetization of the system remains zero. Empirically, it has been found that two characteristics of an interacting spin system that are necessary but not sufficient for glassy behaviour are disorder and frustration [44]. While disorder causes the existence of relaxation times on all timescales, frustration ensures that there is no easy symmetry configuration for the ground state. The interplay of both effects results in a thermodynamic phase transition, most often between a paramagnetic and the glassy phase that shows an abundance of highly non-trivial effects such as anomalously slow relaxation times [45], aging [46] as well as rejuvenation and memory effects in general [47, 48].
A commonly studied model for this kind of system has been introduced by Edwards and Anderson [49]. Considering classical Heisenberg spins pointing in direction $\vec{\sigma}$ in an external field $\vec{B}$, the Hamiltonian is given by

$$\hat{H} = -\sum_{\mathrm{i,j}} J_{\mathrm{ij}} \vec{\sigma}^{(\mathrm{i})} \cdot \vec{\sigma}^{(\mathrm{j})} - \vec{B} \cdot \sum_{i} \vec{\sigma}^{(\mathrm{i})}, \tag{27}$$

where i and j label lattice sites. The spin-spin interactions are considered to be nearest neighbour only and the strength is determined by the J_{ij}, which are independent random variables with zero mean. While this model is conceptually simple, solving it in the presence of an external field already proves to be very difficult.
A full solution has been found by Parisi for a closely related model where the Heisenberg

spins are replaced by Ising like spins and the sum is extended to all particles, a model nowadays known under the term of Sherrington-Kirkpatrick (SK) model [50]. The solution of this model requires a sophisticated mean field theory in combination with an at that time altogether new statistical method of replica symmetry breaking and is able to predict a phase transition together with the occurrence of a new kind of order where individual spins freeze out into random directions.

The corresponding phase diagram is shown in figure 2.4 and features the discussed spin glass phase at temperatures that are small with respect to the variance of the couplings. For higher temperatures, the system behaves like a paramagnet. Interestingly, a bias in the interactions also destroys the spin glass phase, indicating the importance of frustration to the model. The F' region indicates a crossover region where upon lowering the temperature, the system first adopts a ferromagnetic phase and for even lower temperatures transitions to the SG phase.

While the method of replica symmetry breaking [2] has been largely successful, it requires in depth knowledge of statistical physics and a full treatment is out of scope for this thesis. Thus, we are mainly going to present a phenomenological description of the spin glass phase in the following and only briefly highlight how replica symmetry breaking can

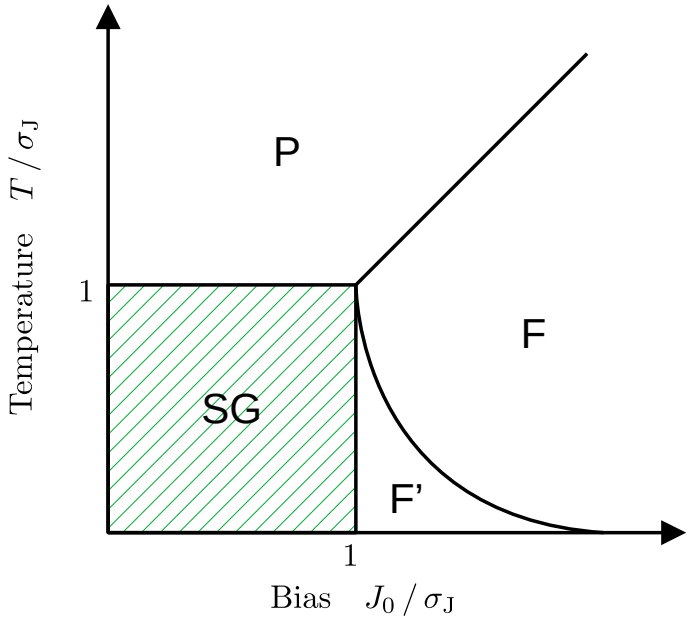

Figure 2.4: Phase diagram of a spin glass obtained in the Parisi solution of the SK model. The spin glass phase occurs at low temperatures if the bias in the interactions is small compared to the variance.

explain some of the observed features of the low temperature glass phase.

2.3.2 Magnetic Susceptibility in the Glass Phase

A very common technique for investigating the frozen phase of a spin glass is to measure the macroscopic linear response function of the system. This is achieved by applying a weak magnetic probe field B_{p} to the sample and measuring the ensuing magnetization. Due to the magnetic irreversibilities below the critical temperature, the response function becomes history dependent, a clear sign of ergodicity breaking.
There are two procedures that are commonly followed when determining said function. For the field-cooled (FC) measurement, the magnetic field is applied in the paramagnetic phase and only afterwards is the sample cooled below the critical temperature. Throughout the whole process, the magnetization is measured as a function of temperature and we obtain the FC magnetization $M_{\mathrm{FC}}(T)$. Notably, the same curve of the magnetization is obtained when reheating the probe.
The second measurement one can conduct is to reverse the order of cooling and applying the probe field. Thus, one first cools the probe below the freezing temperature and only then applies a small magnetic field. The magnetization is then measured upon reheating of the probe. With this procedure, which is termed zero-field-cooled (ZFC), the obtained magnetization curve $M_{\mathrm{ZFC}}(T)$ is not reversible.
An example of such a measurement is given in figure 2.5. Above the critical temperature, we find the typical behaviour of a paramagnet. Thermal fluctuations are strong compared to interactions and the response follows a characteristic Curie-Weiss law, increasing with decreasing temperature as

$$\chi_{\mathrm{mag}} = M/B_{\mathrm{p}} \propto \frac{C}{T-\theta}, \tag{28}$$

where C is the spin dependent Curie-constant and θ a critical temperature determined by the exact interactions of the system. As expected, the FC and ZFC curves overlap in this regime, since the build-up of magnetization is fully reversible.
Below the critical temperature, the FC magnetization is approximately flat, hinting at a collective behaviour of the whole system [7]. Upon entering the low temperature phase, the spins freeze out into a long-time correlated state. This is also the reason why the ZFC measurements in this regime deviate significantly. The freezing of the spins hinder the alignment with the external field and prevents equilibration to the FC value, which results in a weaker response to the external field.

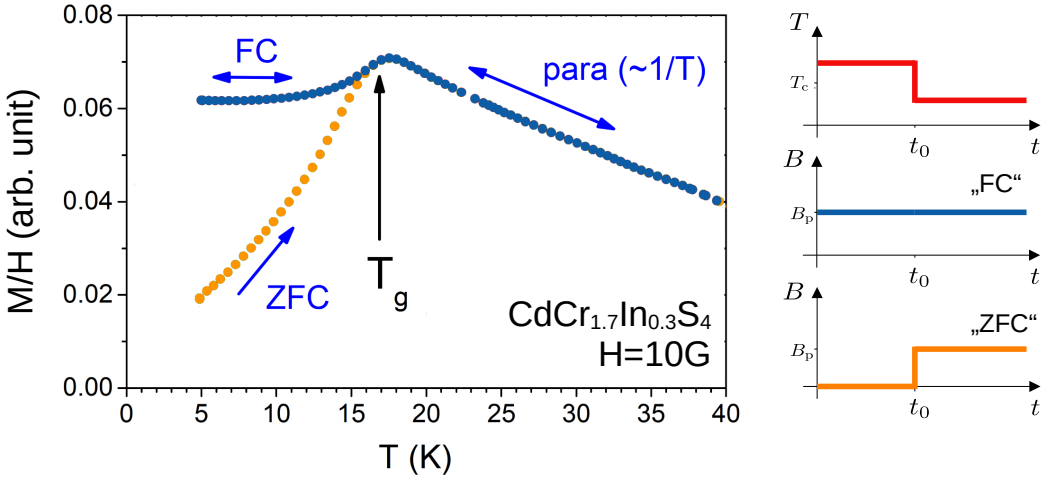

Figure 2.5: Typical susceptibility measurement in a spin glass according to field cooling (FC) and zero field cooling (ZFC) protocols. Above a critical temperature, there is a paramagnetic regime where both curves overlap and follow a Curie-Weiss law. Below the critical temperature, the two different procedures yield different results. Figure adapted from [47]. To the right, the differences in the state-preparation are highlighted.

While this interpretation for difference in both curves is widely spread, it has to be treated with proper care, since there are clear indications such as the aging effect discussed in the next section that even the FC state is not in full thermodynamic equilibrium.
Finally, it is also noteworthy that via a generalization of the fluctuation-dissipation theorem, the linear response measurements can also be related to the magnetization autocorrelation function, in spite of the fact that the system is not in equilibrium [51].

2.3.3 Time Dependent Linear Response Theory and Aging

One of the most prominent effects that unveils the non-thermalizing nature of spin glasses is known as aging. To explain this phenomenon, we have to move from a description in terms of equilibrium expectation values to a more general, time dependent theory. A common way to do this is in the framework of linear response theory, where we can connect time evolution after a perturbation to equilibrium properties of the system. For a more complete introduction to this topic we refer to the lecture notes by David Tong [52]. In the following, we are going to consider the specific interaction of a magnetic system with an external field as a perturbative term in the Hamiltonian

$$\hat{H} = \hat{H}_0 - B(t)\hat{m}(t), \tag{29}$$

the obtained conclusions are however easily generalized to an arbitrary perturbation of the form $\hat{H}_{\text{source}} = \phi(t)\hat{A}(t)$ where $\hat{A}$ is an observable of the system and ϕ any source weakly coupling to it.
If the coupling is weak enough, the time dependent expectation value is governed by the linear response function $R(t, t')$

$$\delta\langle m\rangle(t) \equiv \langle m\rangle(t) - \langle m(0)\rangle = \int_{-\infty}^{t} dt' R(t, t')B(t'), \tag{30}$$

where we neglect terms of quadratic or higher order in the external field. This equation can be interpreted as an average over the past values of the perturbation weighted by the response function. The explicit dependence of $R(t, t')$ on t' allows to keep information on the whole past of the system and thus to even describe possible memory effects.
For a system in thermal equilibrium however, it is intuitive that no memory effects are present and the response can only depend on the difference $\tau = t - t'$ and not the absolute timing of the perturbation, allowing for the simplification

$$\delta\langle m\rangle(t) = \int_{0}^{\infty} d\tau R(\tau)B(t - \tau) \tag{31}$$

At this point, one could continue the investigation in the context of equilibrium physics and derive two very important results from statistical physics, namely the Kubo formula and the fluctuation dissipation theorem, which relate the response function to the equilibrium power spectral density. For the purpose of this thesis, it is however not expedient to delve into this rather extensive topic. Instead we want to take a look at how we can relate the response function to the magnetic susceptibility introduced in the previous sections.
In order to do so, we define the generalized susceptibility as the Fourier transform of the response function

$$\chi(\omega) \equiv \int_{0}^{\infty} R(\tau)e^{-i\omega\tau} d\tau, \tag{32}$$

where the lower limit of the integration is zero due to causality ($R(\tau) = 0$ for $\tau < 0$). The result is a complex number $\chi = \chi' + i\chi''$ that relates the Fourier components of generalized flux (in our case the magnetization) and generalized force (external magnetic field) according to

$$m(\omega) = \chi(\omega)B(\omega), \tag{33}$$

easily verified by Fourier transforming equation (30). This formula essentially states

that the response is local in frequency space. The magnetic susceptibility that has been discussed in the previous section is then obtained in the zero frequency limit:

$$\chi_{\mathrm{mag}} \equiv \left.\frac{\partial m}{\partial B}\right|_{\omega=0} = \lim_{\omega\to 0}\chi(\omega) \tag{34}$$

Having established the very general formalism of how to treat a weak, time dependent perturbation, we now want to take a second look at the FC and ZFC measurements in spin glasses. Empirically, it has been found that in a ZFC measurement, after a fast initial increase to the ZFC susceptibility, the response then features a slow relaxation towards the FC value. The timescale of this relaxation depends on the waiting time t_{w} that has elapsed between the temperature quench and the application of the probe field, a measurement for different waiting times can be seen in figure 2.6.

In terms of the linear response quantities as described above, this means that the substitution of the response function $R(t,t') \to R(\tau)$ is inappropriate. Instead, the system remembers its time of birth and we have to keep an explicit dependence on the waiting time $R(t,t_{\mathrm{w}})$.

This measurement can also be reversed by doing a field cooling and then taking a look at the remanent magnetization when the external field is shut down in the glass phase. This experiment, known as thermoremanent magnetization (TRM), features exactly the same dependence on the waiting time as the upwards relaxation of the ZFC susceptibility. For a given sample, it has been found that $M_{\mathrm{FC}} = M_{\mathrm{TRM}}(t,t_{\mathrm{w}}) + M_{\mathrm{ZFC}}(t,t_{\mathrm{w}})$, the effects are hence exactly mirroring each other. The important takeaway from the TRM measurement is that the waiting is done after a field cooling process. Since we still find this waiting time to change the behaviour of the system, this is a clear indication that even for FC measurements a spin glass is not in a thermal state after the temperature quench.

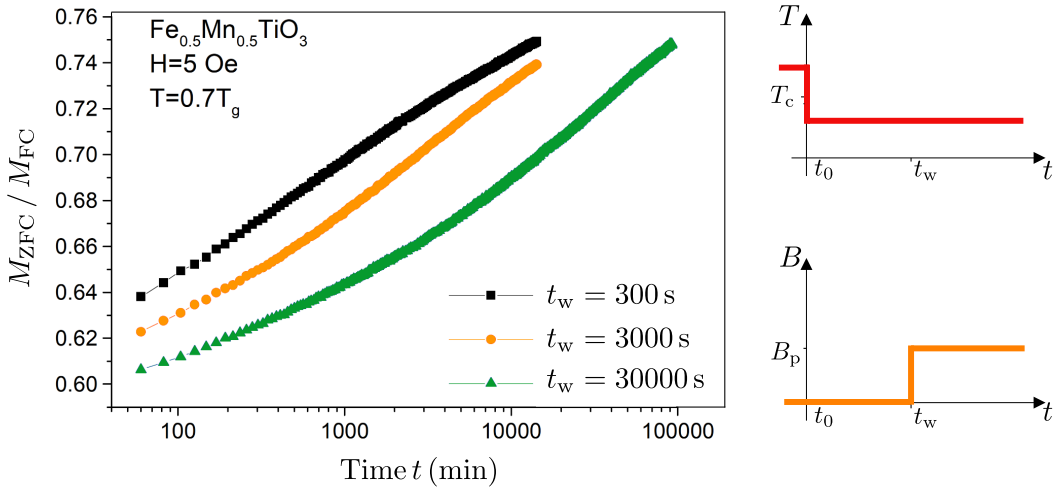

Figure 2.6: Upon measuring the ZFC magnetization in a spin glass, a slow relaxation towards the FC value is observed. The measurement is repeated for different waiting times t_w between cooling the sample at time t_0 and applying the probe field at $t_0 + t_\mathrm{w}$. The time scale of the relaxation process is observed to depends on the waiting time, indicating that the system remembers the time of its birth. The measurement procedure is visualized on the right. Figure adapted from [47]

2.3.4 The Order Parameter and Replica Symmetry Breaking

To complete this introduction into the topic of spin glasses, we want to take a closer look at what happens at the glass transition on a microscopical level. Though it has been a controversial topic over the years, it is nowadays widely accepted that the spin glass transition shows the properties of phase transition in the thermodynamic sense for both Heisenberg and Ising spins. However, there are still competing theories when it comes to the nature of the ground state in the glassy phase.

Within a fully connected model (essentially corresponding to an infintie dimensional model), replica symmetry breaking predicts an infinite amount of ground states and thus in a real spin glass many domains with different order compete with each other. On the other hand, with the droplet model [53, 54], there is a phenomenological description based on scaling theories which predicts simply two spin reversal symmetric ground states. A very nice summary of recent developments and open questions is found in [7].

Throughout this thesis, we are not going to focus on the transition itself, but mostly on the features of the spin glass phase. The low temperature phase is characterized by the Edwards Anderson (EA) order parameter q_EA, named due to the initial paper in which it was proposed [49]. It is based on the experimental observation that spins freeze out in a

certain direction at low temperature, leading to a natural definition of the order parameter as

$$q_{\mathrm{EA}} \equiv \overline{\langle \vec{\sigma}^{(\mathrm{i})}(t_0)\vec{\sigma}^{(\mathrm{i})}(t_1)\rangle} = \frac{1}{N}\sum_{\mathrm{i}=1}^{N} \overline{\langle \vec{\sigma}^{(\mathrm{i})}\rangle^2}, \tag{35}$$

where t_0 and t_1 are fixed points in time that are widely separated. In order for this definition to be meaningful, the order parameter has to be evaluated in the limit of zero external field $B \to 0$, since for a finite global magnetization q is trivially different from zero. As usual, the brackets denote a thermal average whereas the overbar denotes a disorder average.

The Edwards Anderson order parameter is zero in the paramagnetic phase, where the spins are decoupled and each individual expectation value is zero. We can thus define the critical temperature of the spin glass as the temperature T_c where q_{EA} starts increasing, since for temperatures smaller than T_c, the order parameter is non-zero and in the limit of zero temperature even $q = 1$. We note that while the order parameter is increasing, the average macroscopic magnetization in the absence of a magnetic field remains zero in the spin glass phase since the spins freeze in random directions.

Although the order parameter defined above appears to be a very intuitive measure, it is not sufficient for a theoretical description of a spin glass in its totality. The full solution was presented by Parisi in , an effort for which he obtained the noble prize in 2021. It extends on the previously defined order parameter in the following way. Considering the rugged free energy landscape of a spin glass, phase space is partitioned into a large (possibly infinite) number of valleys labeled with the index α. To a good approximation, the thermal average can then be decomposed into the individual valleys

$$\langle \cdots \rangle = \sum_{\alpha} w_\alpha \langle \cdots \rangle_\alpha, \quad w_\alpha \propto \exp(-\beta F_\alpha) \tag{36}$$

where $\langle \cdots \rangle_\alpha$ indicates an ensemble average limited to a single valley and w_α the probability of being located therein. For two given valleys α, γ, we can define the overlap $q_{\alpha\gamma}$ in the following manner

$$q_{\alpha\gamma} = \frac{1}{N}\sum_{i} \langle \vec{\sigma}^{(i)}\rangle_\alpha \langle \vec{\sigma}^{(i)}\rangle_\gamma. \tag{37}$$

As a consequence, the self overlap for a valley $q_{\alpha\alpha}$ is given by the EA order parameter.

The clue of the replica method is now to take two identical copies (replica) of the system and calculate the overlap matrix $q_{\alpha\gamma}$ between the two. In the case that replica symmetry

is not broken, there is only a single value for the overlap, indicating the existence of a single, unambiguous ground state for the system. The more interesting case is however if replica symmetry is broken, which indicates the existence of mutiple or even infinitely many ground states [55].

At this point, much in the same way as for the linear response section before, we could continue the analysis and write a whole section on the topic of replica symmetry breaking. Of course, this is much out of scope for this thesis, more information on the topic can for example be found in the works of Parisi [55], Baity Jesi [56], and Castellani and Cavagna [57].

Finally, we want to conclude this section by linking the order parameter to the magnetic susceptibility in equilibrium

$$\chi_{\mathrm{mag}} = \beta(1 - q_{\mathrm{EA}}) + \beta N^{-1} \sum_{\alpha,\gamma} w_\alpha w_\gamma (M_\alpha - M_\gamma)^2, \tag{38}$$

which is a key result obtained with the use of RSB [55]. The interpretation of this formula is quite natural when remembering the experimental results for the susceptibility in the glass phase.

The first term is what we get if we restrict ourselves to a single valley in the free energy landscape. Since no free energy barriers have to be surpassed, the time scale for this susceptibility is fast and we can experimentallyobserve it when measuring the ZFC magnetization.

The second term originates from the fact that in the presence of a magnetic field, valleys with large magnetization become more likely than those with low magnetization. Accordingly, the system develops towards larger magnetization values. This requires jumping between different valleys separated by free energy barriers, a process to which macroscopically large timescales can be attributed. The final value of the susceptibility can thus only be measured by applying the field already in the ergodic, paramagnetic phase, which is done for FC experiments.

3 Tunable Rydberg Platform for Quantum Simulation

After revisiting fundamental concepts underlying spin glass physics in the previous part of the thesis, this chapter now provides a concise summary of our implementation of a disordered spin model usiung ultracold Rydberg atoms. While a comprehensive description of the experimental setup is for example available here [18], we offer a brief overview of its key components and follow up by a short discussion on how the spin model arises from the Rydberg interactions.

3.1 Experimental State-Preparation and Measurement Procedure

A schematic of the experimental setup can be found in figure 3.1. We utilize a gas of $^{87}\mathrm{Rb}$ atoms confined in an optical dipole trap in their electronic ground state $|\mathrm{g}\rangle = \left|5S_{1/2}, F = 2, m_\mathrm{F} = 2\right\rangle$. The atoms are cooled to a temperature of approximately $20\,\mu\mathrm{K}$, effectively freezing their motional degrees of freedom during the $10\,\mu\mathrm{s}$ duration of the experiment. Rydberg excitation of a large number (~ 1000) of atoms then involves a two-photon transition via the intermediate state $|\mathrm{e}\rangle = \left|5P_{3/2}, F = 3, m_\mathrm{F} = 3\right\rangle$ to the $\left|nS_{1/2}, m_\mathrm{j} = 1/2\right\rangle$ Rydberg state. This excitation is operated at $780\,\mathrm{nm}$ and $480\,\mathrm{nm}$ and involves a detuning $\Delta\nu = 2\pi{\cdot}100\,\mathrm{MHz}$ with respect to the intermediate state such that we can adiabatically eliminate it and effectively consider a two level system for the excitation. During the excitation process, there is an additional effect known as Rydberg blockade that prevents multiple excitations within a blockade radius of

$$r_\mathrm{bl} = \sqrt[6]{\frac{C_6}{\hbar\omega}} \tag{39}$$

depending on the linewidth ω of the excitation laser and the Van-der-Waals interaction coefficient C_6 of the corresponding Rydberg state. We can us this effect to our advantage, since it allow us to tune the disorder strength of the system. In a setting were many atoms are excited from a small volume, the blockade radius will introduce strong correlations between the locations of individual Rydberg atoms and thereby reduce the variance of the distribution of couplings. On the contrary, if the mean inter-particle distance is much larger than the blockade radius, there will be no visible effect and the Rydberg distribution is entirely random.

With the help of a microwave, the $\left|nS_{1/2}\right\rangle$ Rydberg state is then coupled to a second Rydberg state, the specific choice of which determines the dynamics and allows to choose

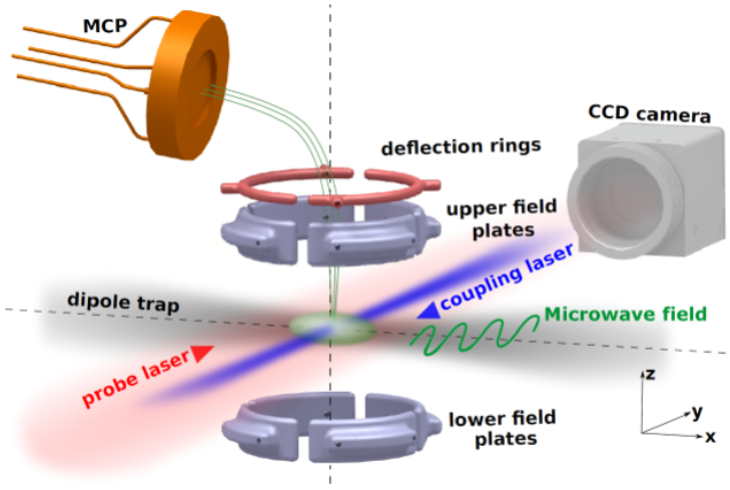

Figure 3.1: Schematic overview of the experimental setup. ^{87}Rb atoms are caught in a dipole trap and subsequently excited to Rydberg states. A microwave is used to couple to a second Rydberg state, the choice of which determines the Hamiltonian of the system. After the experiment has taken place, one of the two Rydberg states is depopulated and the remaining one is detected on the microchannel plate (MCP) after ionization. Additionaly, a CCD camera is installed for absorption imaging of the atom cloud. Figure taken from [58]

between different possible spin models that can be simulated as will be discussed later on. Finally, once the dynamics have taken place, we measure the global z-magnetization per spin via the relative populations of the participating Rydberg states

$$m_z = \frac{N_\uparrow - N_\downarrow}{2(N_\uparrow + N_\downarrow)} \tag{40}$$

By including an additional global readout pulse to rotate the magnetization on the Bloch sphere, it is also possible to measure magnetization in both the x- and y-direction. The relative populations of the Rydberg states are inferred through detection of ionized Rydberg atoms on a microchannel plate. The ionization takes place after optically depopulating on of the two states, to get a state-resolved measurement. This detection scheme, visualized in figure 3.2, requires an additional measurement to calibrate the total number of Rydberg states in the system.

The main limiting factor in the experiment are the lifetimes of the Rydberg states, since they determine for how long we can consider the system to be isolated. They have been calculated previously, an overview of the lifetimes for ^{87}Rb can be found here [59]. For

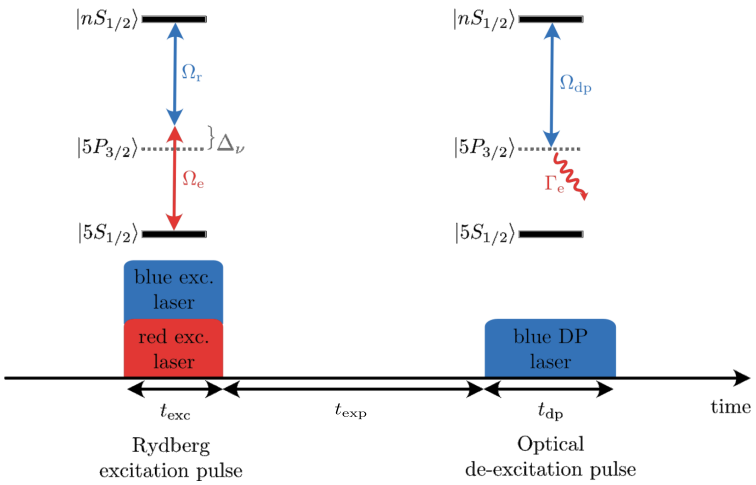

Figure 3.2: Visualization of the two photon excitation process (left) and the optical deexcitation of the Rydberg state after the dynamics have taken place. The necessary frequency shift is created with the help of an acousto-optic modulator (AOM) and we use the rapid natural decay of the intermediate state for the depopulation. Adapted from [18].

our discussion, it is enough to know that the lifetime of the Rydberg $\left|61S_{1/2}\right\rangle$ state is roughly $100\,\mu s$ and the lifetimes of the $\left|61P_{3/2}\right\rangle$ is slightly larger at approximately $120\,\mu s$. These lifetimes are quite substantial and include considerations for losses due to black-body radiation at $300\,K$. By limiting ourselves to experimental times smaller than $10\,\mu s$, we can well approximate the system as isolated.

3.2 Mapping to Disordered Spin System

As highlighted before, the choice of the second Rydberg state greatly affects the Hamiltonian of the system. Different possibilities for mapping the system to Heisenberg like spin Hamiltonians are for example explained by Franz et al. [60], in a paper where they discuss the implications those differences have for spin relaxation. In the course of this thesis however, we will focus on a single Hamiltonian that is obtained when the Rydberg state are chosen to be $|\downarrow\rangle \equiv |61S_{1/2}\rangle$ and $|\uparrow\rangle \equiv |61P_{3/2}\rangle$ such that the transition between the two states is dipole allowed. When considering the interaction between the two states, it is therefore dominated by the dipolar term of a multipole expansion

$$\hat{H}_{\mathrm{DDI}} = \frac{\hat{\mathbf{d}}_i \cdot \hat{\mathbf{d}}_j - 3(\hat{\mathbf{d}}_i \cdot \mathbf{e}_{r_{ij}})(\hat{\mathbf{d}}_j \cdot \mathbf{e}_{r_{ij}})}{r_{\mathrm{ij}}^3}, \tag{41}$$

which expressed in spherical coordinates can be well approximated by

$$\hat{H}_{\mathrm{DDI}} = \frac{1 - 3\cos^2(\theta_{\mathrm{ij}})}{r_{\mathrm{ij}}^3} \left(\hat{d}_{\mathrm{i},0}\hat{d}_{\mathrm{j},0} + \frac{\hat{d}_{\mathrm{i},+}\hat{d}_{\mathrm{j},-} + \hat{d}_{\mathrm{i},-}\hat{d}_{\mathrm{j},+}}{2} \right). \tag{42}$$

For the above formula, we restrict ourselves to the terms in the interaction that couple a $M_{\mathrm{j}} \to M'_{\mathrm{j}} = M_{\mathrm{j}}$ transition, $M_{\mathrm{j}} = m_{\mathrm{j},1} + m_{\mathrm{j},2}$ being the total magnetic quantum number, since other terms are strongly suppressed due to energy conservation. r_{ij} indicates the distance between two atoms and the relevant angle θ_{ij} is the one formed by z-axis and the connection vector of the two particles. Due to the spherical representation of the dipole operator, this formula has the advantage of immediately showing which states are coupled.

The exact mapping to the spin system from here on will not be calculated explicitly, however it is straight forward to do so through a direct evaluation of the the matrix elements of the derived interaction Hamiltonian $\hat{H}_{\mathrm{DDI}}$ with the proper Rydberg states. We obtain a spin-$1/2$ Heisenberg XY Hamiltonian that is going to be the basis for discussion in the rest of this work. In the additional presence of an external field along the x-direction it reads

$$\hat{H}_{\mathrm{XY}} = -\sum_{\mathrm{i,j}} J_{\mathrm{ij}}(\sigma_{\mathrm{x}}^{(i)}\sigma_{\mathrm{x}}^{(j)} + \sigma_{\mathrm{y}}^{(i)}\sigma_{\mathrm{y}}^{(j)}) - \Omega_{\mathrm{ext}} \sum_{\mathrm{i}} \sigma_{\mathrm{x}}^{(i)}. \tag{43}$$

As usual, we work in units where $\hbar = k_{\mathrm{B}} = 1$ and the coupling constants are given in units of frequency. According to the above derivation, they follow a dipolar interaction

$$J_{\mathrm{ij}} = \frac{\mathrm{C}_3(1 - 3\cos^2\theta_{\mathrm{ij}})}{r_{\mathrm{ij}}^3}. \tag{44}$$

While the coupling strength in the experiment is determined through the C_3 coefficient of the participating Rydberg states, we have the freedom to choose an arbitrary coupling strength for the numerical simulations.

Another important measure characterizing the system is the strenght of the nearest neighbour couplings, which govern the early dynamics and therefore set the smallest intrinsic timescale of the system. Hence, we are going to use the median of the nearest neighbour distribution J_{med} as the relevant energy scale of the system and rescale external fields and timescales accordingly.

Unless further specified, the numeric results are discussed in this thesis are obtained from a simulation of 12 spins using the method of exact diagonalization. Positions are drawn

from a uniform distribution over a sphere where additionally a cutoff distance is introduced below which no two spins are sampled. This is physically motivated by the Rydberg blockade and allows to tune the disorder of the system. Based on this geometry, we can calculate the average and give an estimate for the variance of the strong couplings

$$\langle J \rangle \equiv \int d^3r \, p(r) J(r,\theta) = 0, \tag{45}$$

$$\langle J^2 \rangle \equiv \int d^3r \, p(r) J^2(r,\theta) \approx \frac{4}{5} \left(\frac{r_{\mathrm{med}}}{r_{\mathrm{bl}}} \right)^6 J^2_{\mathrm{med}}, \tag{46}$$

which holds only in the strongly blockaded regime, the derivation can be found in appendix A. We see that with decreasing density, corresponding to an increase of r_{med}, the influence of the blockade becomes less important and the variance increases. On top of that, since the average of the interactions is exactly zero due to the dipolar nature of the interaction, the experiment provides a promising setup to study for a possible spin glass transition.

4 History Dependent Magnetization in a Finite Size System

As outlined in the previous section, the Rydberg platform for quantum simulation is versatile and can be used to study different kinds of spin Hamiltonians in a setting that can be well approximated as isolated. Since we are interested in the question of whether a spin glass transition is possible for an isolated quantum system, we are going to focus on the study of the XY model that has been discussed in detail in the preceding section. From all previously realized models, it is the only one with both ferro and antiferromagnetic couplings that arise from the anisotropic dipole-dipole interactions between the Rydberg atoms. In view of the innate disorder present in an atomic cloud, it thereby features both frustration and disorder as necessary components and is a fitting candidate system to investigate the presence of a glassy phase.

Previous work from the group has already started this study and two very interesting results were found. In a first paper [15], the system was shown to demagnetize under unitary evolution. By initializing a fully polarized state and letting the system evolve in time, it has been measured that this relaxation follows the same stretched exponential law seen in conventional spin glasses. While the initial paper dealt with a Heisenberg XXZ Hamiltonian, it has by now also been measured in the XY model [60].

Such a relaxation curve for the model with dipolar interactions is depicted in 4.0.1a, where we see that relaxation takes place on timescales spanning multiple orders of magnitude. By fitting a stretched exponential $e^{-(t/\tau)^\beta}$ to the relaxation, the stretching coefficient is obtained to be $\beta = 0.79$.

The second observation that has already been seen is a non-analycity in the magnetization which indicates ergodicity breaking behaviour [16], at least on experimentally observable timescales. The effect is visible in a spin locking experiment similar to what is common practice in nuclear magnetic resonance (NMR) technologies [61]. After initializing the fully polarized state, an external field is applied parallel to the spins to prevent relaxation. As can be seen in figure 4.0.1b, the corresponding steady state value of the magnetization is then dependent on the strength of the locking field. In the case of strong disorder, the magnetization profile shows a cusp at zero external field, a feature that can be attributed to ergodicity breaking in the system.

Thus, the XY model with dipolar couplings has already been shown to display slow relaxation times and ergodicity breaking behaviour. The question is now whether this can be

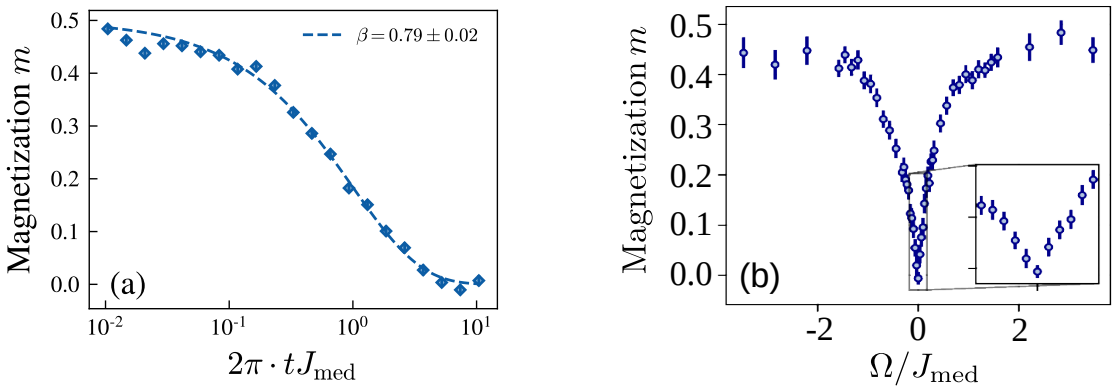

Figure 4.0.1: Previous studies of a disordered spin system with dipolar interactions point towards the existence of a glassy phase. (a) The relaxation of a fully polarized state in the XY-model follows a stretched exponential law, which is also observed in typical spin glass systems (b) Steady state magnetization is measured as a function of an external locking field applied to the fully polarized state. The curve features a cusp at zero field, which can be related to a loss of ergodicity on experimental timescales. Figure adapted from [16]

related to the same principles underlying conventional glasses or if it has to be explained using a different framework.

To address this question, we introduce a new method of state-preparation for the Rydberg system that allows us to prepare states at different energies. We then use a combination of numerical simulations of finite size systems and experimental results obtained from the Rydberg simulator to study the possible existence of a glassy phase.

In this section, we focus on the numerical studies, which provide a large degree of control over the system and thus serve as a good tool to obtain a first intuition for how the system behaves.

4.1 State-Preparation through External Field Ramp

A key tool for the subsequent discussion is going to be the determination of the magnetic susceptibility at different internal energies of the system. While it is easy to initialize these states in a simulation, there are two large problems for doing so in an experiment. First, we are limited to global spin control, which makes it difficult to experimentally initialize states with spin configurations that differ locally. Second, the ground state of the XY model is non-analytic and varies between disorder realizations, which means that we do not know which spin configuration we have to initialize in the first place in order to reach low energies.

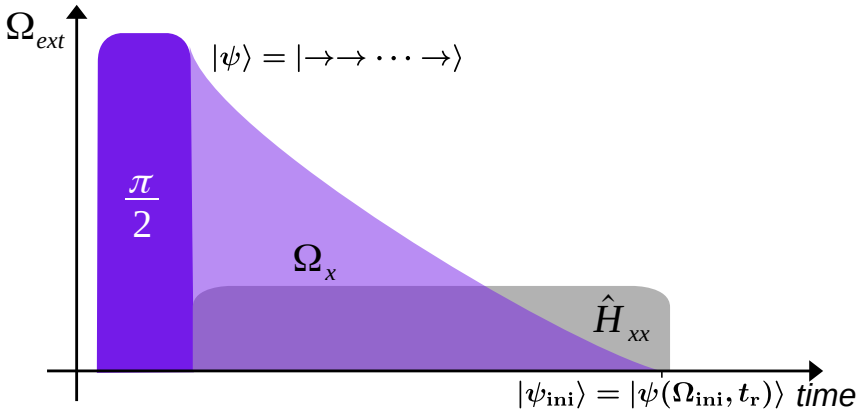

Figure 4.1.1: Sketch of the state-preparation using a ramp of the external field. After performing a global $\pi/2$-pulse, the system occupies the fully polarized state, which is the ground state configuration in the presence of a strong external field Ω_{x}. The field strength is then continuously reduced, which transforms the state to a low energy state of the XY model. The exact state depends on the initial amplitude Ω_{ini} and ramp time t_{r}.

To bypass these problems, in the experiment we want to use state-preparation based on a ramp of the external field from very strong amplitudes to zero. Hence, to keep comparability between the numerics and the experiment, we are also going to use this procedure for the numerical simulations instead of directly populating low energy states. This has the additional advantage of serving as a test for how well the state initialization is expected to work later on.

There are two fundamental ideas underlying the usage of the field ramp as sketched in figure 4.1.1. First, we note that if the external field dominates the spin-spin interactions ($\Omega_{\mathrm{ext}}/J_{\mathrm{med}} >> 1$), the system can be treated as paramagnetic. Hence, the ground state is well known to be the fully polarized state $|\psi_{\mathrm{g}}\rangle = |\rightarrow\rightarrow\cdots\rightarrow\rangle$ which is easy to prepare even with the restriction in global control.

Second, take advantage of the adiabatic theorem in quantum mechanics [62], which for a generic quantum mechanical system states that if the Hamiltonian is changed slowly, the system will adapt its configuration and end up in the corresponding eigenstates of the new system. This is opposed to the notion of a diabatic change, where the state of the system remains identical and is projected onto the new eigenstates.

Combining both concepts, the state-preparation is as follows. We start by preparing the system in the paramagnetic ground state under the influence of a very strong external field. We then proceed to slowly ramp down the external field, thereby continuously changing the configuration of the system. By varying the speed of the ramp, we extrapolate be-

tween the limits of a very slow, adiabatic passage and a very fast, diabatic process that corresponds to quenching the external field.

While, as will be demonstrated below, the above scenario succeeds at initializing energies anywhere between the ground state energy and the middle of the spectrum (all states are equally populated after the quench), it also has some flaws that need to be addressed. To start out with, the timescales needed for a full adiabatic passage are long, usually determined by the inverse energy gap of the spectrum. If the gap approaches zero, as is the case for our system in the limit of large particle number N, the theorem is still applicable but there is no preemptive notion about the timescales needed for an adiabatic passage. This is problematic, since experimental times are limited by decoherence effects. Hence, we will not be able to probe arbitrarily low energies in the experiment.

This ties into the next issue, which is also directly related to the experimental realization of such a ramp. The way it is currently set up, it is not possible to measure the energy of the system after the ramp. Unfortunately, there is also no way to calculate the energy, since the exact energy gap of the system at large particle numbers is unknown and even worse, it changes with each disorder realization. The actual energy in the system after the ramp is thus unknown in an experimental realization and we have no way of knowing how close to the ground state we can get. Having said that, it is still clear that energy will be monotonically decreasing as the duration of the ramp increases, which means that the dependence on the ramp duration will reflect the dependence on the energy.

We continue now with an analysis of how well the state-preparation is expected to work. There are two main tuning parameters that govern the energy at the end of the ramp. The maximum field strength at the start of the ramp, which ascertains how well the ground state can be approximated by the fully polarized state, and the duration of the ramp, which determines the strength of the diabatic effects that inevitably occur during the ramp. In principle, one could also think that the shape of the ramp plays an important role, however we will see that the effects of changing it are almost negligible.

Figure 4.1.2(a) shows the quantum mechanical overlap $|\langle\psi_{\mathrm{p}}|\psi_{\mathrm{g}}\rangle|^2$ between the fully polarized state $|\psi_{\mathrm{p}}\rangle = |{\rightarrow}{\rightarrow}\cdots{\rightarrow}\rangle$ and the exact ground state $|\psi_{\mathrm{g}}\rangle$ of the XY model as a function of the external field strength Ω_{ext}. It approaches unity if the field strength is roughly five times as strong as the interaction strength, thereby justifying the fully polarized state as a good approximation of the ground state. Going to weaker fields, until an amplitude of approximately twice the interaction strength, 90% ground state character is retained, which then falls off rapidly for even lower fields.

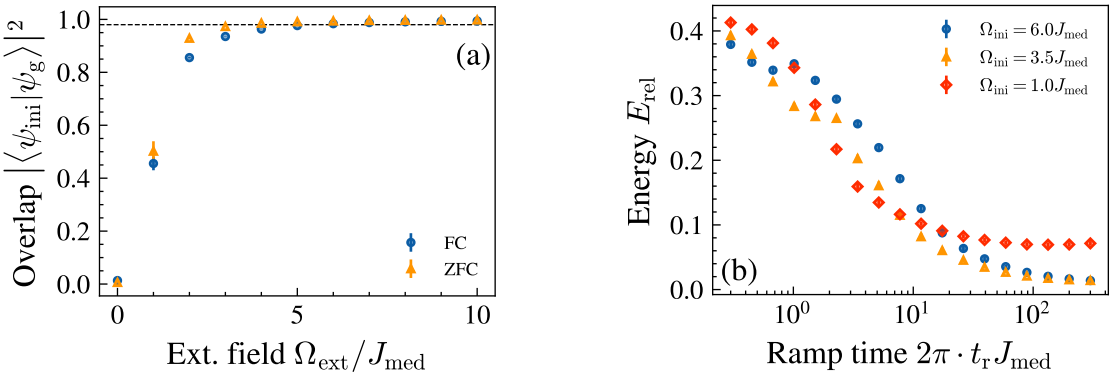

Figure 4.1.2: (a) Overlap between the fully polarized state and the exact ground state of the XY Hamiltonian with strong external field. The dashed line is a reference for 98% fidelity, at large fields the approximation of the ground state as fully polarized state is well justified. The difference between the FC and ZFC curves is explained in the text below. (b) Relative energy $E_{\rm rel}$ after the ramp with respect to the ground state and normalized to the bandwidth of the spectrum. Energy is given as a function of the ramp time $t_{\rm r}$. Three different initial amplitudes are shown, if the initial ground state overlap is large enough, very low energies can be reached. Numerical errorbars are smaller than the marker size.

The distinction between FC and ZFC is done in anticipation of the latter part of the thesis. While the ZFC overlap is obtained in exactly the manner as described above, for the FC curve an additional, small perturbation is applied in y-direction. As can be seen in the plot, this does not severely influence the ground state overlap and thus should not be a problem for the state-preparation in presence of a small field, the reason of which will become clear later on. We conclude that in both scenarios, the fully polarized state is a good approximation for the ground state of the system.

Thus, having confirmed that the basic assumption for an adiabatic passage is fulfilled, we can now study the timescales needed to stay at low energy throughout the field ramp. In the following, we assume a ramp that is shaped according to $\Omega_{\rm ext}(t) = \Omega_{\rm ini}\left(1 - {}^{t}/_{t_{\rm r}}\right)^{\alpha}$ where α determines the curvature of the ramp and for our discussion will be limited to $\alpha = 1$ and $\alpha = 2$. The duration over which the ramp is performed is given by the ramp time $t_{\rm r}$ and the initial field strength by $\Omega_{\rm ini}$. This analytic form is motivated by the fact that as long as α is larger than one, not only the field itself but also its first derivative goes to zero at the end of the ramp.

Figure 4.1.2b shows the energy per particle of the system at the end of a quadratic ramp as a function of the ramp time $t_{\rm r}$ for three different initial amplitudes. As expected, if the initial field is too weak, we do not reach low energies even in the limit of very slow

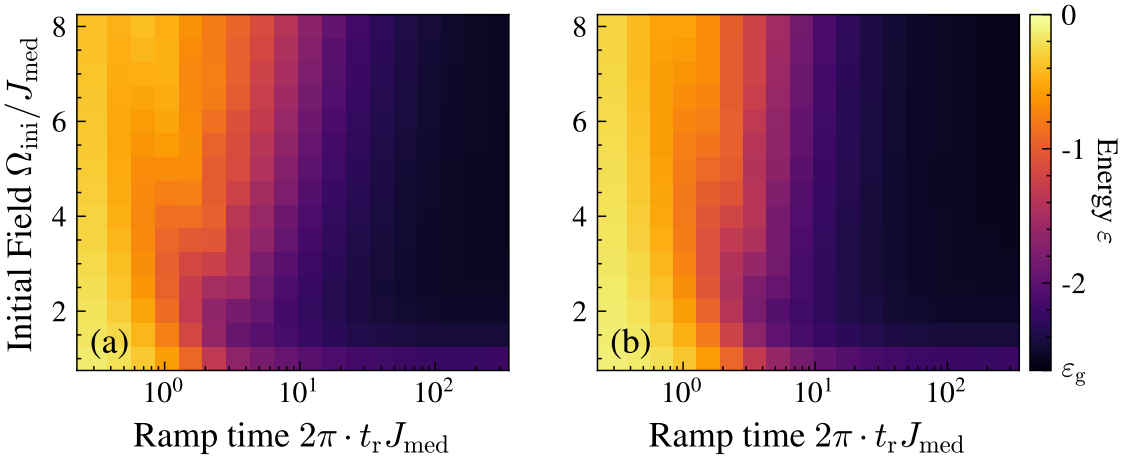

Figure 4.1.3: Energy after state initialization via the ramp as a function of ramp time and initial amplitude. (a) Results for the linear ramp ($\alpha = 1$). The lowest energy that is reached seems to be largely independent from the initial field amplitude, as long as it is above two times the interaction strength. (b) The results for a quadratic ramp ($\alpha = 2$) are very similar to the linear case, indicating that the exact shape has only a minor influence on the diabatic component of the ramp.

ramps. However, if the initial overlap is large enough, we are able to perform ramps that yield almost ground state energy ε_{g}, indicating that the wave function at the end of the ramp stays well localized around the ground state and is not spread out over a large part of the energy spectrum.

To see whether the exact shape of the ramp plays a role, we simulate the energy over a wide range of parameters for linear and quadratic shape of the ramp. In figure 4.1.3, the final energy is depicted as function of both the initial field amplitude and the ramp time, where (a) shows the results for a linear and (b) a quadratic ramp. Both follow the same trends, where the energy decreases with increasing ramp time. Above a critical amplitude, both are also largely independent from the external field amplitude and do not show a clearly preferred set of parameters in the range that was studied.

The timescale for a very slow ramp is at the order of 100 interaction cycles, which is a regime that is expected to be accessible in the experiment without decoherence effects being too strong. However the typical timescale for an adiabatic crossing is inversely proportional to the energy gap, which in the limit of many particles goes to zero.

To see how strong this affects our current system, we perform a finite size scaling for three different ramps. The results are shown in figure 4.1.4, where we plot the relative energy after the ramp with respect to the ground state and normalized to the bandwidth. Interestingly, we find the opposite effect of what was expected and the ramping seems to

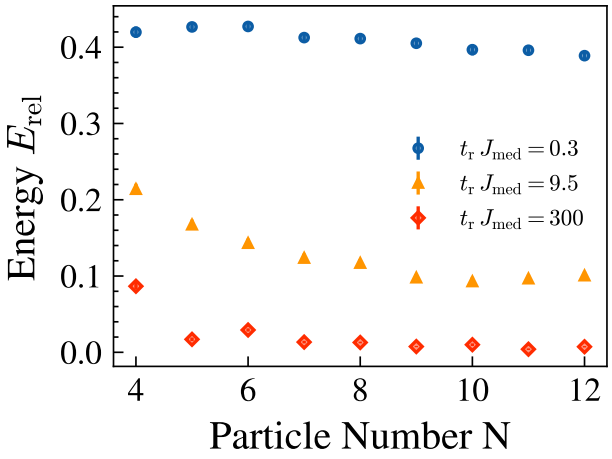

Figure 4.1.4: Finite size scaling for the final energy after the ramp with respect to the ground state and normalized to the bandwidth. All three ramp times seem to be either saturated or even declining as a function of the particle number. Thus, we are confident that the ramping should work in the experiment.

retain lower energies as the system size increases. Since the curves are either saturated or decreasing with particle size, we expect the ramping to be successful also in the limit of large system size.

4.2 Observation of a Linear Response

Having demonstrated the possibility of initializing energetically different states, we now want to explore in what way the energy affects the response of the system to an external probe field Ω_{p}.

To this end, we perform the state-preparation by ramping down over a fixed time t_{r} and afterwards we apply a field of varying strength Ω_{p} to the system (Figure 4.2.1a). The physical picture of what is happening with this kind of response measurement is as follows. Via the ramp, the system adapts a low energy state of $\hat{H_{\mathrm{XY}}}$, which is then probed with an external field. We recall that this bears a close resemblance to the zero field cooled measurements introduced in section 2.3 where we introduced conventional spin glasses. In this kind of measurement, the probe is cooled without the presence of an external field, thereby lowering its energy, and afterwards a probe field is applied. In view of this analogy, we are going to label the state-preparation as described above as ZFC for the rest of the thesis.

Naturally, this also begs the question if we can find an analogy for the field cooled mea-

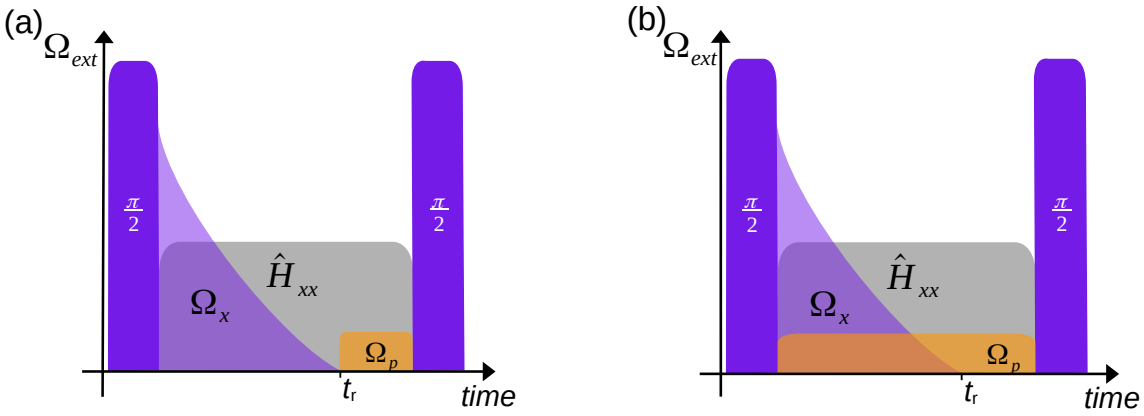

Figure 4.2.1: When probing the response of the system, we have the freedom to choose between two different procedures. (a) We first ramp all the way to zero and then reapply a small probe field followed by a readout pulse. This sequence bears a close analogy to the zero field cooling in spin glasses and is referred to as "ZFC" in the following. (b) We apply the probe field already during the ramp, thus never reaching zero external field. Again, in analogy to conventional spin glasses we term this sequence "FC".

surement as well. Instead of ramping all the way to zero, we can directly ramp to the final value of the external field as visualized in figure 4.2.1b. This implies that the system adapts a low energy state of the combined Hamiltonian $\hat{H}_{\mathrm{XY}} + \hat{H}_{\mathrm{ext}}$, which corresponds with the picture of cooling in the presence of an external field. Hence, the term FC will be used throughout this thesis for ramping directly to the probe field and never reaching zero magnetic field.

With these two different procedures in mind, we now simulate the response for a fixed ramp time of $t_{\mathrm{r}} J_{\mathrm{med}} = {}^{60}/_{2\pi}$ and varying probe field strength, the result of which can be seen in figure 4.2.2. We see that both sequences yield a non-zero magnetization as a response to the probe field.

We first focus on the time development of the ZFC measurement in figure 4.2.2a. We see that at the start of the ramp, the magnetization is spin locked by the strong external field to $m = 0.5$ and as the external field gets weaker, it slowly relaxes towards zero. Once the probe field is applied, there is a rapid build up of magnetization towards a steady state value.

On the other hand, the FC magnetization never relaxes to zero and shows a smooth development towards the equilibrium state, which is reached for a magnetization that is about $\Delta m = 0.1$ larger than the ZFC value.

The exact value of the equilibrium magnetization is found to depend on the external field

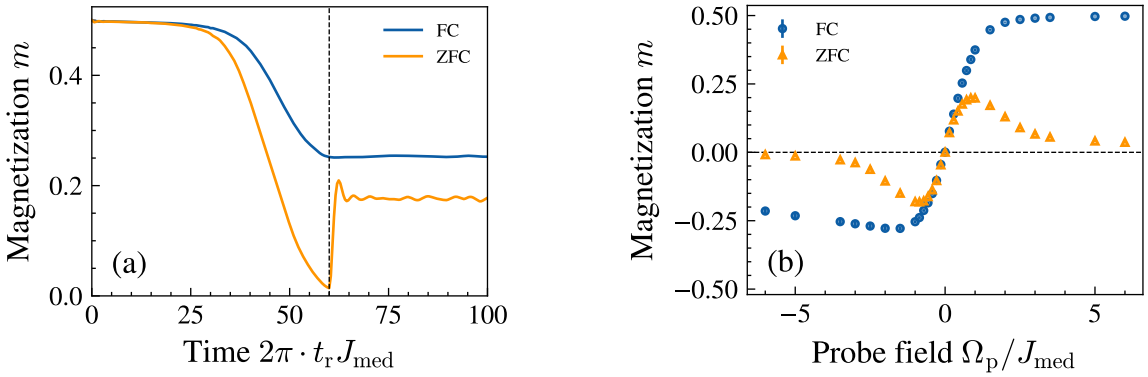

Figure 4.2.2: (a) Time evolution of the magnetization under FC and ZFC procedure at fixed ramp time and probe field amplitude. Dashed line indicates the end of the ramp. (b) Steady state magnetization as a function of the probe field strength. We find a linear response regime for both possible sequences. However, the response is not symmetric around the origin, which would be expected considering the symmetry of the Hamiltonian.

and shown in figure 4.2.2b for different amplitudes. Once again, we focus first on the ZFC measurement, where we see that there is an approximately linear regime around zero that extends to a magnitude of roughly $0.5 J_{\mathrm{med}}$. For external fields larger than that, the magnetization curve $M(\Omega_p)$ reaches a maximum at amplitudes slightly below J_{med}. Probing with even larger field strengths reduces the magnetization again, which seems unintuitive at first glance.

However, the effect can be understood in a relatively simple picture by considering the isolated nature of the system. As the external field strength increases, the eigenstates of the system change accordingly. For large fields, the projection of the low energy state of the XY Hamiltonian onto the new eigenbasis in a strong field spreads out more and more. In the limit of very large field strength, the new eigenbasis is given by the product states in x-direction, and the effect is the inverse of what happens when the fully polarized state is initialized and relaxes. Essentially, the system increases its energy through the quench of the probe field and since it has no way to dissipate it, it cannot develop towards states with large magnetization that would be energetically favored.

At this point, we also want to stress that a relaxation towards a magnetized state in an external field is a clear many-body effect and cannot be understood in the picture of individual spins. For a single spin, applying an external field only leads to a precession and does not change the magnitude of its expectation value along the direction of the field. It follows that the relaxation towards states with large magnetization can only be understood in the framework of statistical mechanics.

For the FC curve, we find a qualitatively different picture. The gradient of the linear regime is slightly larger than for the ZFC measurement, and at very large field strengths, we retain the full magnetization. This is also quite easy to understand, since for strong probe field values in the FC sequence, effectively there is no ramp at all and we perform a spin locking experiment that has been extensively studied in [16].
Both procedures also show the build up of negative magnetization when applying a field in negative direction, in contrast to the spin lock measurements that have been performed until now. However, we find a strong asymmetry around zero for the FC measurement and a very slight asymmetry for the ZFC curve. Considering the symmetry of the Hamiltonian, which is U(1) symmetric in the xy-plane, this cannot be an effect of applying the probe field and has to be an unwanted side effect of the state-preparation.
We can resolve this problem by taking a second look at the time development of the magnetization (figure 4.2.2). As we see, for the FC procedure, the magnetization stays far from zero at all times and even for the ZFC measurement, the system has not fully relaxed before the probe field is applied.
For a non-zero magnetization, we know from previous studies that due to the spin-locking effect, a finite magnetization remains at all times. Hence, we would also expect a finite contribution of this effect to the response when applying a probe field to the system if the magnetization is not zero at the start of the response.
To further quantify the influence of this effect, we compare the positive branch of the FC procedure to a simple spin locking experiment in figure 4.2.3a. It shows that for the same amplitude, the FC procedure retains larger magnetization values than the spin locking. This finding by itself is quite interesting, since in both cases we start with the fully polarized state and end with the same external field. Yet, we see different magnetization values for the system.
At this point, it is tempting to declare this an observation of memory effects and conclude that the system does not coincide with a thermal state. This statement would, however, be premature. While it is true that the isolated system shows different behaviour for an external field ramp compared to a quench of the same magnitude, by performing the ramp we also drastically decrease the internal energy of the system. Plotting the energy instead of the magnetization (figure 4.2.3b), we see that there is a large difference in the final state that we obtain depending on whether we ramp or quench the system. One would thus not expect the same behaviour in the first place, even for a perfectly thermal system with no sort of memory effect.

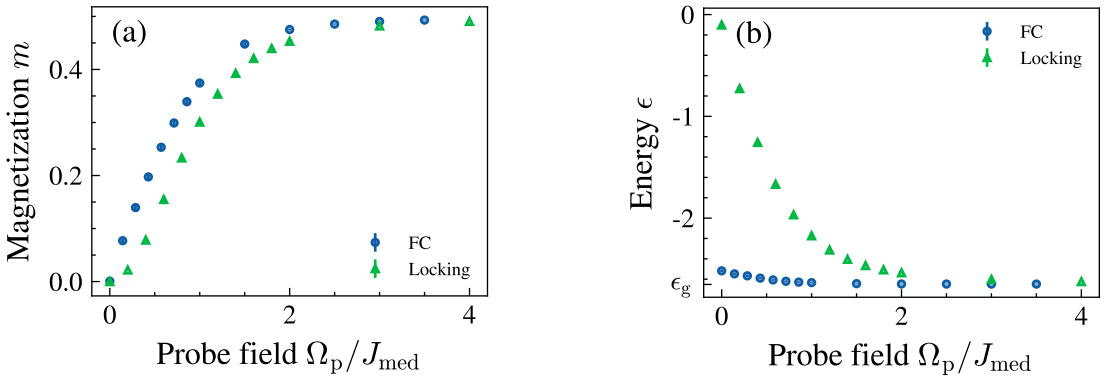

Figure 4.2.3: The asymmetry of the response in x-direction can be explained due to additional effect of spin locking (a) Magnetization after spin locking and FC ramp for different external field strengths. (b) The difference in the corresponding energy explains the discrepancy in magnetization at same field strength.

Having identified the spin locking effect as the reason for the asymmetry of the response, the next question is whether we can get rid of this defect within the state-preparation. A possible way for the ZFC procedure would be to simply wait at zero field until all remanent magnetization has decayed, and only then apply the probe field. This method successfully gets rid of the asymmetry, however it still has a few flaws that make it unpractical.

First of all, the decay of the magnetization is sub-exponential, so it is difficult to define a timescale for which the magnetization is fully decayed and one would have to wait for long times. Second, there might be many-body dynamics such as the aging effect that take place during this additional waiting time. Since this is going to be one of the main focus points in the later part of the thesis, it would be disadvantageous not to have a reference where we can exclude these kind of effects. The last and strongest argument against the waiting time is that there is no analogue for the FC state-preparation, since the field never reaches zero in the first place. Thus, comparability between both methods would severely suffer from a waiting time at zero field.

Fortunately, there is a second, more elegant way of removing the spin locking effect, that is by exploiting the symmetry of the Hamiltonian. Due to the invariance under rotations in the xy-plane, we can simply apply the probe field in the y-direction perpendicular to the initial magnetization. Since there is no y-magnetization to begin with, there is also no spin locking that can take place. Any remanent x-magnetization will simply precess in the xz-plane and thus does not contribute to a response that is measured in y. This is also ap-

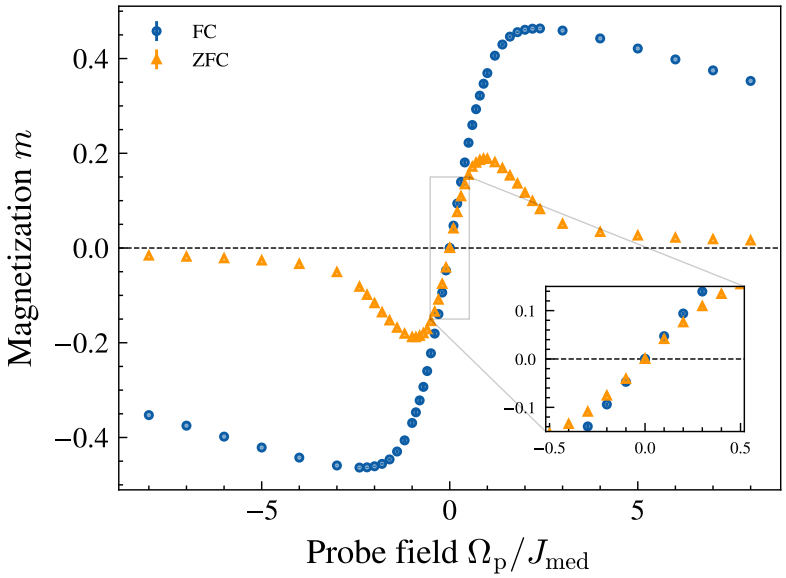

Figure 4.2.4: By using the symmetry of the XY Hamiltonian and applying the probe field along the y-direction we get rid of the asymmetry around the origin. Highlighted in the inset, we find that the regime of linear response is up to an probe field amplitude of $\Omega_\mathrm{p} = 0.5 J_\mathrm{med}$

plicable to the FC scenario, since we can perform the ramp in the x-direction while a small field in y is already applied. This simply corresponds to applying an external field with a time dependent phase $\varphi = \tan(\Omega_\mathrm{y}/\Omega_\mathrm{x}(t))$ and decreasing amplitude $\Omega = \sqrt{\Omega_\mathrm{x}^2(t) + \Omega_\mathrm{y}^2}$. With this new idea we simulate again the response for the two different procedures. This time, the results shown in figure 4.2.4 are perfectly symmetric for both positive and negative field values. The overall trends of the ZFC curve did not change, however we find that the FC values also start declining for large field strengths, albeit much slower than for the ZFC case. This is due to the fact that at some point the small perturbation field in y-direction applied throughout the ramp reaches the same order of magnitude as the initial field strength of the ramp and is thus no longer small. Hence, the initial state which is fully polarized in x-condition no longer fulfils the necessary condition of being the ground state of the system, which would be given by a fully polarized state in the direction of the resulting external field vector.

Both curves also show a linear regime for weak fields, where the slope is slightly larger in the FC case, which can be seen in the inset of the plot. This regime of linear response is where a lot of the signatures for a spin glass can be found, hence we are going to examine it more closely in the ensuing discussion where we investigate the dependence of the response on the ramp duration.

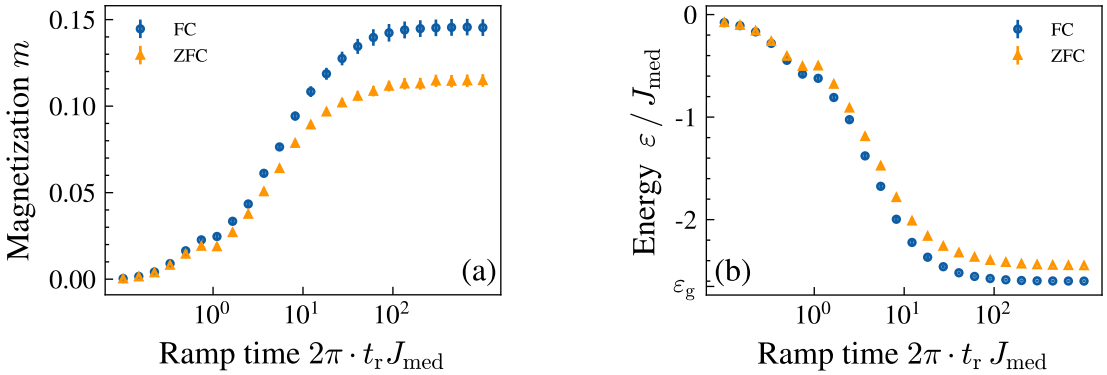

Figure 4.3.1: We simulate the dependence of the linear response on the ramp time. (a) The steady state magnetization shows a monotonous increase towards slower ramp times. FC and ZFC split above critical time, and the difference continues to increase towards slower ramps. Both curves saturate around the same time, however at different magnetization values. (b) This behaviour is mimicked in the energy, the splitting here could be a possible explanation for the difference in the magnetization.

4.3 The Significance of the Ramp Duration for the Response

From a statistical mechanics point of view, the energy of the isolated system is the natural thermodynamic variable and thus the control parameter of the system akin to the temperature in the case of a system coupled to a heat bath. Therefore, knowing that the duration of the ramp determines the energy, we expect it to have a strong impact on the response. Taking care that we stay in the linear regime with a probe field amplitude of $\Omega_p = 0.3 J_{med}$, we now evaluate the influence a change in the ramp speed (trends are reversed when talking about ramp speed instead of ramp duration!) has on the response. The simulation is plotted in figure 4.3.1a, once again repeated for both experimental sequences. There is a small regime for very fast ramps, where FC and ZFC yield an identical response that increases with the ramp time. For ramps that take around ten interaction cycles, the two curves start diverging and the FC curve grows increasingly larger than the ZFC curve. Finally, both ramps saturate for ramp times of roughly 1000 interaction cycles.
Interestingly, this behaviour is mimicked in the energy per spin at the end of the ramp (figure 4.3.1b), depicted in the usual units of the nearest neighbour interaction strength J_{med}. While for very fast ramps, both state-preparation techniques show a similar energy, once the ramp speed decreases, the ZFC simulation shows larger energies. This effect can be traced back to the influence of the small quench in the Hamiltonian when applying the probe field. As previously discussed, this causes the state to slightly spread out in the

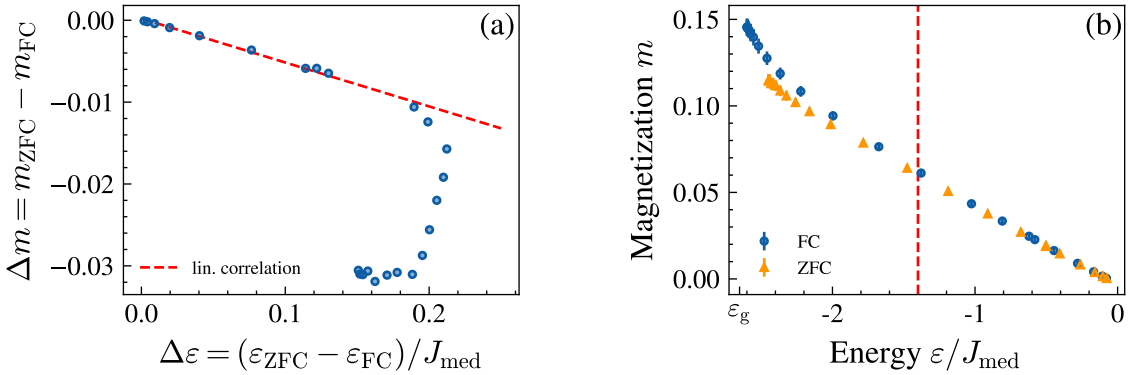

Figure 4.3.2: We further investigate whether the energy splitting explains the splitting in the magnetization. (a) For the faster ramps, a linear correlation between $\Delta\varepsilon$ and Δm is observed, however this breaks down for the slower ramps. (b) Magnetization is plotted as a function of the energy. Indeed, we find a linear regime at large energies which at some point starts splitting slightly. The dashed red line indicates the location where the linear correlation from (a) breaks down.

energy spectrum, thereby increasing its energy by a small amount.

It is now an interesting question to ask whether the difference in the magnetization $\Delta m = m_{\mathrm{ZFC}} - m_{\mathrm{FC}}$ can be strictly explained by the difference in the energy $\Delta\varepsilon = (\varepsilon_{\mathrm{ZFC}} - \varepsilon_{\mathrm{FC}})/J_{\mathrm{med}}$ as a result of the state-preparation. To this end, we plot the differences in figure 4.3.2a and evaluate the correlation between the two. We find that when considering the first ten data points, there is an almost perfect negative correlation of $r = -1$, defined in the usual way via the covariance matrix between ΔE and Δm. Considering that these points are obtained from fast ramps and correspond to large absolute energies, the correlation hints at the existence of a paramagnetic phase at high energies. This would be characterized by a linear relation between magnetization and energy of the system.

Figure 4.3.2b shows both FC and ZFC magnetization as a function of the energy. Quite nicely, we find the linear regime at large internal energies where no significant difference can be observed between the FC and ZFC values, a clear indication of a thermal paramagnetic phase in the system. At small energies however, a splitting becomes apparent. Since its magnitude is very small ($\Delta m \sim 0.02$), determining the exact point of this transition is very difficult from the plot. When considering the correlations, it appears to be around an energy of $\varepsilon = -1.4 J_{\mathrm{med}}$. Of course, this value is obtained from a finite size simulation and at best presents only a first approximation of the actual transition point. At worst, the transition might not even persist in the limit of many particles.

It is interesting to point out that if the regime below the transition line is not a defect of the

system size, it clearly is non-thermalizing. While a detailed analysis will follow below, already at this point it is clear to see that we have a scenario where the equilibrium value of the magnetization at a given energy depends on the history of the system. Since for a thermal description of the system there is no notion of history, no memory effects like this dependence on the details of the state-preparation can be present.

4.4 The Influence of Strong Disorder

For many non-ergodic systems, the strength of disorder plays a fundamental role for the equilibration processes. In the framework of conventional spin glasses, disorder in combination with frustration leads to a rugged free energy landscape with many local minima separated by large energy barriers, which in turn causes diverging timescales for thermalization. In this case, it has been shown [43] that the transition temperature to the glassy phase depends on the statistical variance of the couplings.

On top of that, in the context of many-body localization, disorder plays a major role by preventing efficient exchange between particles and therefore hindering the thermalization process. In this case, there is a critical disorder strength above which localization takes place.

A similar effect has also been observed for our system with dipolar couplings [16], where depending on the strength of the disorder, a breakdown of ergodicity in connection to the

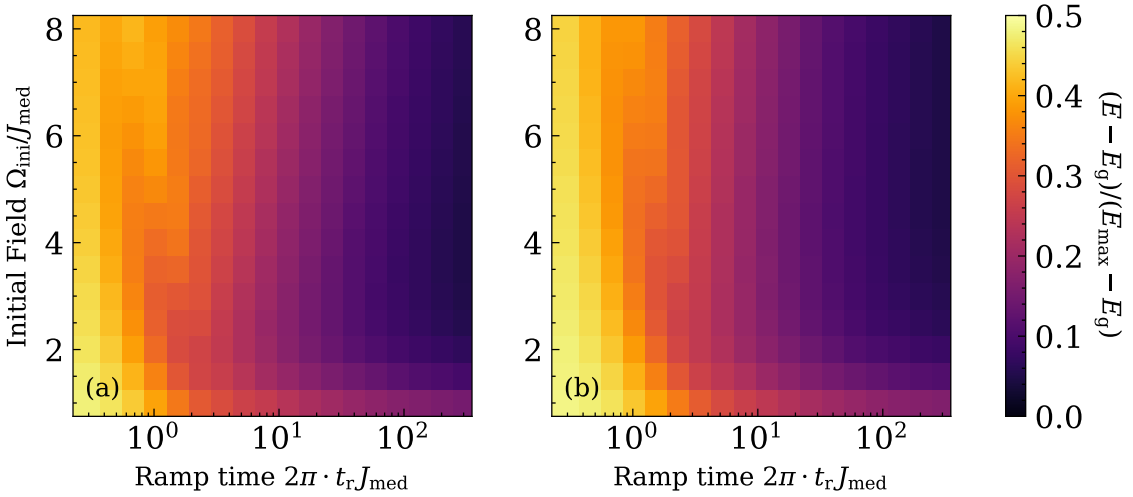

Figure 4.4.1: Ramping process for the disordered regime in the case of (a) linear ramp and (b) quadratic ramp. Comparing to before, we see that we needs slower ramps to reach the same level of energy as for weak disorder. The differences between the two shapes are still mostly irrelevant.

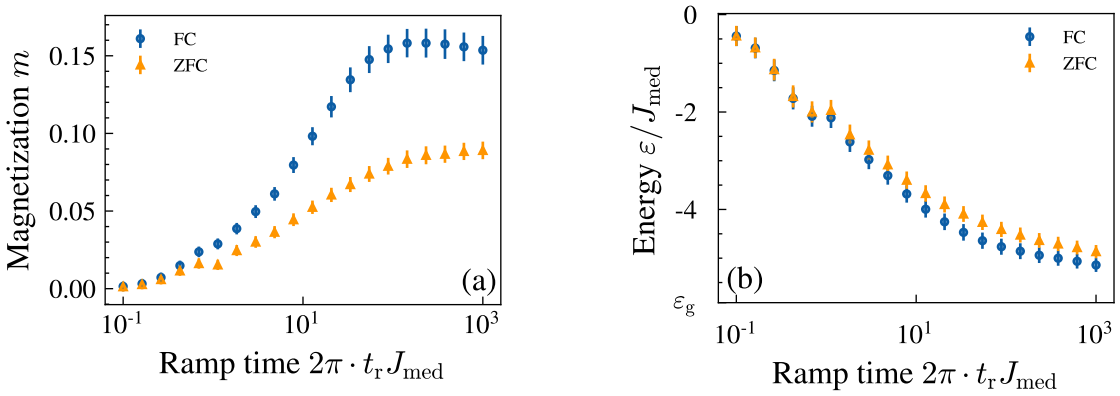

Figure 4.4.2: Ramp speed dependence of magnetization (a) and energy (b) in the case of strong disorder. The behaviour is similar to the ordered case, when considering the energy but the splitting in the magnetization is a lot more pronounced. Also we find a regime where the magnetization decreases with increasing ramp time at very slow ramps.

spin locking effect has been observed at least on experimental timescales. It is thus a logical conclusion to study how the disorder strength changes the previously discussed observations. We therefore change our model parameters, the blockade radius and the spin density, such that we increase the variance of the couplings from $0.6 J_{\mathrm{med}}$ to $1.7 J_{\mathrm{med}}$ and reconduct the same simulations as before. In the following, the model with lower variance that was studied up to now will be referred to as the ordered case and the large variance system as the disordered case. The labeling is done for obvious reasons, however it is important to keep in mind that even the ordered case features disorder.

The first check is to see how the properties of the ramp are influenced by the disorder. As depicted in figure 4.4.1, qualitatively the ramping process stays the same as before. There is a large stability for initial amplitude and shape of the ramp and we can use the ramp duration to tune the energy of the system.

Nevertheless, there are a few notable deviations from the ordered case, the most important one being that the condition for adiabaticity seems more strict. The lowest energy value reached still has an energy of roughly 5% with respect to the ground state and bandwidth of the system. It is thus a lot more difficult to reach the same energy levels as before. While this does pose a small restraint for investigating the low energy states of the system, we expect to be able to use the state-preparation in much the same way as before to probe a large range of different states.

As for the ordered case, we now explore the system by initializing a variety of states, each with a unique energy. The corresponding data is plotted in figure 4.4.2a. In the

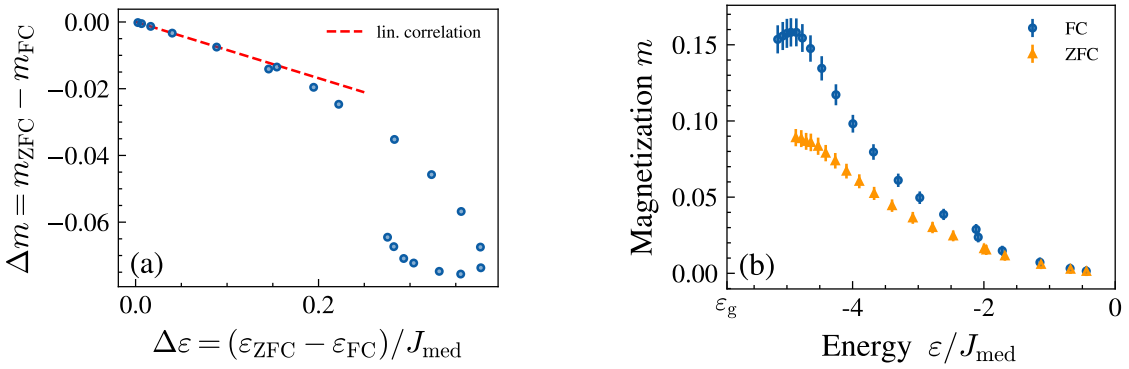

Figure 4.4.3: (a) Correlations between energy and magnetization difference in the case of large disorder. If there is a linear regime at all, it is limited to the very first ramps. (b) The magnetization shows a large splitting even when plotted as a function of the energy. This hints very strongly towards an ergodicity breaking behaviour of the system.

same manner as before, there is a small region where FC and ZFC overlap, followed by a splitting of both curves. Nonetheless, the effect is much more pronounced than in the weakly disordered case, the FC curve showing almost twice the magnetization of the ZFC one. Interestingly, it appears that for very slow ramps, the magnetization of the FC curves starts to decline again. This behaviour is not observed for the ZFC case, where both scenarios were monotonically increasing.

Taking a look at the energy after the ramp in figure 4.4.2b, we see again that it qualitatively behaves in a comparable way, where we have a region of no splitting and a region where the curves separate. Even so, this time the energy difference appears to be almost constant for the different ramps, clearly signaling that the difference in magnetization has a different origin than just a simple energy difference due to the state-preparation.

It is also interesting to see that the energy curve does not appear saturated, slower ramps probably would still lead to less energy in the system. Unfortunately, these timescales are already too large for the numerics to converge and we were not able to investigate a regime of even slower ramps.

Finally, we repeat the same analysis as for the ordered case to estimate the paramagnetic regime. As can be seen in figure 4.4.3a, the regime where the differences in energy and magnetization correlate linearly is very limited in the case of strong disorder. This becomes even more apparent in figure 4.4.3b, where magnetization is plotted as function of the energy. The linear paramagnetic regime is restricted to the very fast ramps, and almost immediately FC and ZFC diverge in a non-linear fashion.

4.5 Relation to Quantum Thermalization in the Context of ETH

Until now, we focused purely on the observations that can be found through the use of a new kind of state-preparation with the help of an external field ramp. Exploiting the fact that as the external field ramp gets slower, the system accumulates less and less energy during the ramping process, we were able to probe dynamics over a large range of energies.

By using the analogy to conventional spin glass methods, like field cooling and zero field cooling, we found magnetic irreversibilities where the steady state magnetization at given energy and external field depends on the preparation of the system. The strength of this effect was found to vary strongly with the amount of disorder present in the system.

In the following, we want to conduct a theoretical analysis of the system to see whether some of this behaviour can be attributed to thermal equilibration in a many-body system. The goal is to consider the previous findings in view of the eigenstate thermalization hypothesis (ETH) and possibly find further analogies to conventional spin glasses.

For the rest of this section, we also move to a description of the magnetic susceptibility instead of the magnetization, which is achieved by dividing through the external field since we are working in the regime of linear response. This is done to remove the external field dependence and for comparability with the results obtained later on where susceptibility can be measured at greater accuracy than magnetization.

We start by pointing out the relation to the ETH. As a reminder, within the context of ETH, there is a set of three conditions that is sufficient for thermalization. (i) The steady state has to be equal to the diagonal ensemble, (ii) the initial state is localized in energy and (iii) the observables follow a smooth function with respect to the energy eigenstates.

To verify the first condition, we calculate the coefficients for the diagonal ensemble by projecting the state immediately after the ramp onto the eigenstates of the Hamiltonian in the presence of a small field. When doing so for the different states initialized through the ramp, we can then calculate a ramp speed dependent diagonal ensemble prediction for the system.

Figure 4.5.1a compares the resulting expectation values from the diagonal ensemble visualized as a dashed line with the previously obtained values from simulating the full dynamics. The results are in perfect agreement, the very slight deviation can be attributed to a truncation of small coefficients in the density matrix to speed up the numerics. Thus, we conclude that the diagonal ensemble predicts the correct steady state values for the system, which considering the universality of the conditions under which it can be proven

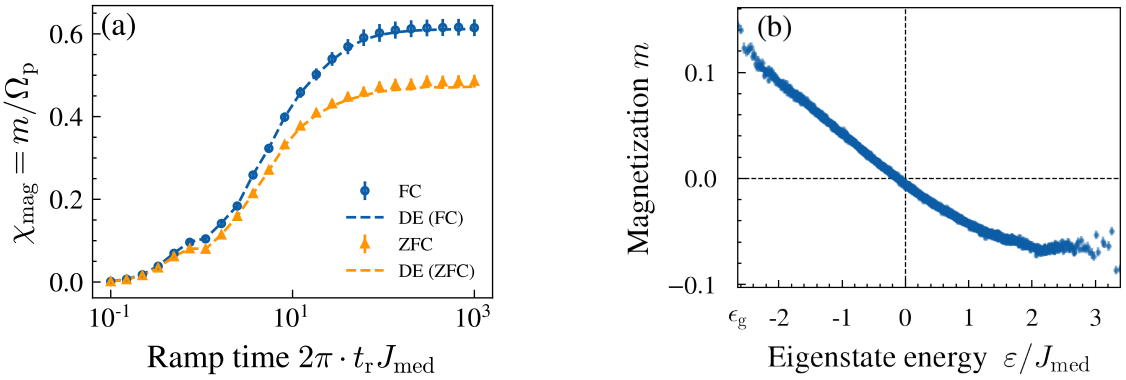

Figure 4.5.1: (a) Diagonal ensemble predictions yield perfect prediction of the magnetic susceptibility. (b) The eigenstate magnetization curve takes on a smooth form for the largest part of the energy spectrum, indicating that the ETH is fulfilled and the system is expected to thermalize.

is not really surprising.

Postponing the evaluation of the second condition for the moment, we continue by taking a look at the magnetization as a function of the eigenstate energy (figure 4.5.1b). The plot shows the disorder averaged magnetization of each eigenstate over its corresponding energy. Apart from the eigenstates at the far ends of the spectrum, the condition of smoothness is nicely fulfilled, indicating that eigenstate thermalization holds for a vast range of the energy spectrum.

This also means that we should be able to describe the system using a thermal ensemble. To verify this, we apply both a microcanonical (MCE) and a canonical ensemble (CE) description to the system. A detailed explanation of how this is done can be found in appendix B, where we also elaborate on the dependence on the energy window in the case of a MCE description and how to fit the CE temperature to obtain specific energy values. The results of the thermal prediction are shown and compared with the diagonal ensemble results in figure 4.5.2. As it turns out, in the region where FC and ZFC follow the same linear trend, the MCE description gives a perfect prediction of the susceptibility. The curves are essentially identical within the very small numerical errorbars from a disorder average over 50 realizations. Interestingly, at the splitting of the FC and ZFC curves, the MCE continues to agree with the ZFC curve over the whole available energy spectra.

The canonical description on the other hand slightly overestimates the susceptibility throughout the linear regime of both diagonal ensembles predictions. Once the splitting occurs, it proceeds slightly above the ZFC curve while staying below the FC curve. Finally, at very low energies it starts to agree with the MCE prediction.

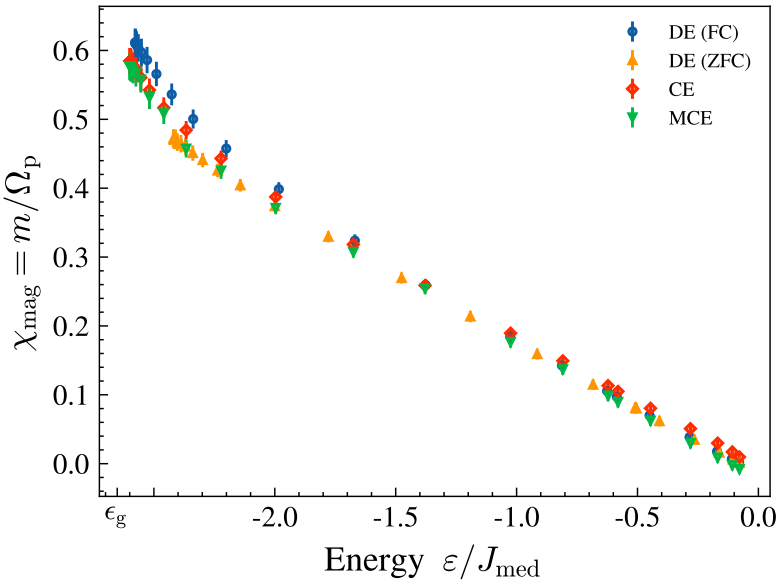

Figure 4.5.2: Comparison between thermal predictions based on a microcanonical MCE and canonical CE ensemble and the diagonal ensemble predictions for both FC and ZFC. In the linear regime at high energies, the MCE prediction gives an accurate value for both state-preparations. It continues to align with the ZFC curve upon the splitting of the FC one. The canonical ensemble slightly overestimates susceptibilities for most of the spectrum.

Considering the fact that this is a twelve particle simulation, we can attribute the differences in both ensembles to finite size effects. Hence, the interpretation of the plot is as follows. Since eigenstate thermalization is fulfilled, we expect a thermal prediction to accurately model the system. This is also the case for the ZFC state-preparation, where a MCE predictions perfectly reproduces the results of exact diagonalization.
That being said, we still want to find an answer to the question of why the FC measurement seems to deviate from the thermal description at lower energies.
To tackle this question, we take a look at the eigenstate population for both FC and ZFC procedure (figure 4.5.3). Both ways of preparing the state show a similar trend, where at fast ramps, they initialize states that are broadly spread throughout the full spectrum. Seeing this, at this point we might question whether condition (ii), which has been conveniently ignored up to here, is fulfilled. The state clearly shows a broad distribution over the spectrum and does not appear to be localized in the energy at all. However, this is strongest for the fast ramps, where as we have seen both FC and ZFC actually agree with thermal procedures. Towards slower ramps, it is clear that the states are more localized in the spectrum, yet this is where the discrepancy can be found for the FC susceptibility.

Considering this, we can assume that condition (ii) is valid for both cases, so a different origin has to be found for the visible splitting of the susceptibility.
Taking a closer look at the eigenstate population after the ramp, we find that the main difference between FC and ZFC becomes visible for very slow ramps. For the FC procedure the distribution becomes very narrow at large ramp times whereas for the ZFC case it seems to saturate and no longer reduce above a ramp time of roughly 100 interaction cycles.
This feature can be understood by remembering that the ZFC simulation contains an additional small quench to the Hamiltonian when applying the probe field that is not part of the FC state-preparation. This causes the state after the ramp to slightly spread out again, disregarding the fact that it initially was more localized after a slower ramp. This also explains why we never reach the same low energies obtainable with an FC ramp using the ZFC state-preparation.
Moreover, this effect also provides a nice explanation for why the diagonal ensemble predictions are not the same for FC and ZFC in spite of the fact that ETH seems to be fulfilled and one would expect a thermal description yielding a single susceptibility no matter the history of the system. Going back to the condition of ETH in figure 4.5.1b, we realize that it breaks down at the edge of the spectrum, where we find discontinuities. Thus, we would not expect states with a large ground state character to thermalize.

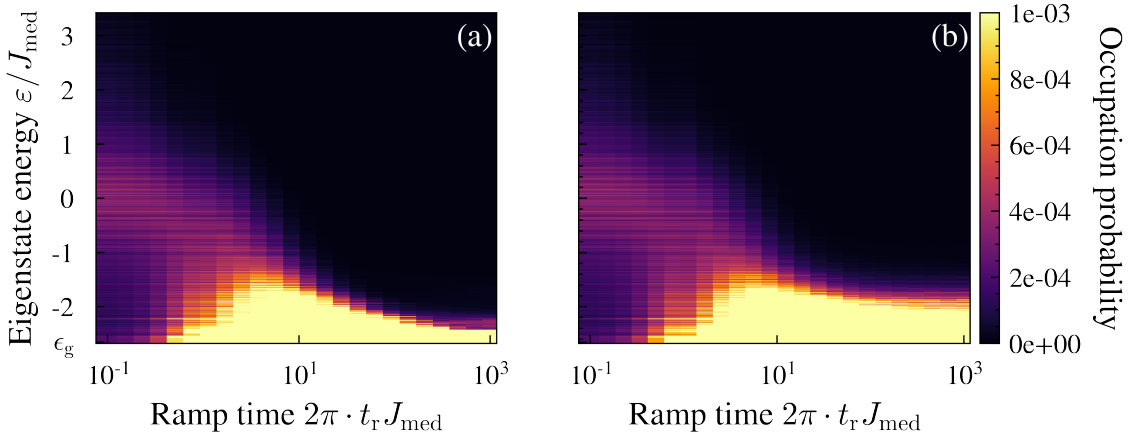

Figure 4.5.3: Population of eigenstates depending on the ramp time. While both state-preparations are similar for fast ramps, they show different features at very slow ramps. (a) The FC scenario is very well localized around the ground state for slow ramps. (b) ZFC states are a lot more spread out. This can be attributed to the small quench to the Hamiltonian that happens when applying the field in the ZFC case.

However, the state population after the ramp shows that the main difference between FC and ZFC is exactly that the former is much more localized around the ground state. By explicitly computing the overlap with the lowest two states, we find that this is already roughly 80% in the FC case and only about 30% in the ZFC scenario. Since the very low energy states also have a considerably larger magnetization compared to the rest, this seems to explain the visible deviation from thermal behaviour in the FC susceptibility.
While the previous discussion nicely explains the onset of irreversibilities in the case of the simulations, it leaves the question of whether this is a result of limited disorder realizations or finite system size unanswered. One could think, for example, that the non-thermal nature of the low energy states vanishes for a larger disorder average. We consider this to be quite unlikely considering how small the errorbars obtained from the disorder average already are. More difficult to answer is the question whether this effect persists for many particles or is a defect of the finite size setting. The observed differences are small and might well vanish in the thermodynamic limit. Answering this question proves to be very difficult and the only feasible way of arguing against it would be to realize the state-preparation in an actual experiment.
Postponing the discussion of larger system sizes to the experimental section, we now continue the numerical studies by increasing again the strength of disorder and doing a similar thermal analysis as before. The corresponding plots for the diagonal ensemble, the smoothness condition of ETH and the thermal ensemble predictions are found in figure 4.5.4.
Unsurprisingly, the diagonal ensemble still reproduces the exact values obtained from simulating the full dynamics. On the other hand, the magnetization as a function of the eigenstate energy shows a vastly different behaviour from before. We see multiple discontinuities of the curve and it is overall a lot broader, which shows that eigenstates can differ significantly even if they are close in energy.
Quite interestingly, the whole spectrum is symmetric around zero energy and there are evenly spaced gaps at an interval of about $2J_{\mathrm{med}}$. We note that this is not just a simple global spin flip symmetry along the axis of the external field. Such a transformation would indeed change the magnetization to negative values but leave the interaction energy invariant. Since the scale of the Zeeman energy is roughly $\Delta\varepsilon \sim 0.05J_{\mathrm{med}}$, the energy between magnetization and external field is essentialy irrelevant for the total energy.
Yet, in contrast to this estimation, the plot shows that the magnetizations seems to be very important for the total energy. Seeing that this behaviour is found in a disorder

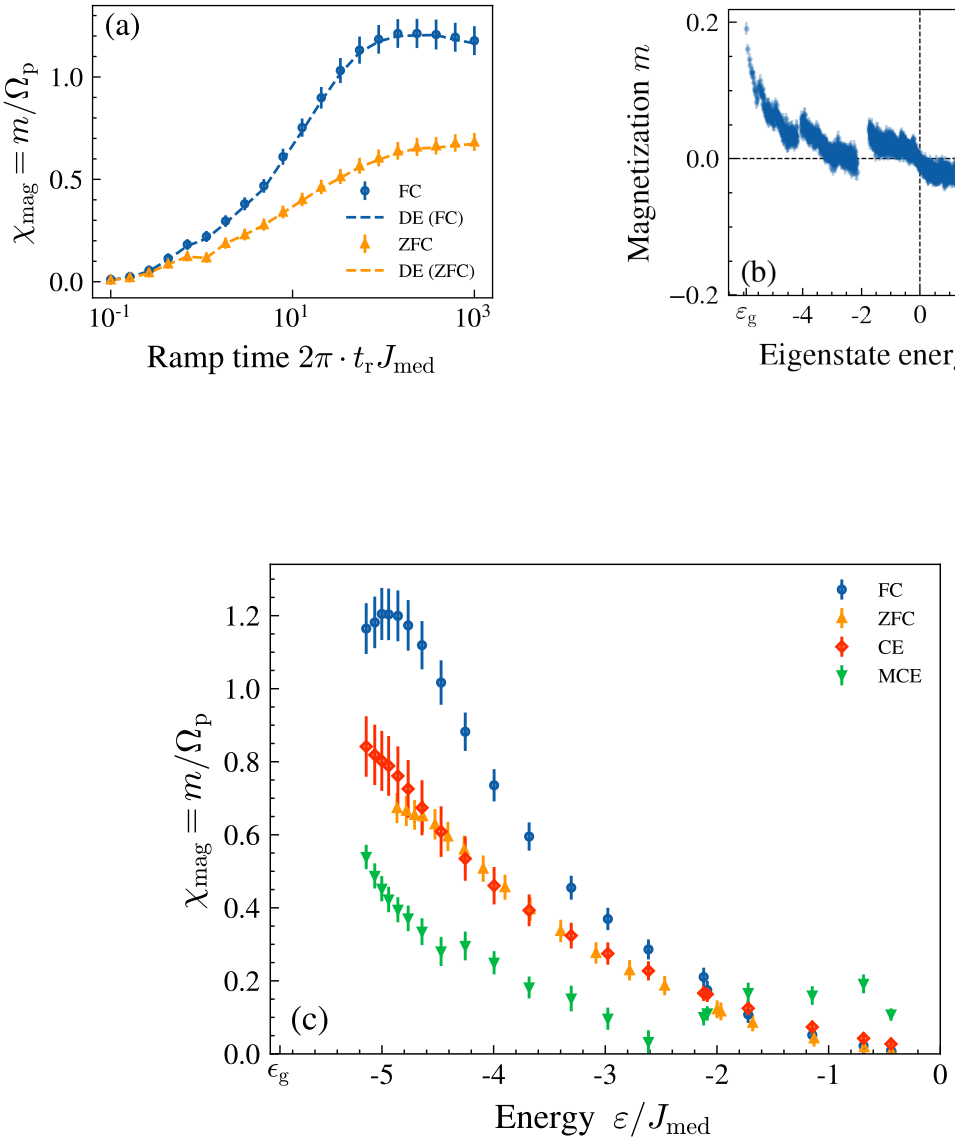

Figure 4.5.4: Thermal analysis of the system with strong disorder. (a) The diagonal ensemble still reproduces the exact values for the susceptibility. Notably, the absolute values are much larger than for the ordered case. (b) ETH is clearly not fulfilled in the system. There are multiple smaller energy values that internally show a smooth dependence on the energy but are separated by discontinuities. (c) Thermal predictions for the system at large disorder. The MCE values severely underestimate the susceptibility of both ramping procedures and are much worse than before. Conversely, the predictions of the CE ensemble seem to match the ZFC values over a large range of energies.

average, it seems to hint at a collective behaviour of the spins. Furthermore, due to the regular spacing of the gaps, it seems to be quantized in some way. A possible explanation might be a global excitation that retains some freedom in the magnetization. In this case, the gaps would be explained by such an excitation whereas the continuous change in energy would be due to the small differences in the magnetization. We stress that this interpretation is purely speculative, and at this point we have no indication for a physical origin of such a quantized collective behaviour. Nonetheless, it is clear that the observed magnetization as function of the eigenstate energy warrants further investigations, which is outside the scope of this thesis.

Next, we want to focus on the thermal predictions. From the previous discussion, it is clear that the system is not expected to thermalize over the full range of the energy spectrum, since ETH is not fulfilled. However, thermalization might still occur in the smooth part around the middle of the spectrum which has roughly the size $4J_{\mathrm{med}}$. Remarkably, a comparison with the diagonal ensemble values shows that the splitting of both curves happens at the location where the first discontinuity is observed in the eigenstate magnetization curve at $-2J_{\mathrm{med}}$. Below this value, an increasingly strong difference between FC and ZFC values is observed, indicating non-thermal behaviour.

Accordingly, we find that the MCE predictions are entirely off and fail to predict the behaviour of the system even in the case of large energies. Instead, it looks very similar to the eigenstate magnetization curve in 4.5.4b. Considering how it is derived, this is not surprising since the MCE obviously predicts a smoothed out version of the eigenstate magnetization curve.

Unexpectedly, the CE predictions show a very large overlap in the high energy regime before the splitting occurs and continues to give a good prediction for the ZFC curve even at lower energies, only slightly underestimating its magnetization. The numerical errorbars in this case are quite large still, and it might even be possible that the curves collapse onto a single one for a larger disorder average.

Based on the notion of ETH, the system would not be expected to thermalize in the first place. Also the clear discrepancy between MCE anc CE predictions indicates that the system is too small for methods of statistical mechanics to converge, as in the thermodynamic they should be equivalent. It is hence difficult to say whether the good prediction from the CE is accidental or whether for a large system the ZFC behaviour can be observed as thermal all the time, which would be quite surprising.

To find some clues on why the FC-ZFC splitting is much larger than for the ordered case

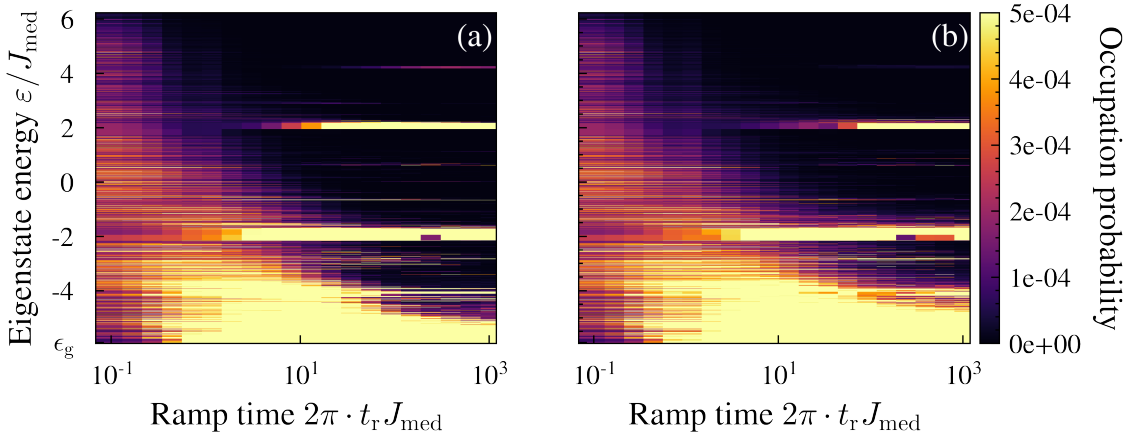

Figure 4.5.5: Population analysis for the disordered case. (a) Eigenstate occupation after FC ramp, overall the behaviour appears quite similar to the ordered case. The apparent high density of populated states at $\pm 2 J_{\mathrm{med}}$ is a defect of the plot, since there are simply no states with such an energy and thus the plot fills up the whole space to the next available state. However this still means that there are highly excited states, only not at the apparent density. They are increasingly populated for slow ramps, which is quite unusual when thinking in terms of an adiabatic passage that supposedly works better at slower ramps. Even more interestingly, they appear to overlap with the discontinuities in the eigenstate magnetization curve 4.5.4b. (b) The ZFC case shows similar effects. Additionally, it shows the same effect of the second quench that already was found in the ordered regime.

and on the question whether the ZFC curve might be thermal, we do a population analysis of the states after the ramps. The plots are shown in figure 4.5.5 and show a striking difference to the ordered case in figure 4.5.3.

The first observation is that in the limit of a quench, the state is distributed a lot more than in the ordered case. While the latter is somewhat localized around the middle of the spectrum, in the disordered case almost all states are occupied. This explains why the canonical prediction, which needs very high temperatures to reach the point of zero energy and is thus also very spread out in the whole spectrum is more accurate than the microcanonical one, which is by definition distributed only in a small energy interval.

Second, we find a similar effect to the ordered case, where the additional quench causes the state to spread out again and thus limits the minimum energy obtained in the ZFC case. Once again, this explains why the ZFC energy is larger at the same ramp speed than the FC one.

Third, the most eye catching observation is that there are higher energetic states that are populated once the ramps are slow enough. These states appear to be evenly spaced in the energy at a distance of $2 J_{\mathrm{med}}$. While the ones at $\pm 2 J_{\mathrm{med}}$ are clearly visible, a

closer inspection also shows them at $\pm 4J_{\mathrm{med}}$, albeit at a much weaker intensity. It is also interesting to see that for slower ramps, higher energetic states start being populated. For the very slow ramps in the FC case, even the state at $+4J_{\mathrm{med}}$ starts being populated. Since this state has a large negative magnetization, this explains why the magnetization of the FC curve starts decreasing again at very long ramp durations.

Additionally, we observe that these states seem to coincide with the gaps in the eigenstate magnetization plot in figure 4.5.4(b). This initially seems like an issue with the simulations, since there should be no states to populate at this energy. However, it is only a defect of the way the data is plotted. This is handled in such a way that if a state is populated, the whole region till the next state is highlighted. Thus in this interval where there are no states, a very broad line appears if the next state after the gap is populated, which is exactly what happens during the ramp.

The intepretation of this effect proves to be quite difficult. While it very strongly hints at some hidden physics, at this point all we can do is speculate about the origin since we discovered it recently and it is not yet thoroughly studied. Nevertheless, we are going to include some thoughts and ideas that could possibly explain the observed behaviour.

There appears to be some kind of collective behaviour in the system, that stepwise lowers the energy. This behaviour is symmetric around zero, however not related by a simple spin flip transformation.

Since for fast ramps, no trace of these excitations remains, they are probably destroyed by sudden large changes of the external field. This is further supported by the fact that we see an increasing amount of high energy excitations for slower ramps, which is completely against the intuition one would have when thinking based on a fully adiabatic passage. On could also think that these states

Summing up the discussion in the context of the ETH, we find that the system at weak disorder is expected to thermalize over a large range of energies. This behaviour is also observed in the simulations, where only at very low energies when the ground state admixture is no longer negligible we find a deviation from thermal behaviour. In the context of state-preparation with an external field ramp, this is only relevant for the FC procedure, since the additional quench in the ZFC simulations always causes an additional spreading in the spectrum such that the ground state population is insignificant and thermal behaviour is restored.

In the case of large disorder, the behaviour changes dramatically. The system no longer fulfills the ETH condition of a smooth eigenstate magnetization curve and is thus no

longer expected to thermalize, which was already observed in a previous work [16]. However, we now extended these findings to a large range of energies instead of just a single one. Both FC and ZFC curves are found to vastly differ from a thermal prediction, at least in the case of a small system size. Since they are also different from each other, the system shows memory effects where the global steady state magnetization at a fixed energy depends on the past. The numerical simulations do of course not guarantee a persistence of this non-thermal behaviour in the thermodynamic limit, however, considering that the system is large enough for a thermal description in the ordered case, we suspect it is unlikely that the effect is a defect of the system size.
Finally, a very interesting result is the existence of highly excited states that are populated in the case of slow ramps, an observation that demands further investigation.
At this point, it might also be interesting to see how a statistical mean-field prediction would compare to the results. However, significant difficulties arise when trying to create a mean-field theory in a setting where the average coupling strength for each particle is zero. These problems and possible ways to bypass them are highlighted in appendix C, since a full adaption of the mean-field theory proved to be out of scope for this thesis.

4.6 Classical Thermodynamic Analysis

Subsequently, we want to further explore whether the observed behaviour can be linked to the physics displayed in conventional spin glasses in any way. As explained in section 2.3, the main feature responsible for ergodicity breaking in a spin glass is a rugged free energy landscape. In our case, the rugged landscape indicating a glass phase should appear in the entropy, which is the appropriate thermodynamic potential for an isolated system. It will thus present the main focus of the succeeding discussion.
To numerically study the entropy, we diagonalize the Hamiltonian for different external field strengths and then simply count the number of states in an energy window $\Delta\epsilon$. The density of states is obtained by normalizing the amount of states counted by the energy window $\Omega(\epsilon, \Delta\epsilon) = \frac{\#\text{states}}{\Delta\epsilon}$, which guarantees the proper behaviour in the limit $\Delta\epsilon \to 0$. Finally, according to the microcanonical definition of the entropy we take the logarithm of the density of states $s(\epsilon, \Delta\epsilon) = \frac{1}{N} \ln \Omega(\epsilon, \Delta\epsilon)$ and divide by the particle number N to study an intensive quantity.
It should be said that the following observations for the entropy are not disorder averaged and should be treated only as qualitative statements. While in principle, entropy should be self-averaging and thus a disorder average should be the appropriate method of dealing

with disorder, this is only the case for very large systems. In our case, we are still limited to a study of 12 particles, which is why interesting features are smoothed out in a disorder average.

With the aforementioned procedure, laid out in the introduction to the thermodynamic potentials 2.2.1, entropy $s = S/N$ is obtained as a function of magnetic enthalpy $h = H/N$ and external field B. A sector of the resulting phase space is plotted in 4.6.1, where the top row shows the ordered system and the bottom row the disordered one.

In the ordered case, we find that for large magnetic fields, we see multiple maxima separated by valleys. Each maxima can be identified with a different magnetization sector defined by the amount of spin flips from the fully polarized state in the x-basis. This effect is already well known, the reason for it being that the external field dominantes the interactions and the Hamiltonian is essentially diagonal in x-basis. The number of states is directly inferred from this picture and follows a binomial coefficient exactly as lined out in the paramagnetic theory.

In the region of interest, which is the linear response regime at small magnetic fields, there appears to be a clear maximum of the entropy around zero enthalpy, which still corresponds to the paramagnetic prediction, only now the magnetization sectors are no longer visibly split since the Zeeman term is too small in the low field limit.

The situation is more interesting in the bottom row. Figures 4.6.1 (c) and (d) show the phase space in the case of large disorder. We find that holes start appearing in the entropy landscape for small external fields. This observation already hints at the existence of interesting physics, as it clearly is no longer explicable in a paramagnetic picture.

However, we find it difficult to extract any information on the dynamics of the system based on this kind of entropy. This is because at fixed enthalpy and external field, the state of the system is constrained to a single point in the phase space. Hence, by evaluating the partial derivatives of the entropy at this point, we would still obtain a single prediction for an apparently unique equilibrium magnetization.

To see whether there is more to this than a single thermal equilibrium state, we need to find a description of the entropy in terms of the magnetization. As lined out in the introduction, the appropriate thermodynamic potential for this is the inner energy $u = U/N$, with natural variables $s = S/N$ and $m = M/N$. By solving for the entropy we thus obtain a function $s(u, m)$.

Consequently, we have to slightly adapt the procedure of how enthalpy is calculated. We once again diagonalize the Hamiltonian in the presence of the external probe field. This

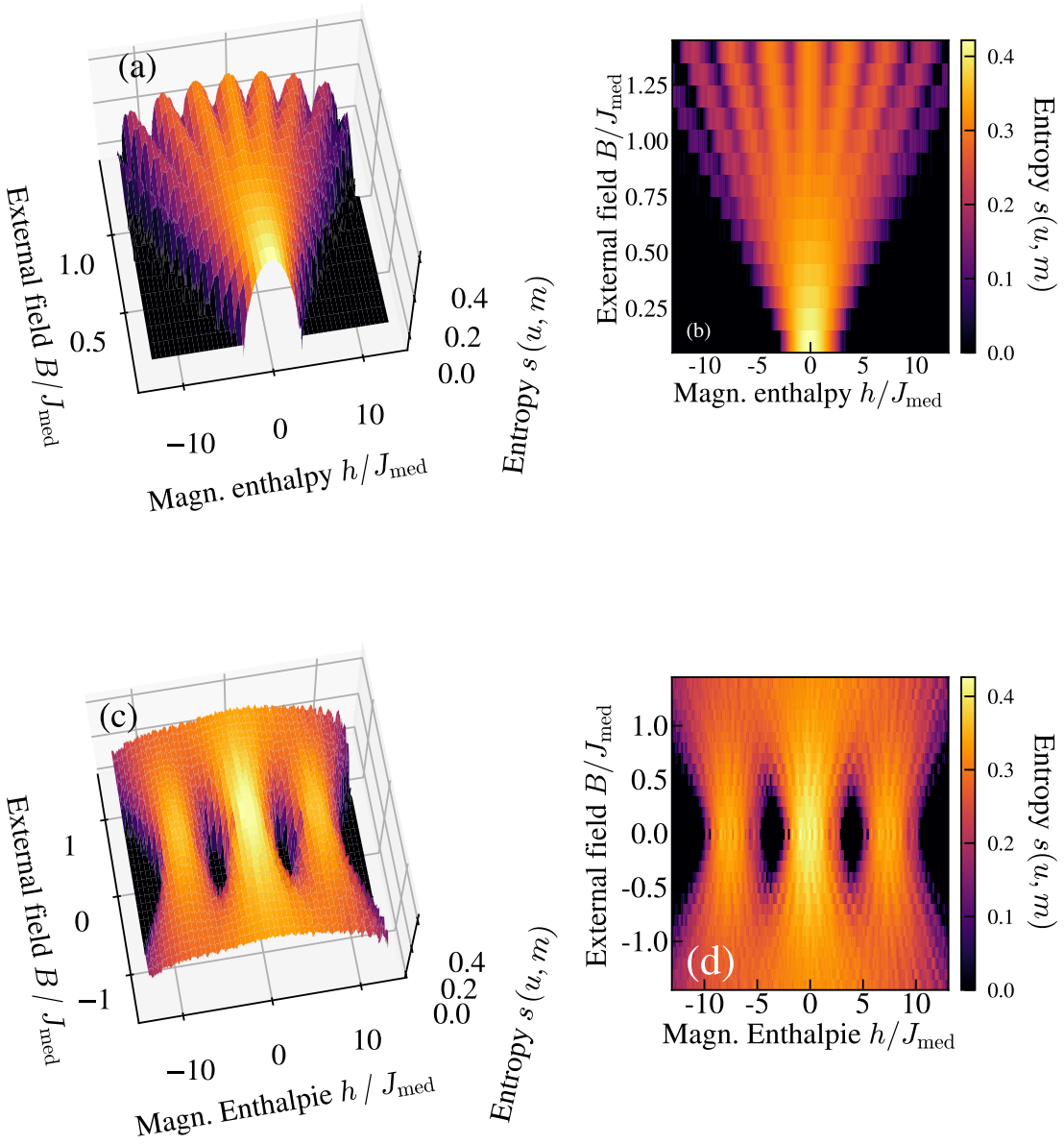

Figure 4.6.1: Top row: MCE entropy of the ordered system in the phase space of magnetic enthalpy (which is the total quantum mechanical energy of the system) and external field. We clearly observe the different magnetization sectors at large external fields. For zero field, there seems to be a single maximum, which still seems to respects a thermal description. **Bottom row:** Same plot but for large disorder. Interestingly, at zero field we now have a landscape with multiple entropy maxima separated by holes where no states are present.

time however, we group the resulting eigenstates $|\mathrm{i}\rangle$ by their magnetization and internal energy, which for a given eigenstate is obtained as $\langle \mathrm{i}|\hat{H}_{\mathrm{int}}|\mathrm{i}\rangle$, where we neglect the external field in the Hamiltonian. By doing so, we can now count the number of states in a 2d window of energy and magnetization. From there on, entropy is again obtained via the microcanonical definition.

This time, we obtain a function of inner energy u and magnetization m. To find the dynamics, we now have to consider the additional constraint on the enthalpy due to the isolated evolution. Hence, the condition of energy conservation is $h = u - Bm$, which defines a line in the u-m plane as physical states. In the plots, states of constant enthalpy are highlighted as white lines.

Using the above condition, we can now take a cross section of the entropy for different values of the enthalpy to obtain entropy as a function of the magnetization given the total quantum mechanical energy of the system. The resulting curves for the ordered system regime are depicted in figure 4.6.3.

We find that for large enthalpy values, there is a single clear maximum of the entropy. As the enthalpy decreases, the position of the maximum shifts to larger magnetization values. This qualitatively agrees with the observations that slower ramps corresponding to lower enthalpies show larger magnetization values.

However for very low enthalpy values, we observe that the single clear maximum in the entropy splits up and starts to form a landscape with multiple local maxima. It should be noted that this effect is not limited to a single realization but shows in every realization. Even though the exact amount and location of the maxima differs, all realizations show some kind of transition from a single maximum in the entropy to a region where there are multiple configurations at different magnetizations with similar entropy and thus no clear thermodynamic ground state.

In the disordered regime, this trend does not exist. When trying to assign physical states to the system, we find that even at large energies, entropy does not necessarily have a clear maximum. On top of that, there is no clear trend towards positive or negative magnetization as the enthalpy decreases. Thermodynamic predictions clearly are inaccurate, which is again strengthens the statement that a large disorder prevents thermalization in the system.

Nevertheless, we can gain additional information on the system by considering that the entropy is derived from the density of states. We see that in terms of the inner energy, the density of states appears to be discretized. While this does not always manifest in groups

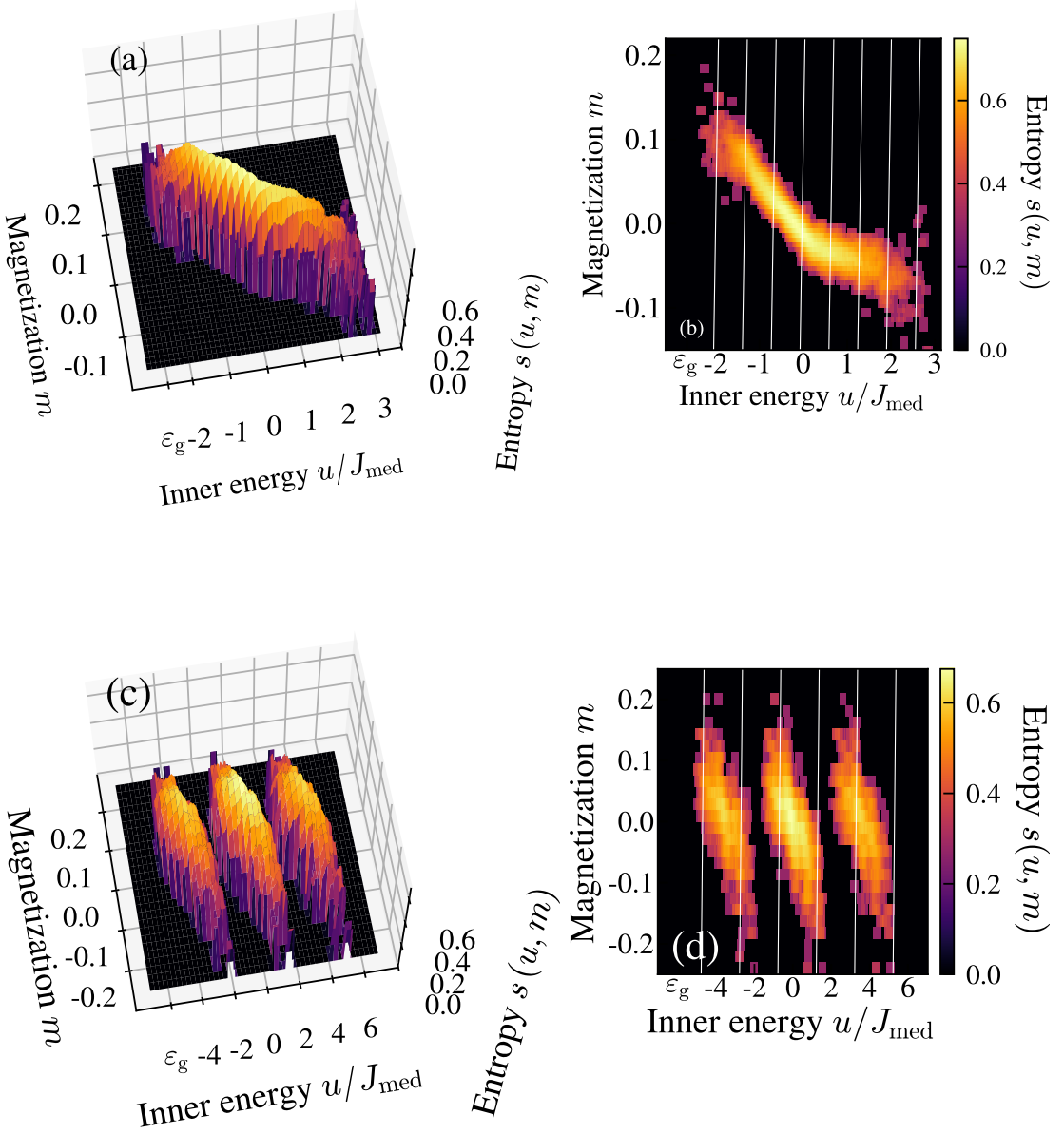

Figure 4.6.2: Top row: Entropy as a function of magnetization and inner energy for the ordered regime. In general, we find that lower energetic states feature larger magnetization. To find the equilibrium state, we have to consider the physical restriction of a conserved enthalpy. Different values of enthalpy are indicated as white lines in the 2d plot. Interestingly, there is a transition from a clear entropy maximum in the middle of the spectrum to a rugged landscape at the edges. **Bottom row:** Same plots at large disorder. Here, there is no clear relation between magnetization and inner energy that can be found and the magnetization depends very much on the specific value of the enthalpy. There are also gaps in the inner energy where no states are present. Both observations indicate a breakdwon of thermal predictions for the disordered case.

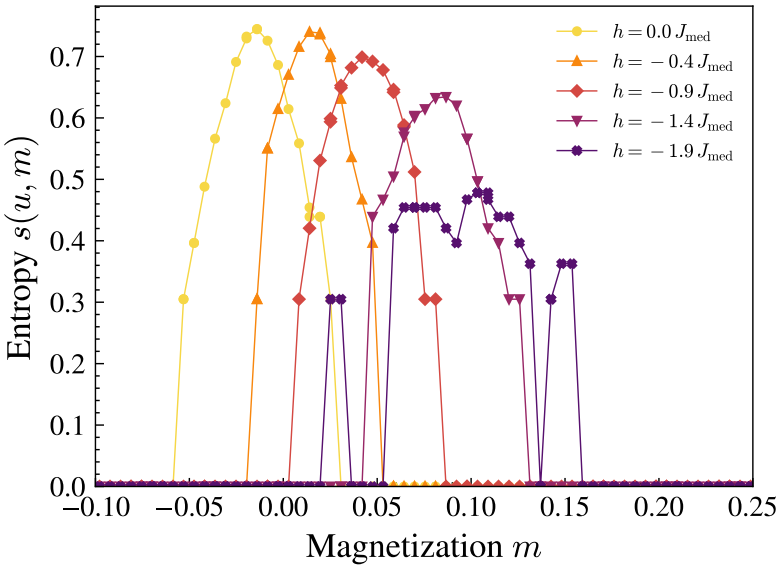

Figure 4.6.3: Cross section through the entropy along lines of constant enthalpy in the ordered regime. The transition from a paramagnetic phase with clear entropy maxima to a region with multiple entropy maxima and no clear thermodynamic ground state becomes apparent.

of three as depicted above, there still has to be a mechanism explaining the existence of a gap in the interaction energy at large disorder. Especially since this is clearly not present in the ordered regime. It would, for example, be interesting to see whether a description in terms of pairs of spins that was previously developed by our group and shown to accurately capture the spin-locking dynamics [16, 60] also gives insight into the discrete internal energies.

While the analysis of the disordered regime shows quite intriguing features, it does not seem to be compatible with typical observation in a spin glass, since the thermal prediction for the magnetization completely fails as it is zero at all energies. In a spin glass on the other hand, the thermal prediction still gives an accurate value for the FC (referring to the actual field cooling done in CMP systems) magnetization.

The situation seems to be different in the ordered regime, here the analysis of the entropy yields exactly what one would expect for a spin glass, as it transitions from a paramagnetic to a non-trivial regime.

5 Experimental Indications of Aging in the quantum XY-Model

In the course of the thesis so far, we have focused on a numerical study of the quantum XY model in three dimensions with a dipolar distribution of couplings. Exploring the possibility of preparing initial states at different energies with the help of a slow ramp of the external field, we were able to gain considerable insights on the nature of the system and its behaviour in the presence of an external field.

In the strong disorder limit, we found ergodicity breaking behaviour that displays different equilibrium magnetization values depending on the history of the system. Thermal predictions in this regime seem to break down as indicated by the failure of the micro-canonical ensemble prediction and the structure that is displayed by the phase space in the classical limit, where the entropy maxima are at seemingly random values of the magnetization for a given enthalpy. This is also in accordance with the nowadays established picture of eigenstate thermalization, which is found to not be fulfilled at strong disorder. In view of these results, a spin glass transition seems unlikely in the strong disorder regime, since ergodicity breaking in a spin glass is based on infinitely slow thermalization and not a complete absence thereof.

However, the situation changes for the ordered regime, where we are left with conflicting results concerning the question of a spin glass transition. While the ergodicity breaking at low energies and a thermodynamic analysis show qualitatively similar features as are observed in conventional spin glasses, interpretation is always hindered by the small system size. Moreover, the specific shape of FC and ZFC magnetization, the analysis of the order parameter in appendix E and the absence of aging in numerical simulations that is presented in appendix F all speak against a spin glass transition. We should note that for the analysis of the order parameter, we did not yet properly address the spontaneous symmetry breaking nature of the spin glass phase. Also, since a theoretical description of aging relies heavily on many-body physics, namely a formation of many individual domains in the glass phase that slowly merge with each other, it is not surprising to see it absent in a finite size system.

A physical interpretation for why a spin glass phase might only occur in the dense regime can be found when considering the requirements leading to glass phase. As discussed in section 2.3, the main components needed are frustration and disorder. While disorder obviously increases in the regime at larger variance, at the same time the number of spins

with strong couplings decreases dramatically, which reduces possible frustration in the system. It has even been shown that a good approximation in the strong disorder case is to simply considering nearest neighbour interactions [16, 60], a limit in which there is no frustration at all since every pair of spins has a clearly preferred state between alignment and anti-alignment depending on the sign of the coupling. Frustration hence increases in the dense regime, where this pair approximation breaks down and one has to consider interactions between multiple spins. Since there is still disorder present even in the case of a fully blockaded regime, both necessary conditions are fulfilled, allowing for a possible glass phase.

Ultimately, it is difficult to reach a satisfactory answer to the question based solely on the investigation with a system of only twelve particles. Hence, in the following we want to use the advantages of the Rydberg quantum simulator introduced in section 3 to study larger system sizes. While the experiment provides an experimental setting with a system size of thousands of spins, there are also a lot more constrictions to bear in mind.

5.1 Measuring Linear Response for Large System Size

The main limiting factor for conducting measurements is the black body lifetime, which limits the experimental time for which we can consider the system to be isolated. Since we want to perform a very slow field ramp, we want to maximize the time at hand. Considering the black body rates, we realize that large n values are beneficial since the lifetime increases as n^3. On top of that, they comes with the additional advantage of an increased interaction strength, since the strength of dipolar interactions between the Rydberg atoms also scales as $C_3 \propto n^4$. This is helpful, since it immediately plays into the effective ramp time tJ_{med}.

Thus, in order to maximize the effective ramp time $2\pi \cdot t_{\mathrm{r}} J_{\mathrm{med}}$, we choose the high lying Rydberg states $|\downarrow\rangle \equiv |61S\rangle$ and $|\uparrow\rangle \equiv |61P\rangle$ for our mapping to the spin Hamiltonian. With this setting, the coupling constant is given by $\mathrm{C}_3/2\pi = 3.14\,\mathrm{GHz}\,\mu\mathrm{m}^3$ and the blockade radius can estimated to be $r_{\mathrm{bl}} = 7\,\mu\mathrm{m}$ where we assumed a Fourier limited laser linewidth of $1\,\mathrm{MHz}$. In an experimental window of $10\,\mu\mathrm{s}$ we are thus able to achieve on the order of 100 interaction cycles, the same order of magnitude that has been numerically investigated for the slow ramps.

Since this is the first time that state-preparation using an external field ramp is performed in the system, we start by trying to reproduce the linear response found in the simulations. We limit ourselves to a study of the ZFC sequence, since the experimental realization

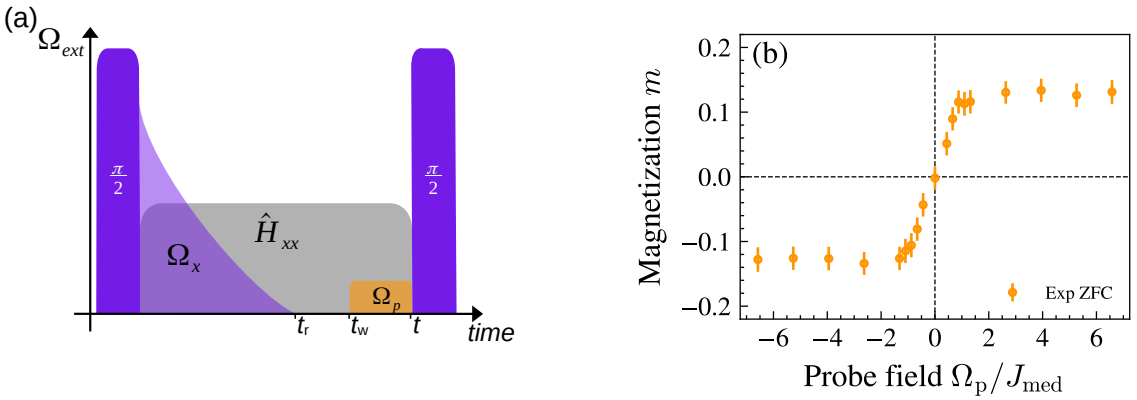

Figure 5.1: (a) Visualization of experimental sequence. We adapt the ZFC procedure from before with an additional waiting time t_w. The time t is set to zero when the probe field is applied. (b) Experimental values for the response to a small external field. The linear regime seems to extend a bit further than in the numerical analysis, spanning roughly the interval $[-J_{med}, J_{med}]$. Interestingly, we do not observe the same decline of the response for large values of Ω_p that was found in the numerical simulations, at least for the regime that is considered.

of the ZFC state-preparation is a lot simpler than the FC one, where the phase of the microwave becomes time dependent.

Thus, the experimental sequence (Figure 5.1a) is as follows: Starting with a global $\pi/2$-pulse to initialize the fully polarized state, we subsequently apply a strong field in x-direction that is ramped down to zero amplitude over a duration of $t_r = 3\mu s$. To ensure that no remanent magnetization is present when applying the field, we additionally introduce a small waiting time $t_w = 0.35\mu s$ after the ramp. Then, the probe field is applied along the y-direction and the magnetization is measured at $t = 0.5\mu s$ after the probe field has been applied. This time is expected to be large enough for the magnetization to reach a steady state value, since it exceeds the relaxation time of the system which the numerical analysis has shown to be slower than the timescales of the response.

The results of this measurement are seen in figure 5.1b . The measured response is nicely symmetric around zero and reaches magnetization values in between $m = \pm 0.12$. We also find the linear regime to extend to $\pm J_{med}$, where the value for the experimental coupling strength $J_{med}/2\pi = 1.66\,\mathrm{MHz}$ has been estimated as the inverse of the time constant that we fit to the relaxation process in figure 4.0.1a. The main qualitative difference with respect to the numerical simulation is the behaviour when probing at larger external field values. The experimental data points seem to saturate at a given field strength and

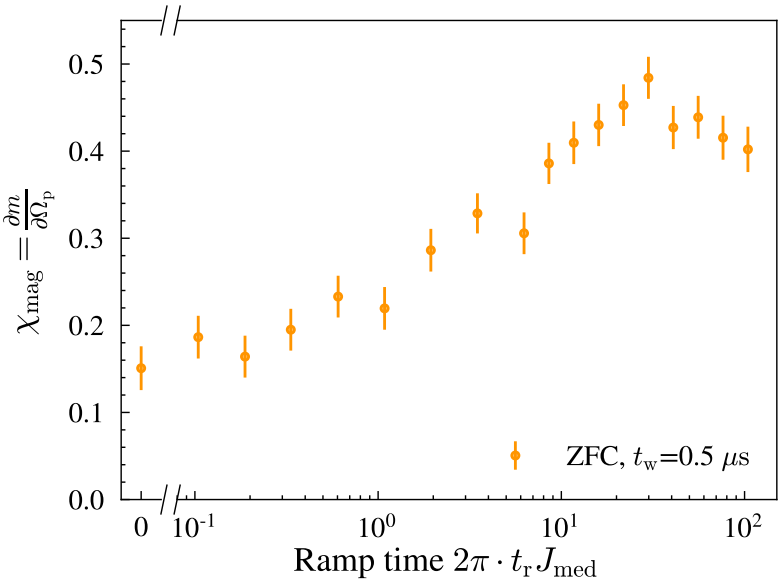

Figure 5.2: The magnetic susceptibility is plotted as a function of the ramp time. Additionally, the value for applying a field without any ramp is plotted at $t_{\mathrm{r}} = 0$. The measurement yields the expected increase of the susceptibility with increasing ramp times. However, there are two notable deviations when compared to the numerical data. First, even in the limit of quenching the external field, the susceptibility is not zero. Second, it features a clear maximum and starts declining again for very slow ramps, which is the same behaviour that a glassy phase would show.

show no sign of decreasing, at least up to the maximum amplitude that was measured at $\Omega_{\mathrm{p}} = 6J_{\mathrm{med}}$. Considering the isolated nature of the system, we would expect that the response is zero again for large fields, since quenching the field always causes some heating for the isolated system. It is thus interesting to see that at larger system size, this effect seems to be suppressed very strongly.

Now that we have verified the existence of a response in the experiment, we want to extend also the numerical analysis of the ramp time dependence to a larger system size. Thus, we continue the experimental measurements with by varying the ramp duration in the following. However, we realize that measuring changes in the magnetization at an order of magnitude of $\Delta m \sim 0.02$ proves to be quite a challenge. In order to improve our accuracy, we measure every ramp duration at four probe field strengths in the linear regime. This allows us to perform a linear fit and thereby obtain a value for the magnetic susceptibility of the system.

In general, the data in figure 5.2 fits quite well to our expectations. With increasing ramp duration, the susceptibility of the system rises as well. Even the magnitude of the response

matches surprisingly well to the numerical ZFC curve in the ordered regime.
There are however two notable differences from the numerical simulations. We observe that even when quenching the external field to zero, we still measure a finite response, the origin of which is as of now uncertain. While one could consider the finite fall-time of the waveformgenerator as a possible reason, it is three orders of magnitude smaller than the slowest ramp and thus should not contribute to the finite response that is seen for slow ramps.
As previously discussed, the experimental data also shows a qualitatively different behaviour from numerical studies in the inverse limit of applying a strong probe field to the system. Hence, it might be possible that the influences of a strong external field quench in the many-body system are not quite the same as what is observed for a few particle system, where the state is redistributed equally among the new eigenstates. If that was the case, no magnetization should be measured in the quench limit in both experiments discussed so far, since the spectrum stays symmetric with respect to the magnetization. We infer that further studies in a setting with more control would be needed to find the reason for a finite magnetization in these scenarios.
The second observation found when considering the ramp time dependence is the decrease of the susceptibility at very slow ramp values. This effect is not at all seen in the numerical simulations, where in the ordered regime both FC and ZFC curves simply saturate for slow enough times and in the regime of strong disorder only the FC curve shows a similar feature. As such it is an effect that appears to be relevant only at large system sizes.
Interestingly, such a behaviour is also what we would expect for the magnetization if a transition from a paramagnetic towards a glassy phase occurred. In this scenario, the spins would freeze out below the transition energy and the system would take much longer times to develop towards an equilibrium state.

5.2 Observation of Short Term Aging Effects

The form of the magnetic response curve as a function of the ramp duration indicates a non-trivial behaviour of the system when probed with an external field at low energies. Notably, the observed behaviour differs severely from what is seen upon exact diagonalization of a small system, indicating a complex behaviour that only appears in a many-body setting. Furthermore, it bears a close resemblance to what is seen in typical spin glass systems realized by metallic alloys. This hints at the existence of a possible glass phase, which is characterized by a freezing of the spins random directions.

A clear indication for such a behaviour would be a non-zero EA-order parameter as introduced in section 2.3. Unfortunately, the measurement of said parameter would require the ability to measure temporal correlations, which due to the destructive nature of the measurement procedure and the random spatial distribution of the atom cloud is impossible with the current experimental setup. Thus, we have to rely on indirect measurements in order to find further information on the quest for searching a glassy phase in our system.
A typical feature of spin glasses that we might be able to observe in our system is the aging effect, as it directly manifests in the global magnetization, which we can measure using the usual methods of the Rydberg quantum simulator. As a reminder, aging stands for the dependency of the linear response not only on the strength, but also on the timing of a perturbation. The system remembers its birth and depending on the time that has elapsed since, it responds at different timescales.
To probe for such an effect, we repeat the above measurement for two different waiting times before applying the probe field. If the system transitions to a glass phase below a critical ramp speed, aging effects should be present and accordingly the build-up of the magnetization should be slowed down for the longer waiting time. Since we measure magnetization at a fixed time, we would then expect to see a splitting of the two curves below a critical ramp duration, where the long waiting time shows smaller magnetization values.
Amazingly, we find a behaviour that is comparable to typical spin glass physics (figure 5.1). Initially, for fast ramps in the high energy regime, there seems to be no noticeable difference between the curve at a waiting time of 1μs and the one for 6μs. Both are simply monotonously increasing with the ramp time.
The situation changes at a ramp duration of about 10 interaction cycles. From here on, every consecutive data point from the long waiting time lies below the one obtained at a shorter waiting time. Also, the absolute value of the susceptibility stops increasing and even start to decline. Unfortunately, the splitting is very small and hard to resolve. The average difference between both ramp times is barely significant with respect to the errorbars. Nonetheless, in view of the amount of consecutive points that show the same trend, we consider the findings to be meaningful.
Still, we perform an additional measurement for a fixed ramp time in the regime where aging is observed and measure the susceptibility for a large range of waiting times. This is shown by the inset of the figure, clearly reproducing the trend of a weaker response at larger waiting times.

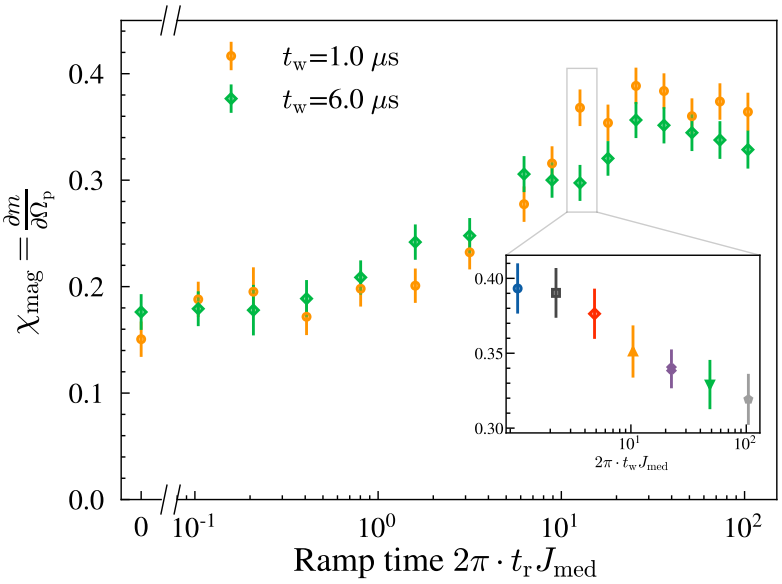

Figure 5.1: The susceptibility of the system is investigated for two different waiting times. We find that a splitting between the waiting times occurs if the ramp for state-preparation is slow enough, which indicates the presence of aging effects in the system at low energies. The statement is further supported by the inset, which shows the waiting time dependence for a single ramp time measured in a separate run. A clear trend towards a weaker response at longer waiting times can be observed.

A simple qualitative argument also rules out a possible explanation of these observations based on decoherence of the system during the waiting time. Since we calibrate the magnetization for the loss of atoms, black body radiation effectively only reduces the coupling strength in the system. However, since the difference in the waiting time is constant for all points and the effects of black body radiation are approximately linear at early times, it should affect all data points in the same way. It is thus clear that if a splitting occurs only in part of the plot, it cannot be attributed such a difference.

Next, we also want to measure a time resolved build up of the susceptibility, to ascertain that it is indeed slowed down. The measurement can be found in figure 5.2, once again for two different waiting times. While there is a fast increase independent of the waiting time at the beginning, the curves split after roughly one interaction cycle and show the expected dependence on the waiting time. It is however very difficult to resolve the splitting at later times, since it becomes very small.

While the observations qualitatively agree very well with the known aging effect in a spin glass, we also want to highlight some very important differences. First of all, the

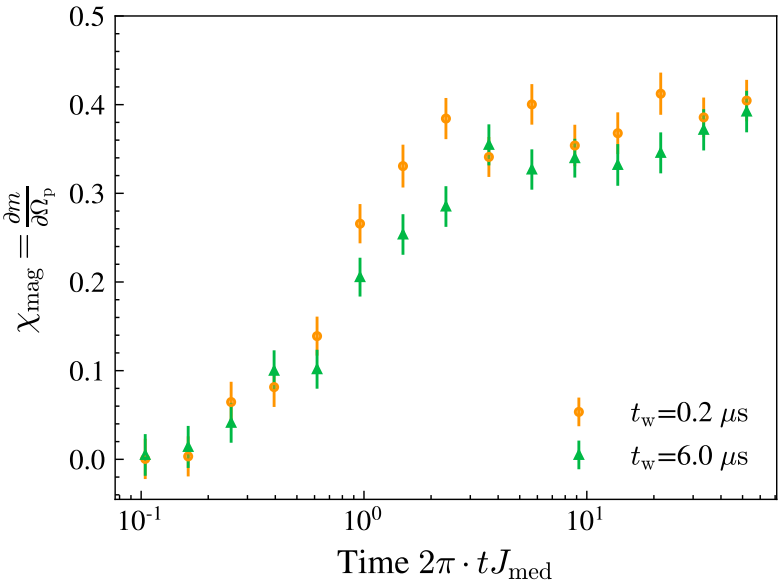

Figure 5.2: Build up of the response. At every point in time, the magnetization is determined for multiple probe fields and the slope of a linear fit determines the plotted susceptibility. We observe that after an initial increase that seems independent of the waiting time, the build up of the response is slower in the case of a larger waiting time. Unfortunately, the absolute magnetizations that are measured are very small, which makes it difficult to resolve the splitting ($\Delta m < 0.05$) at late times

timescales applied for our system are vastly different than what is measured in a condensed matter setting. Aging phenomena are seen for macroscopic timescales at the order of $10^0 - 10^5$ s, whereas a typical paramagnetic spin flip time of for these systems is estimated to be $\tau \sim 10^{-12}s$ [7]. Thus, they explore roughly $10^{12} - 10^{17}$ interaction cycles in their measurements, to which we now compare about $100\,tJ_{\mathrm{med}}$ cycles in our system that are used for state-preparation, aging and probing the system all together. Thus, the observed features are on extremely short timescales, which makes a comparison, that is inherently difficult due to the difference between isolated and open systems, even more difficult. On the flip side, such a short term measurement is impossible for to perform on condensed matter systems and could thus offer valuable new insights if a spin glass transition could be confirmed for our system.

We also want to quickly address the fact that the behaviour deviates significantly from what is found in numerical simulations. For small systems, no effect at all is observed when introducing the additional waiting time, the corresponding simulations can be found in the appendix. Thus, the aging effect appears to be an effect that only becomes relevant

at large system sizes. This statement is also naturally supported by the droplet picture that can be used as a phenomenological description for a spin glass. Within this picture, many small domains start forming below the freezing temperatures. As the system ages, these domains start to merge, which causes the temporal dependence of the response. Obviously, they cannot form in a small system, at least not a relevant number of them. Thus, if this was the case in our system and could explain our findings, it would be reasonable that the effect vanishes in the analysis of a system of only twelve particles.

To conclude, we demonstrated the possibility of using an external field ramp for state-preparation to initialize states that show a response when probed with an external field. This response was investigated as a function of the ramp time, which effectively varies the internal energy. At presumably low energies, a discrepancy with numerical results based on exact diagonalization is found and the system starts to display a short term aging effect, a strong indication for the possibility of a glassy phase in an isolated quantum setting.

6 Conclusion and Outlook

The main question we set out to answer in this thesis is the potential occurrence of a spin glass transition in an isolated system of Rydberg atoms that exhibit dipolar XY interactions. To address this question, we introduced a new of state-preparation protocol for the Rydberg quantum simulator that enables the initialization of states at different internal energies. With its help, we conducted a thorough investigation of the system based on a combination of experimental measurements supported by numerical studies.

For the state-preparation, we used a protocol where the fully polarized state is initialized in the direction of a strong external field, which is subsequently ramped down to zero. Knowing that the fully polarized state is a good approximation for the ground state in the presence of a strong field, we made use of the adiabatic theorem in quantum mechanics to initialize energetically different states based on the speed of the ramp. While this concept of state-preparation using adiabatic passage was not new by itself, the question remained whether it is applicable to our platform.

Usually, the condition for adiabaticity depends on the energy gap between the eigenstates, which determines what is considered to be a slow change of the Hamiltonian. Thus, in a setting of thousands of spins where the gap becomes very small and we are limited in the experimental times due to decoherence effects, it is not guaranteed that we can conduct slow enough ramps to reach low energetic states. Furthermore, we are dealing with a disordered system and the meaning of ”slow” could change from shot to shot.

Nevertheless, a numerical analysis with finite size scaling showed that low energies can be initialized at good fidelity for ramp durations within the limits of the experiment. We are helped by the fact that we do not have to stay perfectly adiabatic and only need to avoid a large spreading out into the energy spectrum. The successful application of this scheme to the experiment was demonstrated in the later parts of the thesis, where we directly measured the influences of the ramp duration on the response of the system when probed with an external field.

Numerically, the fidelity of the state preparation was also found to be largely independent of the initial amplitude and exact analytic form of the ramp for the studied scenarios. We expect, however, that it is possible to considerably improve the efficiency of the state-preparation protocol by adjusting the ramp speed based on the momentary energy gap of the spectrum. Unfortunately, such a procedure would require a great deal of fine tuning with respect to the experimental parameters and would be hard to optimize for the current

setup where only indirect feedback on the energy can be obtained.
Throughout the thesis, we distinguished between the application of a small orthogonal probe field during the ongoing ramp or conversely probing the system with such a field after the ramp has finished. This approach allowed us to draw an analogy to the conventional methods of field cooling and zero field cooling commonly utilized in condensed matter experiments, which we used in the first part to numerically study the system at different disorder strengths.
In the strongly disorder regime, we extended on previous findings that ETH is not fulfilled and found a clear sign of ergodicity breaking behaviour over a large range of energies. While energy and external field are the same, the steady state magnetization differs largely between the FC and ZFC procedures. This observation complements nicely recent studies conducted in a spin locking field, which showed the absence of thermalization on experimental timescales [16]. The key signature in this experiment was a non-analycity of the magnetization at zero field, which is now complemented by our explicit demonstration of the existence of multiple equilibrium states for the same macroscopic parameters of the system. Unfortunately, we have to be a bit careful with this interpretation since so far, only the ZFC state-preparation has been employed in the experiment and we did not yet measure multiple equilibrium states for large system sizes. However, since the previous result of non-thermal behaviour on experimental timescales was observed for large systems, we are confident that our findings will persevere in this limit aswell.
The situation changes drastically when studying the system at reduced disorder, where ETH starts to be fulfilled and the system is expected to thermalize. This was also confirmed for a large range of energies since the predictions from FC and ZFC were shown to corresponded to those obtained from a thermal ensemble. However, we found a slight deviation from thermal behaviour at low energy states, where the FC and ZFC curves still start splitting off. While this effect could be a defect of the system size, it is a first indicaction for a possible ergodicity breaking phase at low energies even for the ordered system.
An analysis of the thermodynamic entropy in both cases strengthened the previous findings. In the regime of strong disorder, it confirmed the non-thermal behaviour as predictions for the magnetization seemed largely random, which indicates that a thermal analysis does not help for understanding the behaviour of the system. In contrast, for the ordered scenario, we found that the entropy qualitatively predicts very well the increase of magnetization towards lower energies. Surprisingly, in the low energy regime where a

possible ergodicity breaking was observed, it matches very well to what one would expect for a spin glass. In this regime, the entropy transitions from showing a clear maximum that indicates an unambiguous thermal equilibrium state to developing a landscape with many local maxima. Thinking back, this bears a striking resemblance to what is seen in the free energy landscape of a classical spin glass. Of course, due to the limited system size that restricts all of the numerical observations, we again cannot put too much emphasis on this observation. However, we still note that if it persisted in the many particle limit, it would be a strong argument in favor of a spin glass transition.

It should be noted that the numerical results also provided some arguments against a spin glass transition, even for the ordered regime. First of all, the shape of the FC and ZFC curves is such that the magnetization for both processes continues to increase as the energy approaches the ground state energy. This stands in opposition to what is observed in typical spin glasses, where it is seen to saturate or even slightly decline when approaching zero temperature. Second, any kind of aging is completely absent in the numerical simulations. The values of FC and ZFC are independent of a possible waiting time and in accordance with the diagonal ensemble. This fact guarantees that the difference persists at almost all times. In a typical spin glass, a relaxation from the ZFC to the FC value is present, even though it happens on astronomical timescales. Finally, we found that in our scenario, thermal predictions agree with the ZFC value more than with the FC prediction. Conversely, in a conventional spin glass FC values generally follow a thermal prediction whereas ZFC values are non-thermal at low temperatures. In the same way as the observations in favor of a spin glass transition, all of the above statements do however suffer heavily from the restriction on the system size, making it difficult to reach a conclusive statement based on the numerical analysis alone.

In the second part of the results, we focused on the experimental findings for a large system of spins. We were able to successfully apply the state-preparation protocol to the Rydberg quantum simulator and for the first time measure a response to an external field after the magnetization has previously relaxed to zero. Using the ZFC procedure, we were able to measure the influence of the ramp duration on the magnitude of the response. Notably, the behaviour significantly deviates from the numerical observations. At slow ramps, we find a decrease of the ZFC magnetization as it would be expected for a typical spin glass. On top of that, we were able to measure an aging effect that seems to occur only after a critical ramp duration is reached, also in accordance with what is expected as spin glass behaviour.

To conclude, we think it unlikely that a glass transition persists in the case of strong disorder. While ergodicity breaking is clearly present in this regime, the system seems to be completely non-thermalizing and thermal predictions fail at all energy levels. This is in stark contrast to what one would expect to find in a spin glass, where ergodicity breaking is a result of astronomically long relaxation times. Such a situation is quite different from a complete absence of thermalization since thermal predictions are still relevant and successfully predict for example the FC magnetization. In some cases, it is even possible to adapt the fluctuation-dissipation theorem, a result purely based on thermal equilibrium physics, to the aging regime. In general, the observations for this strong disorder regime seem to be more in line with the scenario of may-body localization, however further studies would be needed for a clear statement about the nature of the system.

The situation changes however for the case of weak disorder. Here, while the numerical considerations yield conflicting results on the nature of the system, the experimental evidence seems to point towards a possible existence of a glass phase. A physical interpretation for why glassy behaviour vanishes at strong disorder might be found in the pair picture that has recently been established within the group [16, 60]. It allows for a description of the strongly disordered system based solely on nearest neighbour couplings. At the same time, a system where only nearest neighbour couplings are relevant for the description cannot feature any kind of frustration, since any spin easily finds a ground state configuration with respect to only its nearest neighbour. As such, once the pair picture is valid in the presence of strong disorder, no spin glass behaviour should be found for the system. However in the opposite limit of a blockaded regime, frustration effects are clearly part of the system and since disorder is still present, such a system might well display a transition towards a glassy phase.

That being said, with the current experimental data it is not yet possible to make a confident statement that such a transition is indeed present. In order to make such a claim in the future, there are a couple of interesting measurements one could still conduct. A very important measurement would be the experimental realization of a field cooling curve, to see whether we find a splitting with respect to the ZFC curve even in the ordered regime. Additionally, one could extend the aging measurements to the regime where no aging is expected, to confirm that the observed effect is not simply a defect from an as of now unknown experimental error.

In view of the method of fluorescence imaging that is currently prepared to be implemented to the experiment and expected to greatly increase the efficiency of state de-

tection, one could also think of possibly measuring the non-linear susceptibility, which should diverge at the point where the system enters the glass phase and would provide an unequivocal sign for a glass transition.
To extend the numerical studies, one could consider an in depth analysis of the spin glass order parameter. While a naive analysis can be found in the appendix, it shows no increase of order at all. This can, however, be attributed to the fact that a spin glass shows spontaneous symmetry breaking in the ground state. When analyzing it with exact diagonalization, one has to explicitly break the symmetry of the Hamiltonian with a small perturbation. Otherwise, all eigenstates will obviously respect the symmetry and hide the nature of the true, symmetry broken ground state.
Finally, one could also take a look at a different transition that is known as chiral-glass transition. For such a transition, the handedness of the spins with respect to rotation freezes out at finite temperatures, an effect commonly seen for the XY model [63]. It would be interesting to see how such a scenario could be relevant for our system.

Acknowledgements

Of course, this thesis would not have been possible if not for the help of many invaluable people that I would like to thank at this point.
First, I would like to express my gratitude to my supervisor, Prof. Dr. Matthias Weidemüller for allowing me to work in an awesome group and the freedom of pursuing both theoretical and experimental physics simultaneously.
Second, I want to thank Dr. Martin Gärttner for agreeing to read this thesis as a second referee.
Next I would like to address the whole Rydberg team, it has been a pleasure working with you all and the amount of knowledge I was able to (hopefully) retain from this past year is incredible. Thank you Gerhard, the number of times you helped me during the lab phase of my studies is uncountable and your knowledge about experimental details of (not just the !!!!) Rydberg lab is simply amazing. Thank you Titus for introducing me to the intriguing topics of aging and the world of 5 cups of coffee a day, the wonders of which I only recently fully grasped when starting to write up this thesis :) Many thanks to Sebastian for withstanding the barrage of questions I had when I first joined in the lab and patiently explaining the details to me, no matter how often I kept asking the same things. Thank you Eduard, I do not think that I was able to come up with a single theory related question during our time together that you were unable to answer. At some point you are going to have to tell me where exactly in your head you store all those little details. Dillen, I loved our friday afternoon philosophy sessions and Amar, the short time we spent together was hugely enjoyable. I also want to thank Maximilian and Oliver, the mario cart evening was simply legendary, we definitely should have repeated that more often.
Of course, many thanks to all the people proofreading parts of this thesis.
Lastly, I would also like to thank my family for the continuous support throughout all of my studies and for handling it quite well when I forget to send signs of life from time to time.

7 References

[1] Alexander F. Siegenfeld and Yaneer Bar-Yam. “An Introduction to Complex Systems Science and Its Applications”. In: *Complexity* 2020 (July 2020), pp. 1–16. DOI: 10.1155/2020/6105872. URL: https://doi.org/10.1155%2F2020%2F6105872.

[2] Giorgio Parisi. *The physical Meaning of Replica Symmetry Breaking*. May 18, 2002. arXiv: cond-mat/0205387. URL: http://arxiv.org/abs/cond-mat/0205387 (visited on 05/15/2023).

[3] Ayaka Sakata, Koji Hukushima, and Kunihiko Kaneko. “Replica symmetry breaking in an adiabatic spin-glass model of adaptive evolution”. In: *EPL (Europhysics Letters)* 99.6 (Sept. 2012), p. 68004. DOI: 10.1209/0295-5075/99/68004. URL: https://doi.org/10.1209%2F0295-5075%2F99%2F68004.

[4] Linda Albanese et al. “Replica Symmetry Breaking in Dense Hebbian Neural Networks”. In: *Journal of Statistical Physics* 189.2 (Sept. 2022). DOI: 10.1007/s10955-022-02966-8. URL: https://doi.org/10.1007%2Fs10955-022-02966-8.

[5] Rémi Monasson. “Optimization problems and replica symmetry breaking in finite connectivity spin glasses”. In: *Journal of Physics A: Mathematical and General* 31.2 (Jan. 1998), pp. 513–529. DOI: 10.1088/0305-4470/31/2/012. URL: https://doi.org/10.1088%2F0305-4470%2F31%2F2%2F012.

[6] K. Binder and A. P. Young. “Spin glasses: Experimental facts, theoretical concepts, and open questions”. In: *Reviews of Modern Physics* 58.4 (Oct. 1, 1986), pp. 801–976. ISSN: 0034-6861. DOI: 10.1103/RevModPhys.58.801. URL: https://link.aps.org/doi/10.1103/RevModPhys.58.801 (visited on 08/15/2022).

[7] Eric Vincent. “Spin glass experiments”. In: 2023, B9780323908009000706. DOI: 10.1016/B978-0-323-90800-9.00070-6. arXiv: 2208.00981[cond-mat]. URL: http://arxiv.org/abs/2208.00981 (visited on 07/05/2023).

[8] Immanuel Bloch, Jean Dalibard, and Sylvain Nascimbène. “Quantum simulations with ultracold quantum gases”. In: *Nature Physics* 8.4 (Apr. 1, 2012), pp. 267–276. ISSN: 1745-2481. DOI: 10.1038/nphys2259. URL: https://doi.org/10.1038/nphys2259.

[9] J. Ignacio Cirac and Peter Zoller. “Goals and opportunities in quantum simulation”. In: *Nature Physics* 8.4 (Apr. 1, 2012), pp. 264–266. ISSN: 1745-2481. DOI: 10.1038/nphys2275. URL: https://doi.org/10.1038/nphys2275.

[10] Iulia Buluta and Franco Nori. “Quantum Simulators”. In: *Science* 326.5949 (2009), pp. 108–111. DOI: 10.1126/science.1177838. eprint: https://www.science.org/doi/pdf/10.1126/science.1177838. URL: https://www.science.org/doi/abs/10.1126/science.1177838.

[11] Sepehr Ebadi et al. “Quantum phases of matter on a 256-atom programmable quantum simulator”. In: *Nature* 595.7866 (July 2021), pp. 227–232. DOI: 10.1038/s41586-021-03582-4. URL: https://doi.org/10.1038%2Fs41586-021-03582-4.

[12] Florian Kranzl et al. “Controlling long ion strings for quantum simulation and precision measurements”. In: *Physical Review A* 105.5 (May 2022). DOI: 10.1103/physreva.105.052426. URL: https://doi.org/10.1103%2Fphysreva.105.052426.

[13] Pascal Scholl et al. “Quantum simulation of 2D antiferromagnets with hundreds of Rydberg atoms”. In: *Nature* 595.7866 (July 2021), pp. 233–238. DOI: 10.1038/s41586-021-03585-1. URL: https://doi.org/10.1038%2Fs41586-021-03585-1.

[14] Hannes Bernien et al. “Probing many-body dynamics on a 51-atom quantum simulator”. In: *Nature* 551.7682 (Nov. 2017), pp. 579–584. DOI: 10.1038/nature24622. URL: https://doi.org/10.1038%2Fnature24622.

[15] A. Signoles et al. “Glassy Dynamics in a Disordered Heisenberg Quantum Spin System”. In: *Physical Review X* 11.1 (Jan. 19, 2021). Publisher: American Physical Society, p. 011011. DOI: 10.1103/PhysRevX.11.011011. URL: https://link.aps.org/doi/10.1103/PhysRevX.11.011011 (visited on 10/03/2022).

[16] Titus Franz et al. *Absence of thermalization in an interacting system of thousands of quantum spins*. 2022. arXiv: 2207.14216 [quant-ph].

[17] H Takayama. “Aging phenomena in spin glasses: theory, experiment, and simulation”. In: *Journal of Magnetism and Magnetic Materials*. Proceedings of the International Conference on Magnetism (ICM 2003) 272-276 (May 1, 2004), pp. 256–

260. ISSN: 0304-8853. DOI: 10.1016/j.jmmm.2003.12.383. URL: https://www.sciencedirect.com/science/article/pii/S0304885303020511 (visited on 09/12/2022).

[18] Titus Franz. "Simulating Disordered Heisenberg Spins out of equilibrium with Rydberg Atoms". PhD thesis. Heidelberg University, 2022.

[19] Dennis Schubert et al. "Quantum versus classical dynamics in spin models: Chains, ladders, and square lattices". In: *Phys. Rev. B* 104 (5 Aug. 2021), p. 054415. DOI: 10.1103/PhysRevB.104.054415. URL: https://link.aps.org/doi/10.1103/PhysRevB.104.054415.

[20] Maksym Serbyn, Dmitry A. Abanin, and Zlatko Papić. "Quantum many-body scars and weak breaking of ergodicity". In: *Nature Physics* 17.6 (May 2021), pp. 675–685. DOI: 10.1038/s41567-021-01230-2. URL: https://doi.org/10.1038%2Fs41567-021-01230-2.

[21] Sanjay Moudgalya, B. Andrei Bernevig, and Nicolas Regnault. "Quantum Many-Body Scars and Hilbert Space Fragmentation: A Review of Exact Results". In: *Reports on Progress in Physics* 85.8 (Aug. 1, 2022), p. 086501. ISSN: 0034-4885, 1361-6633. DOI: 10.1088/1361-6633/ac73a0. arXiv: 2109.00548[cond-mat,physics:quant-ph]. URL: http://arxiv.org/abs/2109.00548 (visited on 06/29/2023).

[22] Dmitry A. Abanin et al. "Many-body localization, thermalization, and entanglement". In: *Reviews of Modern Physics* 91.2 (May 2019). DOI: 10.1103/revmodphys.91.021001. URL: https://doi.org/10.1103%2Frevmodphys.91.021001.

[23] J. Smith et al. "Many-body localization in a quantum simulator with programmable random disorder". In: *Nature Physics* 12.10 (June 2016), pp. 907–911. DOI: 10.1038/nphys3783. URL: https://doi.org/10.1038%2Fnphys3783.

[24] Michael Schreiber et al. "Observation of many-body localization of interacting fermions in a quasirandom optical lattice". In: *Science* 349.6250 (Aug. 2015), pp. 842–845. DOI: 10.1126/science.aaa7432. URL: https://doi.org/10.1126%2Fscience.aaa7432.

[25] John von Neumann. “Proof of the Ergodic Theorem and the H-Theorem in Quantum Mechanics”. In: *The European Physical Journal H* 35.2 (Nov. 2010), pp. 201–237. ISSN: 2102-6459, 2102-6467. DOI: 10.1140/epjh/e2010-00008-5. arXiv: 1003.2133[cond-mat,physics:physics,physics:quant-ph]. URL: http://arxiv.org/abs/1003.2133 (visited on 07/03/2023).

[26] Mark Srednicki. “Chaos and quantum thermalization”. In: *Phys. Rev. E* 50 (2 Aug. 1994), pp. 888–901. DOI: 10.1103/PhysRevE.50.888. URL: https://link.aps.org/doi/10.1103/PhysRevE.50.888.

[27] Joshua M. Deutsch. “Eigenstate Thermalization Hypothesis”. In: *Reports on Progress in Physics* 81.8 (Aug. 1, 2018), p. 082001. ISSN: 0034-4885, 1361-6633. DOI: 10.1088/1361-6633/aac9f1. arXiv: 1805.01616[cond-mat,physics:quant-ph]. URL: http://arxiv.org/abs/1805.01616 (visited on 05/10/2023).

[28] Luca D’Alessio et al. “From Quantum Chaos and Eigenstate Thermalization to Statistical Mechanics and Thermodynamics”. In: *Advances in Physics* 65.3 (May 3, 2016), pp. 239–362. ISSN: 0001-8732, 1460-6976. DOI: 10.1080/00018732.2016.1198134. arXiv: 1509.06411[cond-mat,physics:quant-ph]. URL: http://arxiv.org/abs/1509.06411 (visited on 06/29/2023).

[29] Peter Reimann. “Foundation of Statistical Mechanics under Experimentally Realistic Conditions”. In: *Physical Review Letters* 101.19 (Nov. 7, 2008), p. 190403. ISSN: 0031-9007, 1079-7114. DOI: 10.1103/PhysRevLett.101.190403. URL: https://link.aps.org/doi/10.1103/PhysRevLett.101.190403 (visited on 06/29/2023).

[30] Asl ı Çakan, J. Ignacio Cirac, and Mari Carmen Bañuls. “Approximating the long time average of the density operator: Diagonal ensemble”. In: *Phys. Rev. B* 103 (11 Mar. 2021), p. 115113. DOI: 10.1103/PhysRevB.103.115113. URL: https://link.aps.org/doi/10.1103/PhysRevB.103.115113.

[31] Takashi Mori et al. “Thermalization and prethermalization in isolated quantum systems: a theoretical overview”. In: *Journal of Physics B: Atomic, Molecular and Optical Physics* 51.11 (June 14, 2018), p. 112001. ISSN: 0953-4075, 1361-6455. DOI: 10.1088/1361-6455/aabcdf. arXiv: 1712.08790. URL: http://arxiv.org/abs/1712.08790 (visited on 04/25/2022).

[32] Charlie Nation and Diego Porras. “Off-diagonal observable elements from random matrix theory: distributions, fluctuations, and eigenstate thermalization”. In: *New Journal of Physics* 20.10 (Oct. 2018), p. 103003. DOI: 10.1088/1367-2630/aae28f. URL: https://doi.org/10.1088%2F1367-2630%2Faae28f.

[33] Lea F. Santos and Marcos Rigol. “Localization and the effects of symmetries in the thermalization properties of one-dimensional quantum systems”. In: *Physical Review E* 82.3 (Sept. 2010). DOI: 10.1103/physreve.82.031130. URL: https://doi.org/10.1103%2Fphysreve.82.031130.

[34] Rubem Mondaini et al. “Eigenstate thermalization in the two-dimensional transverse field Ising model”. In: *Physical Review E* 93.3 (Mar. 2016). DOI: 10.1103/physreve.93.032104. URL: https://doi.org/10.1103%2Fphysreve.93.032104.

[35] W. Beugeling, R. Moessner, and Masudul Haque. “Finite-size scaling of eigenstate thermalization”. In: *Physical Review E* 89.4 (Apr. 2014). DOI: 10.1103/physreve.89.042112. URL: https://doi.org/10.1103%2Fphysreve.89.042112.

[36] R. Steinigeweg et al. “Pushing the Limits of the Eigenstate Thermalization Hypothesis towards Mesoscopic Quantum Systems”. In: *Physical Review Letters* 112.13 (Apr. 2014). DOI: 10.1103/physrevlett.112.130403. URL: https://doi.org/10.1103%2Fphysrevlett.112.130403.

[37] Nicholas Hunter-Jones, Junyu Liu, and Yehao Zhou. “On thermalization in the SYK and supersymmetric SYK models”. In: *Journal of High Energy Physics* 2018.2 (Feb. 2018). DOI: 10.1007/jhep02(2018)142. URL: https://doi.org/10.1007%2Fjhep02%282018%29142.

[38] Marcos Rigol, Vanja Dunjko, and Maxim Olshanii. “Thermalization and its mechanism for generic isolated quantum systems”. In: *Nature* 452.7189 (Apr. 17, 2008), pp. 854–858. ISSN: 0028-0836, 1476-4687. DOI: 10.1038/nature06838. arXiv: 0708.1324[cond-mat]. URL: http://arxiv.org/abs/0708.1324 (visited on 07/05/2023).

[39] Gustavo Castellano. “Thermodynamic potentials for simple magnetic systems”. In: *Journal of Magnetism and Magnetic Materials* 260.1 (Mar. 2003), pp. 146–150. ISSN: 03048853. DOI: 10.1016/S0304-8853(02)01286-6. URL: https://linkinghub.elsevier.com/retrieve/pii/S0304885302012866 (visited on 05/24/2023).

[40] Konstantin Likharev. *EssentialGradPhysics*.

[41] Leticia F Cugliandolo. “Advanced Statistical Physics: Quenched disordered systems”. In: *RANDOM FIELDS* ().

[42] Lev Vidmar and Marcos Rigol. “Generalized Gibbs ensemble in integrable lattice models”. In: *Journal of Statistical Mechanics: Theory and Experiment* 2016.6 (June 28, 2016), p. 064007. ISSN: 1742-5468. DOI: 10.1088/1742-5468/2016/06/064007. arXiv: 1604.03990[cond-mat,physics:quant-ph]. URL: http://arxiv.org/abs/1604.03990 (visited on 04/11/2023).

[43] K. Binder and A. P. Young. “Spin glasses: Experimental facts, theoretical concepts, and open questions”. In: *Reviews of Modern Physics* 58.4 (Oct. 1, 1986), pp. 801–976. ISSN: 0034-6861. DOI: 10.1103/RevModPhys.58.801. URL: https://link.aps.org/doi/10.1103/RevModPhys.58.801 (visited on 08/15/2022).

[44] Eric Vincent and Vincent Dupuis. “Spin Glasses: Experimental Signatures and Salient Outcomes”. In: *Frustrated Materials and Ferroic Glasses*. Ed. by Turab Lookman and Xiaobing Ren. Vol. 275. Series Title: Springer Series in Materials Science. Cham: Springer International Publishing, 2018, pp. 31–56. ISBN: 978-3-319-96913-8 978-3-319-96914-5. DOI: 10.1007/978-3-319-96914-5_2. URL: http://link.springer.com/10.1007/978-3-319-96914-5_2 (visited on 07/05/2023).

[45] P. Nordblad et al. “Time decay of the remanent magnetization in a CuMn spin glass”. In: *Physical Review B* 33.1 (Jan. 1, 1986). Publisher: American Physical Society, pp. 645–648. DOI: 10.1103/PhysRevB.33.645. URL: https://link.aps.org/doi/10.1103/PhysRevB.33.645 (visited on 09/27/2022).

[46] Gerardus Koper. *On The Dynamics of Spin Glasses: A Theory of Aging*.

[47] Eric Vincent. *Aging, rejuvenation and memory : the example of spin glasses*. Vol. 716. 2007. DOI: 10.1007/3-540-69684-9. arXiv: cond-mat/0603583. URL: http://arxiv.org/abs/cond-mat/0603583 (visited on 09/27/2022).

[48] M. Baity-Jesi et al. "Memory and rejuvenation effects in spin glasses are governed by more than one length scale". In: *Nature Physics* 19.7 (Apr. 2023), pp. 978–985. DOI: 10.1038/s41567-023-02014-6. URL: https://doi.org/10.1038%2Fs41567-023-02014-6.

[49] S F Edwards and P W Anderson. "Theory of spin glasses". In: *Journal of Physics F: Metal Physics* 5.5 (May 1975), p. 965. DOI: 10.1088/0305-4608/5/5/017. URL: https://dx.doi.org/10.1088/0305-4608/5/5/017.

[50] David Sherrington and Scott Kirkpatrick. "Solvable Model of a Spin-Glass". In: *Phys. Rev. Lett.* 35 (26 Dec. 1975), pp. 1792–1796. DOI: 10.1103/PhysRevLett.35.1792. URL: https://link.aps.org/doi/10.1103/PhysRevLett.35.1792.

[51] Jean-Philippe Bouchaud et al. *Out of equilibrium dynamics in spin-glasses and other glassy systems*. Feb. 7, 1997. arXiv: cond-mat/9702070. URL: http://arxiv.org/abs/cond-mat/9702070 (visited on 03/15/2023).

[52] David Tong. *Lecture Notes on Kinetic Theory*. 2012. URL: http://www.damtp.cam.ac.uk/user/tong/kintheory/ (visited on 07/21/2023).

[53] Daniel S. Fisher and David A. Huse. "Nonequilibrium dynamics of spin glasses". In: *Phys. Rev. B* 38 (1 July 1988), pp. 373–385. DOI: 10.1103/PhysRevB.38.373. URL: https://link.aps.org/doi/10.1103/PhysRevB.38.373.

[54] C. M. Newman and D. L. Stein. "Ground-state stability and the nature of the spin glass phase". In: *Physical Review E* 105.4 (Apr. 2022). DOI: 10.1103/physreve.105.044132. URL: https://doi.org/10.1103%2Fphysreve.105.044132.

[55] Giorgio Parisi. *The overlap in glassy systems*. Oct. 20, 2013. arXiv: 1310.5354[cond-mat]. URL: http://arxiv.org/abs/1310.5354 (visited on 05/15/2023).

[56] Marco Baity Jesi. *Spin Glasses: Criticality and Energy Landscapes*. 1st ed. 2016. Springer Theses, Recognizing Outstanding Ph.D. Research. Cham: Springer International Publishing : Imprint: Springer, 2016. 1 p. ISBN: 978-3-319-41231-3. DOI: 10.1007/978-3-319-41231-3.

[57] Tommaso Castellani and Andrea Cavagna. "Spin-Glass Theory for Pedestrians". In: *Journal of Statistical Mechanics: Theory and Experiment* 2005.5 (May 31, 2005), P05012. ISSN: 1742-5468. DOI: 10.1088/1742-5468/2005/05/P05012. arXiv: cond-mat/0505032. URL: http://arxiv.org/abs/cond-mat/0505032 (visited on 05/28/2023).

[58] Renato Ferracini Alves. "Realization of a Heisenberg XXZ spin system using Rydberg atoms". PhD thesis. Heidelberg University, 2021.

[59] Eduard Jürgen Braun. *Driving of a quantum many-body spin system of Rydberg atoms out of equilibrium*. 2022.

[60] Titus Franz et al. *Observation of universal relaxation dynamics in disordered quantum spin systems*. 2022. arXiv: 2209.08080 [quant-ph].

[61] Jack L. Koenig. "Chapter 8 - High-resolution NMR spectroscopy of solid polymers". In: *Spectroscopy of Polymers (Second Edition)*. Ed. by Jack L. Koenig. Second Edition. New York: Elsevier Science, 1999, pp. 353–396. ISBN: 978-0-444-10031-3. DOI: https://doi.org/10.1016/B978-044410031-3/50008-6. URL: https://www.sciencedirect.com/science/article/pii/B9780444100313500086.

[62] Joseph E. Avron and Alexander Elgart. "Adiabatic Theorem without a Gap Condition". In: *Communications in Mathematical Physics* 203.2 (June 1999), pp. 445–463. DOI: 10.1007/s002200050620. URL: https://doi.org/10.1007%2Fs002200050620.

[63] Tota Nakamura and Shin-ichi Endoh. "A Spin-Glass and Chiral-Glass Transition in a +- J Heisenberg Spin-Glass Model in Three Dimensions". In: *Journal of the Physical Society of Japan* 71.9 (Sept. 2002), pp. 2113–2116. DOI: 10.1143/jpsj.71.2113. URL: https://doi.org/10.1143%2Fjpsj.71.2113.

[64] K. R. Fratus. "Spontaneous Symmetry Breaking and Eigenstate Thermalization". PhD thesis. UC Santa Barbara., 2017. URL: https://escholarship.org/uc/item/1c68q1fh.

A Estimation of the Variance for Dipolar Couplings

Here we explicitly show the calculations for the estimate of the variance in section 3.2. For the calculation, we assume an isotropic distribution of atoms that only depends on the radial distance, such that we can separate angular from radial integration. This means we have to evaluate expressions of the form

$$\langle J \rangle = \frac{1}{\mathcal{N}} \int dr\, \rho(r) r^2 \int d\Omega\, \sin(\theta) J(r, \Omega), \tag{47}$$

where $\rho(r)$ is the probability distribution for finding an atom at distance r from the first one.

We start by evaluating the angular dependencies. Considering the anisotropy of the dipolar couplings, we find for the angular integral $\Omega(J_{\mathrm{DDI}})$

$$\begin{aligned}
\Omega(J_{\mathrm{DDI}}) &= \int d\Omega\, \sin\theta(1 - 3\cos^2\theta) \\
&= 2\pi \int_0^\pi d\theta\, \sin\theta(1 - 3\cos^2\theta) = 2\pi \int_{-1}^1 du\, (1 - 3u^2) \\
&= 2\pi \left[u - u^3\right]_{-1}^{1} = 0.
\end{aligned} \tag{48}$$

In the same way, we can compute the integral for the variance

$$\begin{aligned}
\Omega(J_{\mathrm{DDI}}^2) &= 2\pi \int_0^\pi d\theta\, \sin\theta(1 - 6\cos^2\theta + 9\cos^4\theta) \\
&= 2\pi \int_{-1}^1 du\, (1 - 6u^2 + 9u^4) \\
&= 2\pi \left[u - 2u^3 + \frac{9}{5}u^5\right]_{-1}^{1} = \frac{16}{5}\pi.
\end{aligned} \tag{49}$$

The evaluation of the radial dependency is a little more tricky. While we could integrate over the whole space by assuming a cutoff and extending it to infinity, due to the fact that we have a r^{-3} dependence in the coupling, both mean and variance of the couplings would simply go towards zero in the limit of infinite system size, which clearly does not represent the system. We realize that it is mostly the strong couplings that determine the behaviour of the system. Thus, a first approximation can be obtained for the blockaded regime by assuming that most of the strong couplings are given by the upper limit of the blockade. In this case, we can substantially simplify the radial integration by introducing

a delta function $\delta(r - r_{\mathrm{bl}})$ such that we only consider strong couplings. Taking care of proper normalization by dividing out a shell of $4\pi r_{\mathrm{bl}}^2$, we get an approximation solution for the blockaded regime

$$\langle J_{\mathrm{DDI}} \rangle = 0 \tag{50}$$

$$\langle J_{\mathrm{DDI}}^2 \rangle = \frac{1}{4\pi r_{\mathrm{bl}}^2} \frac{\mathrm{C}_3^2}{r_{\mathrm{bl}}^4} \cdot \Omega(J_{\mathrm{DDI}}^2) = \frac{4}{5} \frac{\mathrm{C}_3^2}{r_{\mathrm{bl}}^6} = \frac{4}{5} \left(\frac{r_{\mathrm{med}}}{r_{\mathrm{bl}}} \right)^6 J_{\mathrm{med}}^2, \tag{51}$$

where in the last step we reallowed for a small deviation between r_{med} and r_{bl}, that is obviously only justified in the case that $|r_{\mathrm{med}} - r_{\mathrm{bl}}| << 1$.

B Numerical Details for the Thermal Ensembles

In order to obtain the thermal predictions in section 4.5, we numerically estimate properties for both microcanonical (MCE) and canonical ensembles (CE). In the following, we give a quick summary of how this is done and show the corresponding populations as well as a convergence analysis for the MCE predictions that depend on an energy window $\Delta\varepsilon$. For the microcanonical ensemble, the density matrix $\hat{\rho}_{\mathrm{MCE}}$ at a given energy ε is obtained in a straightforward manner. After exact diagonalization of the system in presence of the small probe field, we define an energy window $\Delta\varepsilon$ and populate all states within the energy window $[\varepsilon - \Delta\varepsilon, \varepsilon + \Delta\varepsilon]$ at equal probability. Then, expectation values for an

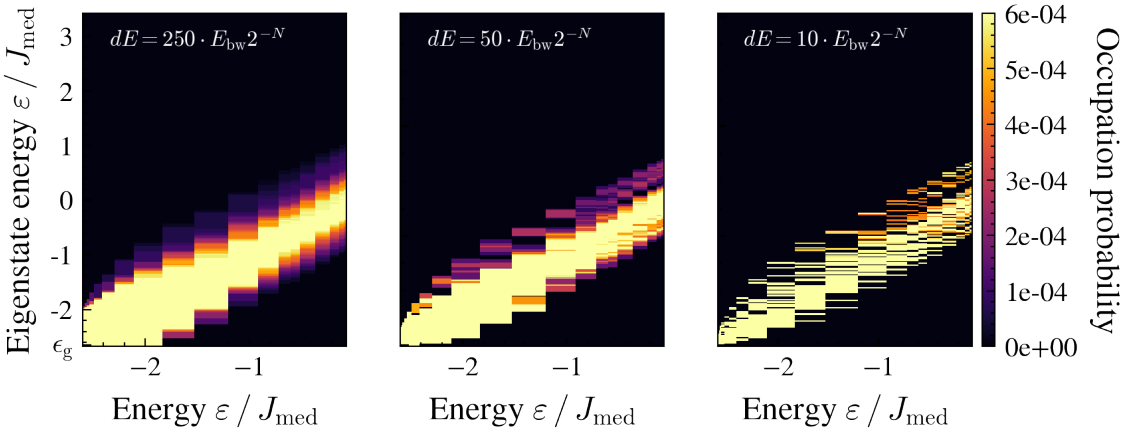

Figure B.1: Disorder averaged populations of the MCE for different $\Delta\varepsilon$. We see that at larger $\Delta\varepsilon$, the disorder average converges faster, as can bee seen by a smooth shape of the distribution. However, large $\Delta\varepsilon$ also decrease the accuracy of the prediction.

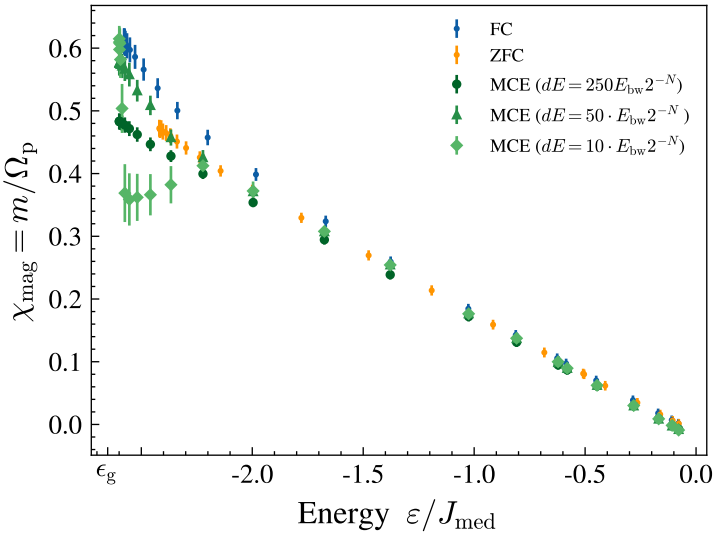

Figure B.2: Microcanonical predictions for different energy windows $\Delta\varepsilon$. At too large values, the prediction converges to a wrong value. At too small windows, we need a very large amount of disorder realizations for the ensemble average to converge. In an intermediate setting where roughly 50 states are on average in the energy window, convergence is achieved within a reasonable amount of disorder realizations.

Observable $\hat{A}$ are obtained as $\mathrm{Tr}(\hat{A}\hat{\rho}_{\mathrm{MCE}})$. This process is repeated for different disorder realizations and then averaged. Of course, the specific values in principle depend on the size of the energy window and we should show that the predictions converge for the chosen value.

We find that for larger energy windows $\Delta\varepsilon$, the disorder average converges faster (figure B.1. However we have to also care that it does so to the right value. We therefore compare the predictions for the different $\Delta\varepsilon$ in figure B.2.

We see that while for large energy windows the disorder average converges, it does so to the wrong value. On the contrary, for small $\Delta\varepsilon$, the average has not yet converged which is apparent when considering the large errorbars and confirmed by looking at the populations in figure B.1, where we see a lot of discontinuities for the smallest energy window.

For the CE prediction, we once again diagonalize the system in presence of the small field. Then the states are populated according to their canonical probabilities

$$p_{\mathrm{i}} = \frac{1}{Z} e^{-\beta E_{\mathrm{i}}}, \quad Z = \sum_{\mathrm{i}} e^{-\beta E_{\mathrm{i}}}. \tag{52}$$

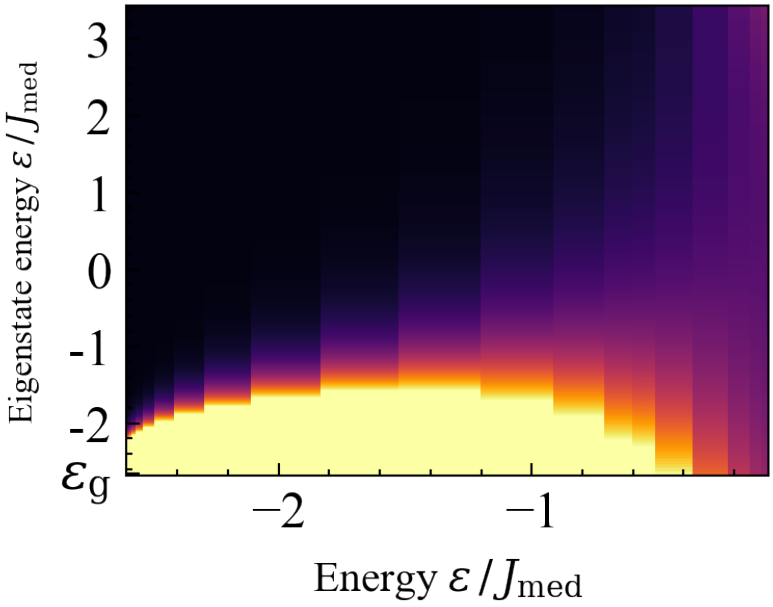

Figure B.3: Disorder averaged populations of the CE for different. We see that it looks quite similar to the actual population after the ramp.

However, in this case the control parameter is given by the inverse temperature β. Since we want to initialize the states at specific energies, we initialize a state at given beta and evaluate the energy of the initialized state numerically. We then adapt beta and repeat the process. This allows us to fit beta such that the energy of the CE corresponds to the energy of the MCE. The corresponding populations at different energies are plotted in figure B.3. The procedures do not change for the different disorder cases, however we find that for the case of large disorder, we need a larger disorder average of 150 realizations for the MCE to converge, which can be seen in figure.

C Problems with Simple Mean Field Theory

In this part, we want to quickly highlight the difficulties arising when trying to adapt a Weiss molecular field theory to our system. When considering the XY Hamiltonian of our system

$$\hat{H}_{\mathrm{XY}} = \sum_{\mathrm{i,j}} J_{\mathrm{ij}} (\sigma_{\mathrm{x}}^{(\mathrm{i})} \sigma_{\mathrm{x}}^{(\mathrm{j})} + \sigma_{\mathrm{y}}^{(\mathrm{i})} \sigma_{\mathrm{y}}^{(\mathrm{j})}) + b \sum_{\mathrm{i}} \sigma_{\mathrm{x}}^{(\mathrm{i})} \tag{53}$$

molecular field theory describes the system by considering the couplings to all other spins in a mean field picture, simplifying the Hamiltonian to

$$\hat{H}_{\mathrm{MF}} = \sum_{\mathrm{i,j}} J_{\mathrm{ij}}(\langle s_{\mathrm{x}}\rangle \sigma_{\mathrm{x}}^{(\mathrm{i})} + \langle s_{\mathrm{y}}\rangle \sigma_{\mathrm{y}}^{(\mathrm{i})}) + b \sum_{\mathrm{i}} \sigma_{\mathrm{x}}^{(\mathrm{i})} \tag{54}$$

Since we know that the average magnetization is only non-zero in the direction of the external field, we furthermore have $\langle s_{\mathrm{y}}\rangle = 0$ and can write

$$\hat{H}_{\mathrm{MF}} = \sum_{\mathrm{i}} \left(\langle s_{\mathrm{x}}\rangle \sum_{\mathrm{j}} J_{\mathrm{ij}} + b \right) \sigma_{\mathrm{x}}^{(\mathrm{i})} \tag{55}$$

So far, this is exactly in analogy to the mean field theory for a ferromagnet, and we would expect it to yield the same benefits. Indeed, we see that in this form, the Hamiltonian is diagonal in the x-product basis and it appears as if we could derive a self consistent equation for the magnetization in the same way as it is done for the ferromagnet. However, the problem occurs when considering the sum in the brackets. We realize that

$$\sum_{\mathrm{j}} J_{\mathrm{ij}} = N \cdot \frac{1}{N} \sum_{\mathrm{j}} J_{\mathrm{ij}} = N \langle J \rangle_{\mathrm{i}} = 0 \tag{56}$$

since as we demonstrated above (appendix A), the average couplings for any particle are zero. Thus, we find that Hamiltonian for a global mean field reduces to the Hamiltonian of a paramagnet, and does not help at improving predictions for the system.
The proper way of doing mean field theory for a system where the average couplings are zero is by introducing a local mean field for each spin $\langle s_{\mathrm{x}}^{\mathrm{j}}\rangle$, which gives the mean field Hamiltonian

$$\hat{H}_{\mathrm{MF}} = \sum_{\mathrm{i}} \left(\sum_{\mathrm{j}} J_{\mathrm{ij}} \langle s_{\mathrm{x}}^{\mathrm{j}}\rangle + b \right) \sigma_{\mathrm{x}}^{(\mathrm{i})} \tag{57}$$

that is still diagonal in x-basis. In the framework of the canonical ensemble, it is then possible to derive N coupled equations for the local expectation values that can be solved numerically to be self-consistent. The full mean field theory for spin glasses also introduces an additional term based on the variance of the coupling to correct for the importance of fluctuations. This Ansatz is known under the name of Thouless-Anderson-Palmer (TAP) equations and it would be interesting to see whether it can be applied to our specific system with dipolar couplings.

D Thermodynamics Disorder Averaged

In this section, we include for the sake of completeness the disorder averaged entropy of the system. However we caution against a strong interpretation of these plots, since twelve particles are not enough for the self-averaging property of the entropy to show and thus interesting features are lost in the disorder average. We mainly want to prove the point that in the strongly disordered regime, even at low energies there is no bias towards positive magnetizations as shown in figure D.1. Thus, we coclude that in the strong disorder regime thermal predictions completely break down. Entropy over the full phase space is shown in figure D.2.

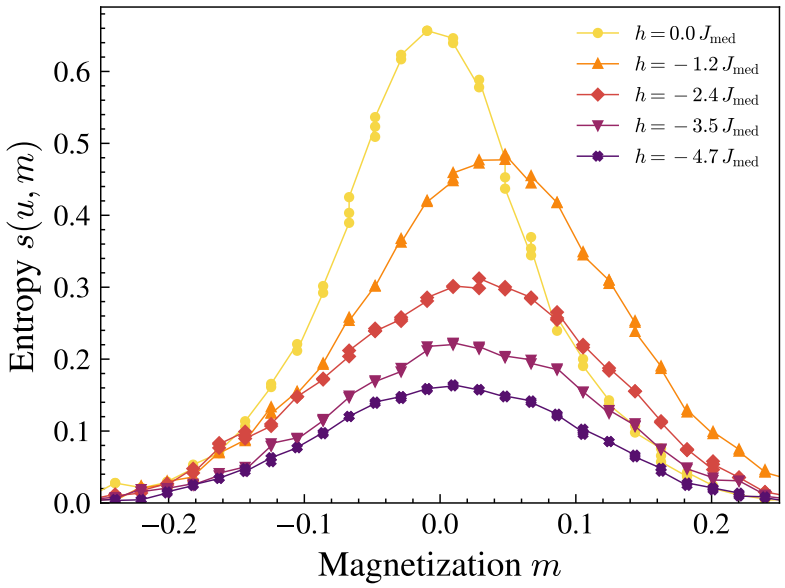

Figure D.1: Physical states for the disorder averaged entropy in the strong disorder regime. We realize that on average, zero magnetization is predicted even for low energies and conclude that thermal predictions fully break down.

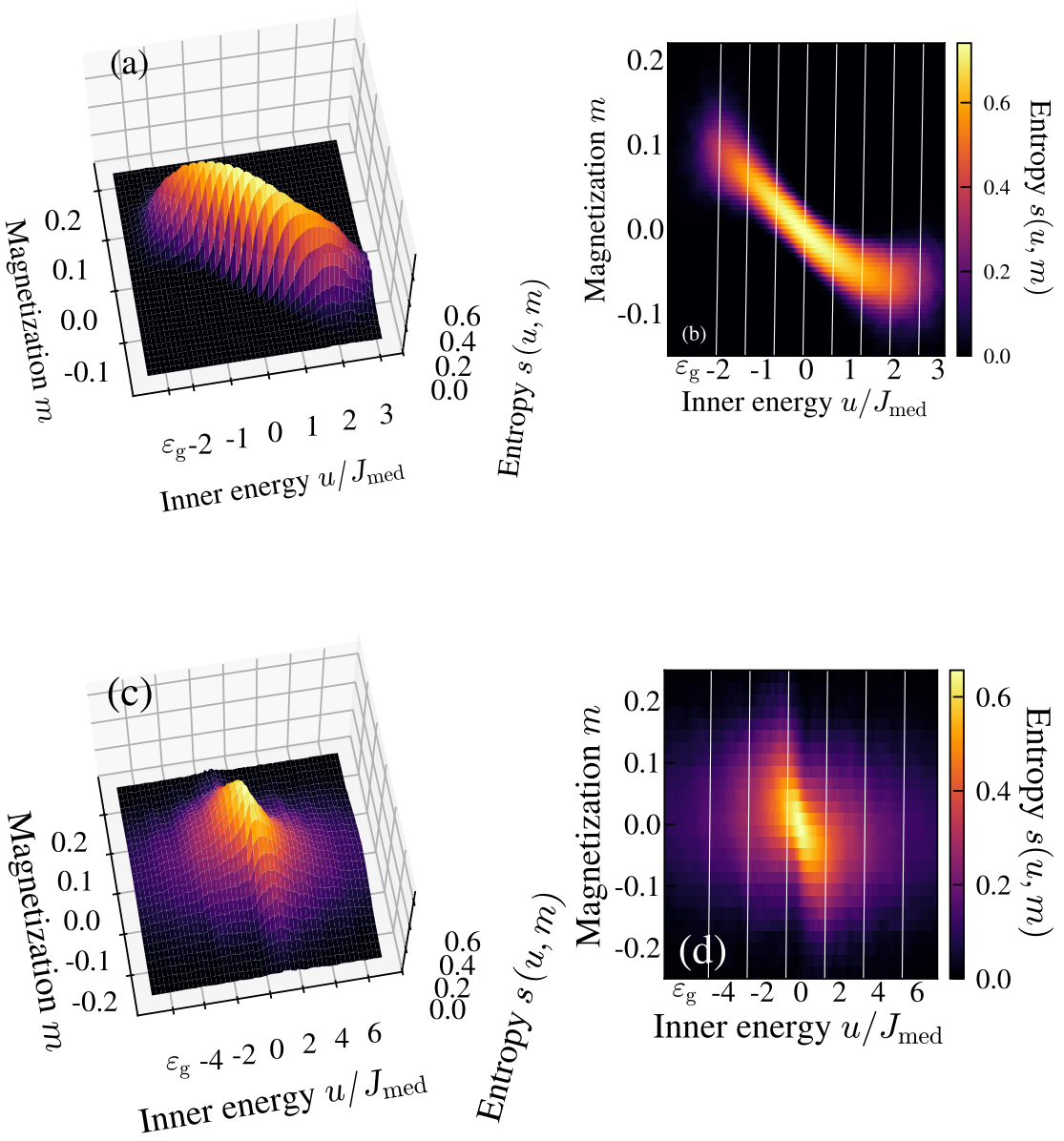

Figure D.2: Disorder averages for the thermodynamic entropy. We realize that all interesting features are lost in the proces of averaging, since twelve particles is simply not enough for the self-averaging property of the entropy to show

E Naive Analysis of EA-Order Parameter

A naive analysis of the EA-order parameter is shown in figure E.1. We plot the self overlap of a single eigenstate for three different amplitudes of the external field. While we do see an increase of the order towards low energy states, it is far from reaching unity and decreases as we decrease the amplitude of the probe field. This indicates that the effect does not persist in the limit of zero field and is simply the result of a magnetization that is globally non-zero.

However, we did not account for the spontaneous symmetry breaking nature of the spin glass ground state. The Hamiltonian has a global $\mathcal{U}(1)$ symmetry corresponding to rotations around the z-axis. Thus, the eigenstates obtained from exact diagonalization respect this symmetry. Considering the definition of the order parameter

$$q_{\mathrm{EA}} = \frac{1}{N} \sum_{\mathrm{i}=1}^{N} \overline{\langle \vec{\sigma}^{(\mathrm{i})} \rangle^2}, \tag{58}$$

it is apparent that if the eigenstates respect global rotation symmetry and do not show any preferred direction, all individual expectation values in the sum are zero and thus the whole order parameter also is zero.

The reason why the order parameter is non-zero in a spin glass is that the ground state features spontaneous symmetry breaking and is thus not invariant under rotation. While the initial direction of freezing is random, the spins afterwards point strictly in a specific

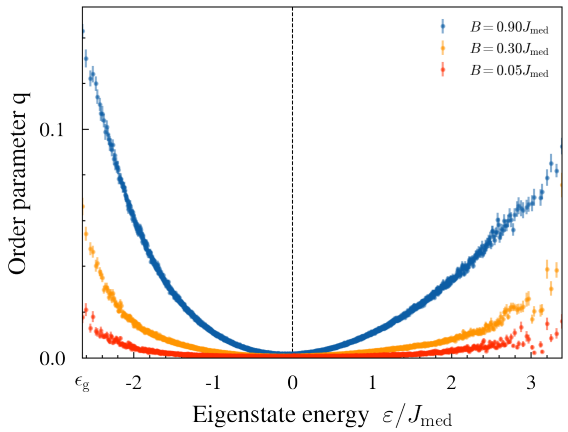

Figure E.1: Analysis of the order parameter using exact diagonalization. It appears that in the limit of no external field there is no spin glass order present. However, we did not account for the spontaneous symmetry breaking nature of a spin glass.

direction and the individual expectation values are no longer strictly zero, which violates the symmetry of the Hamiltonian.

To study systems that display spontaneous symmetry breaking, we have to explicitly apply a small, symmetry breaking perturbation to the system, as this reveals the nature of the symmetry broken ground state [64]. One could argue that we already break the symmetry of the system by applying our probe field, however this only reduces the global $\mathcal{U}(1)$ symmetry to a global $\mathcal{Z}(2)$ spin-flip symmetry with respect to the axis of the field, which is still enough to hide the spontaneously symmetry broken nature of the ground state. This reduction of the symmetry is however the reason why the order parameter deviates a little from zero in the presence of an external field, as it is observed in figure E.1.

It would be quite intriguing to find an appropriate perturbation that breaks the full symmetry and explore whether in this case the order parameter shows the expected increase for low energy states.

F Absence of Aging in Numerical Simulations

We also investigated an influence of the waiting time numerically (figure F.1), however we do not observe any difference in the response at all. This might be a defect of the small system size, since, in the droplet picture that commonly is used to explain aging, there are not enough particles in the numerical simulation to form the different domains needed for an aging effect.

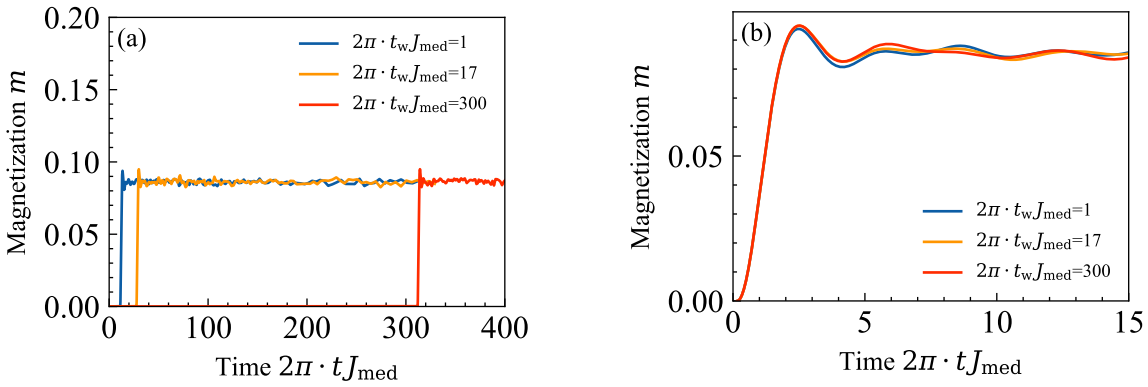

Figure F.1: (a) Build up of response after different waiting times. All curves look quite similar on a large scale (b) The response for different waiting times is plotted on top of each. The observation from before is confirmed, clearly we do not observe any effect of the waiting time in the numerical simulations

Declaration of Authorship

I certify that this thesis is the product of my own work and no other than the cited sources were used.

Ich versichere, dass ich diese Arbeit selbstständig verfasst und keine anderen als die angegebenen Quellen und Hilfsmittel benutzt habe.

Heidelberg, den 31.07.2023,

Moritz Hornung